Universiteit Utrecht

MSC THESIS

Geochemical analysis of the marginal eastern basin facies of the German Wealden (Berriasian, Lower Cretaceous)

Author:
DUSTIN A. MARQUARDT

Supervisors:
DR. ULRICH BERNER
DR. HANS DE BRESSER

April 30, 2012

Advisors

Dr. Ulrich Berner

Geochemistry of Petroleum and Coal

BGR - Federal Institute for Geosciences and Natural Resources

Hannover, Germany

Dr. Hans de Bresser

Experimental Rock Deformation (HPT) Laboratory

Department of Earth Sciences

Utrecht University

Utrecht, The Netherlands

Abstract

Organic-rich shales of the German Wealden, Lower Cretaceous, are a target for gas and oil shale exploration in Germany. Results of published organic petrographic investigations as well as oil shows and hydrocarbon gases extracted at the historical Lüdersfeld shaft of the Stadthagen syncline confirm the hydrocarbon potential of the Wealden sediments at the eastern margin of the Lower Saxony Basin. These former observations suggest that the shales of the eastern sub-basin that comprise several hundreds of meters of thickness have reached thermal maturities compatible of the oil and gas generation windows. We present results of a surface geochemical study in which seventeen outcrop samples collected along a profile across the Stadthagen syncline (Bückeberge to Rehburg anticline) have been used for re-assessment of the hydrocarbon potential of the Wealden sub-basin. The analytical methods comprise porosity measurements, elemental analysis (x-ray fluorescence, total and organic carbon and total sulfur analyses), Rock-Eval pyrolysis, hydrocarbon extraction, fractionation of extracted hydrocarbons and gas chromatography on aliphatic fractions as well as stable carbon isotope analyses and gas geochemical investigations .
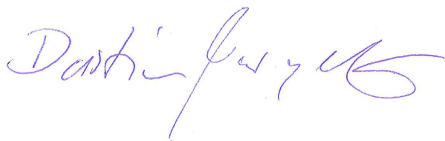
The investigated Wealden sediments comprise sandstones and shales and the latter contain high relative concentrations of carbon with an average of 3.2 wt.-%. Rock-Eval pyrolysis suggests variable contributions of different types of organic organic matter (land plant, phytoplankton). The depositional environment of the sediments was predominantly oxic with the exception of three samples that were deposited under dysoxic to anoxic conditions. Thermal maturities range from the oil to the wet gas window (samples from the basin center). Two samples from the Rehburg anticline contain phytoplankton dominated kerogens and show thermal maturities of the oil window, the latter also confirmed by stable isotope geochemistry of extracted hydrocarbon gases. Hydrogen indices suggest excellent generative potentials for algae-rich sediments; however, most samples have comparatively low hydrogen indices related to either high thermal maturities or unfavorable organic matter types.

Thermal maturities and measured shale porosities indicate changes of probable maximum burial depths from about 1800 m at the Rehburg anticline (Wealden V/VI) to about 3600 m in the basin center (Wealden III/IV). The estimated maximum burial depth of the Bückeberge amounts to about 2600 m (Wealden I/II). Although, initial results suggest good shale gas potential in the Stadthagen syncline, our investigations indicate a horizontal and vertical variability of the hydrocarbon potential within the basin.

Assertion

I herewith ensure that this thesis has been written self-dependently. Only the mentioned references were used.

Dustin A. Marquardt

Utrecht/Hanover, April 30, 2012

Acknowledgements

Contents

List of Figures

List of Tables

1 Introduction

During the Lower Cretaceous a large variety of sediment types were deposited in the Lower Saxony Basin (LSB). In the eastern sub-basin organic-rich German Wealden (Berriasian) sediments reach thicknesses of several hundreds of meters. Extensive research has been conducted on the LSB (cf. Chapter 2), the adjacent sedimentary systems and the German Wealden (Betz et al. 1987, Strauss et al. 1993, Elstner & Mutterlose 1996, Petmecky et al. 1999, Mutterlose & Bornemann 2000, Berner et al. 2010, Kahl 2010, Vejbæk et al. 2010, Berner 2011).

The LSB has been the most prolific hydrocarbon-bearing province in Germany for many decades (Betz et al. 1987). However, attempts to exploit oil from the fine-grained German Wealden shales were not economically feasible (Kahl 2010). In a time in which alternative energy sources become more popular Germany is investigating the LSB and other German provinces for their unconventional hydrocarbon potential. BGR's «NIKO» project (German acronym for 'non-conventional hydrocarbons') investigates Germany's shale oil and gas potential. It is within this framework that the research of this thesis was conducted.

The main objective of this thesis is to analyze the Stadthagen syncline in the eastern sub-basin of the LSB for its hydrocarbon potential. Additionally, the depositional environment and the subsidence in the area will be investigated.

For this purpose the sediment samples that were recovered from the Stadthagen area are investigated using a geochemical-analytical approach. The applied methods comprise x-ray fluorescence and LECO (carbon and sulfur) elemental analysis, Rock-Eval pyrolysis, hydrocarbon extraction and fractionation, gas chromatography, porosity measurements, stable carbon isotope analysis and gas geochemistry.

The thesis gives an introduction into the sample material (Chapter 3) and the applied methods (Chapter 4). The analytical results which are compiled in the appendix are discussed in Chapter 5. A conclusion at the end will summarize the findings.

2 Geological & Geographical Overview

During the time of the Lower Cretaceous Central Europe comprised several basin systems: the North Sea Basin, the Danish-Polish Basin, the Paris Basin and a few smaller basins extending from the Netherlands to east Germany, including the Lower Saxony Basin (cf. Littke et al. 2008 and Doornenbal & Stevenson 2010 for detailed information). These basins were surrounded by highlands such as the London-Brabant Massif, the Rhenish Massif, the Bohemian Massif or the Pompeckj Block, amongst others (cf. Figure 2.1).

The Lower Saxony Basin (LSB) plays an important role with respect to the hydrocarbon potential of Germany. The LSB is located in northern Germany and is bordered by the East Netherlands Triassic Plate on the western side, the Gifhorn Through in the east, the Pompeckj Block in the north and the Harz and Lower Saxony Mountains and the Rhenish Massif in the south. These borders form an ESE-WNW trending intra-continental basin c. 300 km long and 65 km wide (cf. Betz et al. 1987 and Vejbæk et al. 2010, see also Figures 2.2 and 2.3).

The LSB subsidence began in the Late Jurassic and the Early Cretaceous contemporaneously with the major rifting pulses of the North Sea Rift that caused subsidence and continued until Albian times. Subsidence involved a reactivation of some late Carboniferous WNW-ESE trending fracture systems. The LSB, as Betz et al. (1987) further point out, was created due to the termination of the differential extensional tectonics in the surrounding areas (i.e. Emsland, Weser and the Thuringian-West Brandenburg depression). The new stress regime that formed the LSB from Late Jurassic times onwards and governed the Early Cretaceous evolution of the LSB is also responsible for the transtensional subsidence of the en-echelon arranged sub-basins (Betz et al. 1987).

An important period in the formation and evolution of the LSB is the change in depositional environment during the Berriasian. According to Betz et al. (1987) and Elstner & Mutterlose (1996) a sea-level lowstand is reflected by the change of the depositional environment
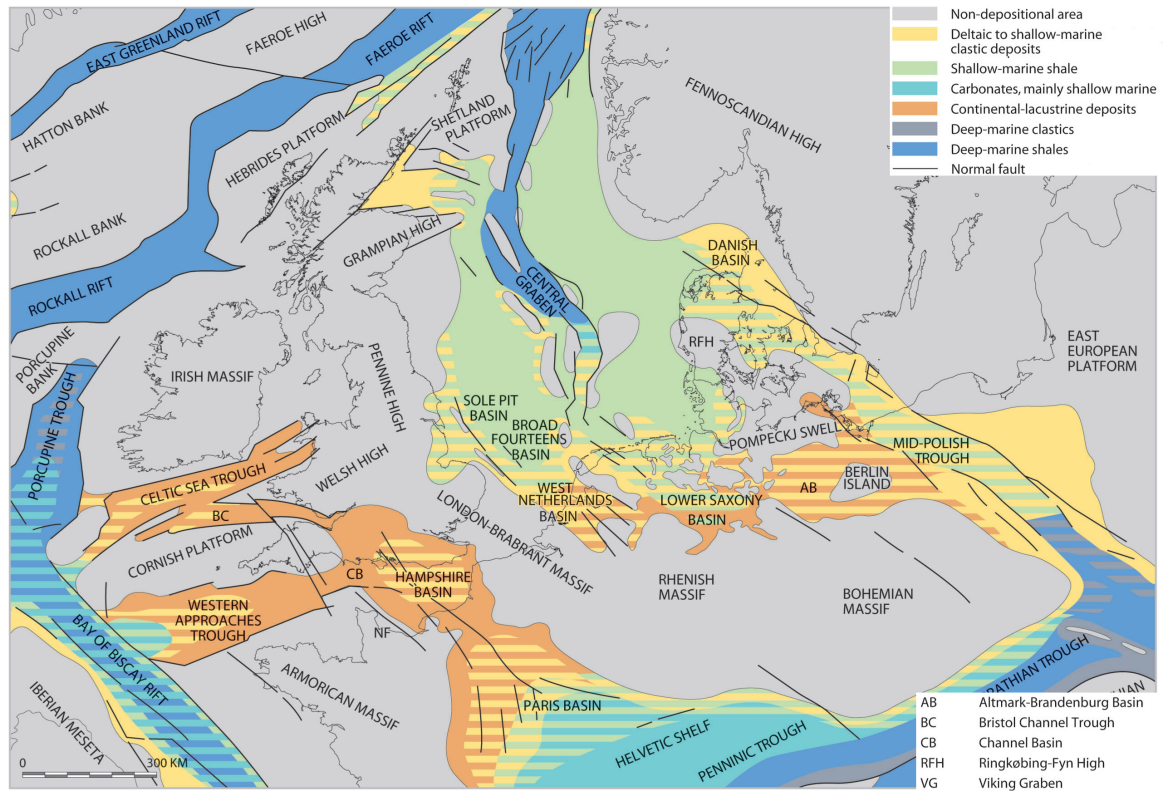
Figure 2.1: Central European paleogeography in Berriasian to Barremian times (after Vejbæk et al. 2010).

from restricted evaporitic, shallow marine conditions that were present in the Late Jurassic to fluvio-lacustrine to brackish and fresh-water lacustrine conditions in the Upper Berriasian (Lower Cretaceous). The predominantly fluvio-lacustrine to shallow lagoonal depositional environment causes an absence of marine macrofossils, especially ammonites, which is seen in the biostratigraphy of the area (Strauss et al. 1993, Elstner & Mutterlose 1996).

Palynological and micropalaeontological studies show several periods of short lived marine flooding during the German Wealden sea-level low stand (Strauss et al. 1993). According to Elstner & Mutterlose (1996), these short lived marine transgressions must have come from the west over the East Netherlands High since marine influence diminishes towards the center and eastern parts of the LSB. Also, geochemical investigations of Berner et al. (2010), Kahl (2010) and Berner (2011) support that marine ingressions have a significant influence on the preservation of the organic matter.

The Berriasian in NW Germany is subdivided into a lower Münder Formation and an up-

per Wealden Formation (cf. Fig. 2.4). As the Wealden that deposited in NW Germany is too different from the name-giving Wealden Formation in England the 'German Wealden' is more precisely called Bückeberg Formation and divided into six sub-units (Wealden I to VI according to the 'WOLBURG zonation', cf. Strauss et al. 1993). The Bückeberg Formation – or as it will be commonly referred to in this thesis: the German Wealden – is further subdivided into the Obernkirchen and Osterwald Members (Strauss et al. 1993).
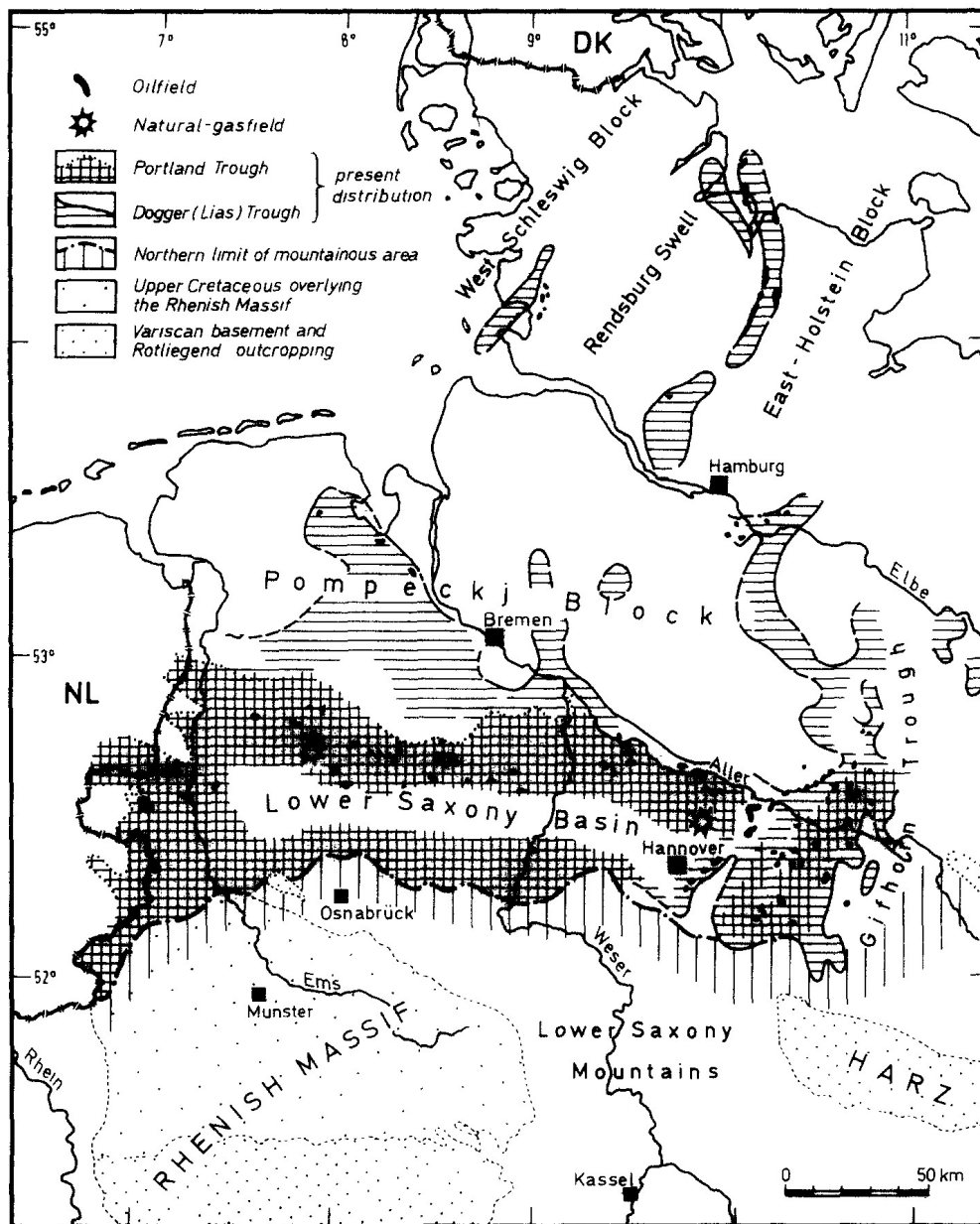
Figure 2.2: The Lower Saxony Basin and its bordering areas (Betz et al. 1987).
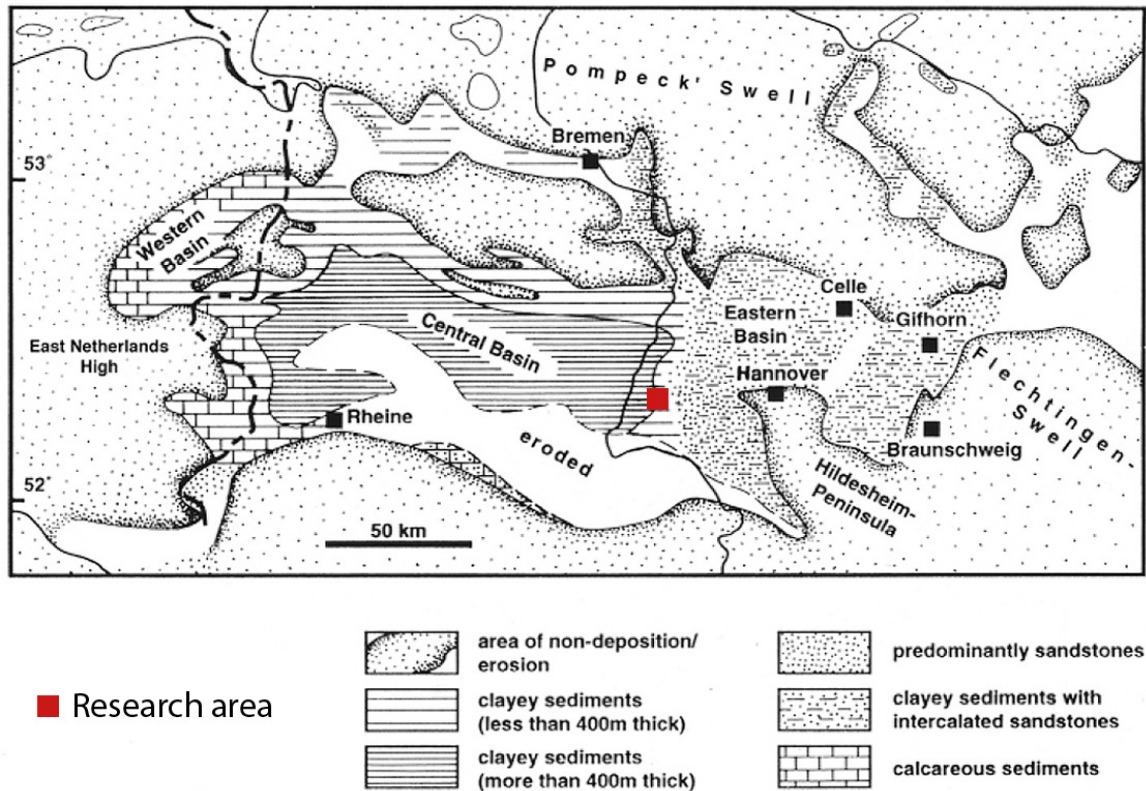
Figure 2.3: This figure displays the paleogeography of the German Wealden during the Berriasian, Lower Cretaceous (after Elstner & Mutterlose 1996, modified by Mutterlose & Bornemann 2000).

Figure 2.3 displays the paleogeography during the German Wealden. According to Strauss et al. (1993), the marine ingression came into the LSB via the channel that is seen SW of where the city of Rheine is located today (Fig. 2.3). In the same figure it is seen that the main basin displays sediment thicknesses of over 400 meters. Towards the margins the sediment thicknesses diminish and eventually become intercalated with sandstones.

The end of the Berriasian and hence the onset of the Valanginian (stratigraphic younger unit adjacent to the German Wealden) was marked by a regional marine transgression (Betz et al. 1987). The depositional area then returned to its full marine conditions that were paused during the Berriasian.

Later, at the transition from the Turonian to the Coniacian, basin inversion started, culminated in the Santonian and continued into Campanian times (Mutterlose & Bornemann 2000). Reactivation of fault systems controlling the subsidence occurred during Late Jurassic and Early

Cretaceous times (Betz et al. 1987). Petmecky et al. (1999) state that the LSB and Pompeckj Block were tilted northwards in Oligocene and Miocene times resulting in partial removal of Lower Tertiary clastics.

Distribution and facies patterns as well as sediment thicknesses and geometry in the LSB are influenced by differential subsidence, local tectonics and sea-level changes (cf. Doornenbal & Stevenson 2010). It is possible to distinguish between these factors in various parts of the basin. The sediment thicknesses arise from differential subsidence in Kimmeridgian to Aptian times. This subsidence is controlled by tectonic movements along NW-SE trending faults. Local tectonics are the result of salt diapirism mainly in the east but also at the western, eastern and southern margins of the basin. Sea-level change is reflected by different facies patterns and by fossils of different origins (Mutterlose & Bornemann 2000). The most important sea-level change is the Wealden regressive phase.

The LSB, on the verge of the most important hydrocarbon-bearing province of Europe (Permian Basin, cf. Doornenbal & Stevenson 2010), is the most important and most prolific hydrocarbon-bearing area in Germany. The organic rich shales that are found in the LSB have been investigated for over 50 years for their hydrocarbon potential (Betz et al. 1987, Elstner & Mutterlose 1996, Petmecky et al. 1999, Littke et al. 2008, Berner et al. 2010, Doornenbal & Stevenson 2010, Kahl 2010, Berner 2011).

2.1 The German Wealden Lithostratigraphy

The German Wealden is a period characterized by non-marine conditions. However, several short lived marine flooding phases occurred (Strauss et al. 1993). These changes in depositional environments are responsible for a strong variability of the vertical and horizontal facies. The change between the depositional environments causes the deposition of coals, carbonates, shales and sands depending on the state of regression and transgression. A regressive sequence shallows the water and increases the eroding surfaces of the surrounding areas, the water-covered
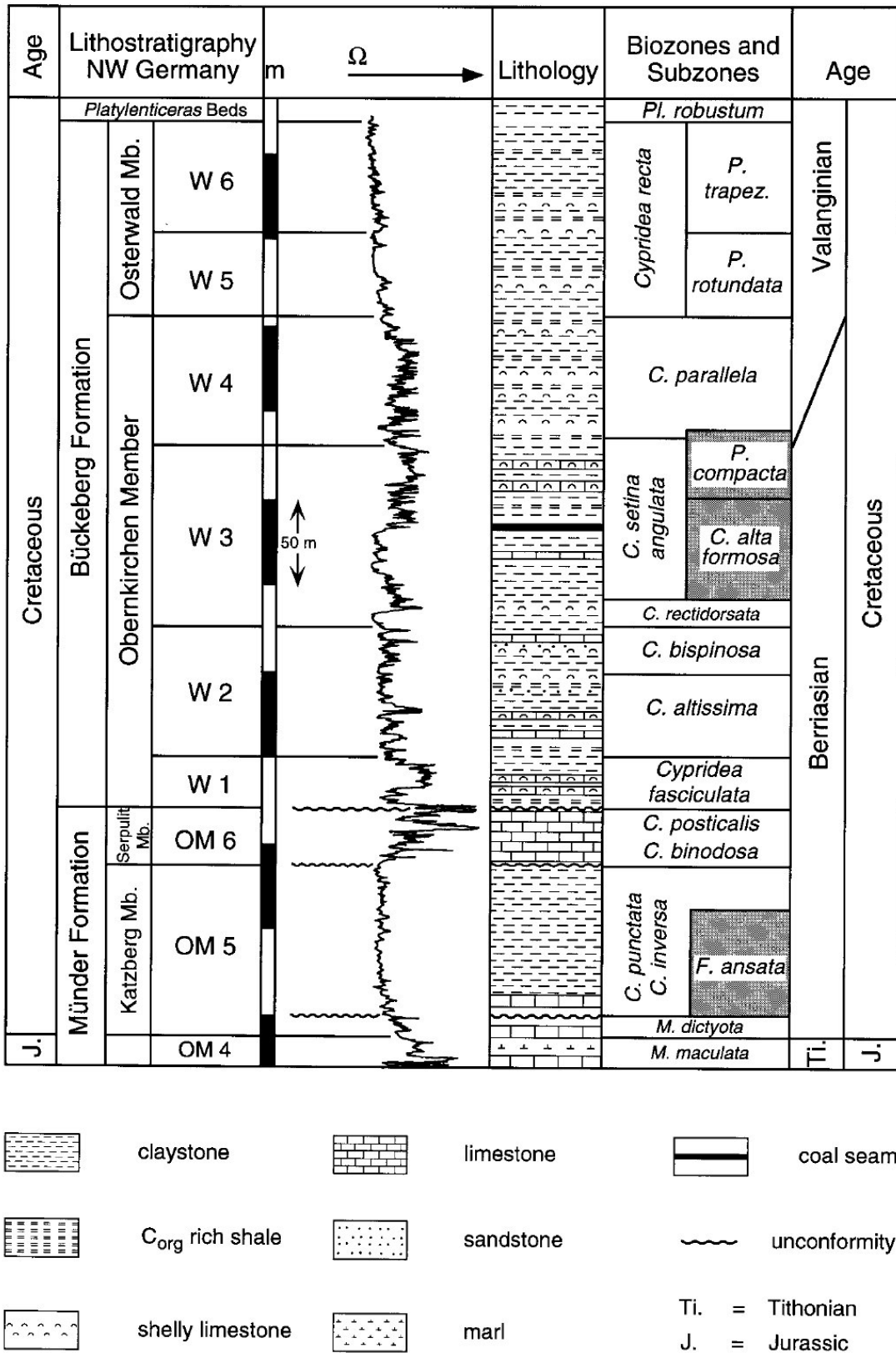
Figure 2.4: Chart of the bio- and lithostratigraphy in NW Germany for the Lower Cretaceous. Also included is a resistivity log of the oil well Rühlertwist 3 (Elstner & Mutterlose 1996).

area becomes smaller and sand is deposited. When the water is shallow evaporites may form. At times of lowest lake-level, swamps remained that facilitated the formation of peat and coals. When lake-level was higher and hence the lakes deeper, shales could deposit in quiet environments. Additionally, in the process of level rise and fall, lake sediments can be reworked and oxidized (Berner et al. 2010, Kahl 2010).

2.2 Geological Map & Cross-Section

The geological map (Fig. 2.5) has been obtained from the digital geological map of Lower Saxony (1:50000; NIBIS®Kartenserver 2011). Essentially, it shows the distribution of Jurassic, Cretaceous and Quaternary sediments in blue, green and pink colors, respectively. The red line marks the location of the cross-section of Figure 2.6. The localities of the samples that were collected for this study (cf. Chapter 3) are displayed in Fig. 2.5 with their according sample numbers.

The cross-section of Fig. 2.6 shows the subsurface geology and the orientations and thicknesses of the Wealden formations. It was constructed using information contained in the digital geological and topographical map of Lower Saxony (1:25000; NIBIS®Kartenserver 2011) combined with layer orientation measurements done at the outcrops.

In close proximity to the cross-section lies the Lüdersfeld mine shaft. An old vertical geological profile of the Lüdersfeld mine shaft (profile done by 'Bergamt Hannover', the former mining agency of Hanover, Krassmann 2010) allowed us to correlate the layer boundaries at the surface to fit the profile in the subsurface. However, the Lüdersfeld profile was not adopted entirely as published and was thus re-interpreted.

Leading to this re-interpretation are the annotations accompanying the Lüdersfeld mine shaft vertical cross-section. The annotations of the profile (Krassmann 2010) state that the upper layer – in this thesis interpreted as German Wealden instead of Valanginian – consists of hard, dark gray shale. Valanginian sediments usually are of lighter colors. It is plausible that these hard, dark gray shales belong to the German Wealden formation. The dark color may be

the result of the high contents of organic carbon in the Wealden sediments. The dipping angle of the sediment layers at the surface is small and the mine shaft showed that the German Wealden in the basin center is at least 550 meters deep (cf. Krassmann 2010).

The above observations give reason to re-interpret the Wealden vertical cross-section in the Stadthagen syncline. A Valanginian thickness of 300 meters (cf. Krassmann 2010) would imply that the Wealden shale units become thinner towards the basin center. The re-interpretation (i.e. Valanginian thickness of c. 70 meters) gives a more logical basin geometry (cf. Fig. 2.6).
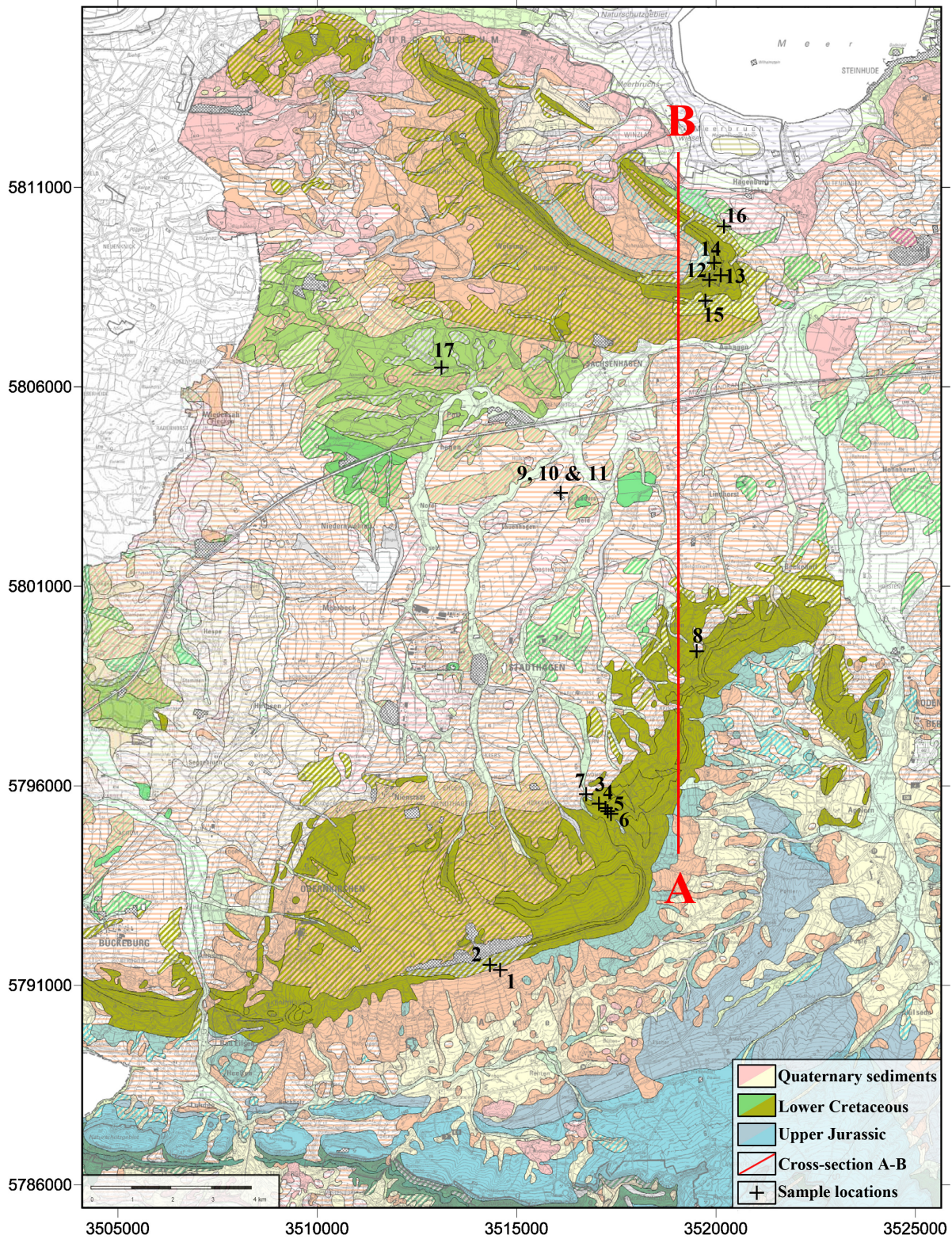
Figure 2.5: Map modified after the 1:50000 digital geological map of Lower Saxony (NIBIS®Kartenserver 2011). The red line marks the cross-section of Figure 2.6. Numbers indicate the samples described in Chapter 3.
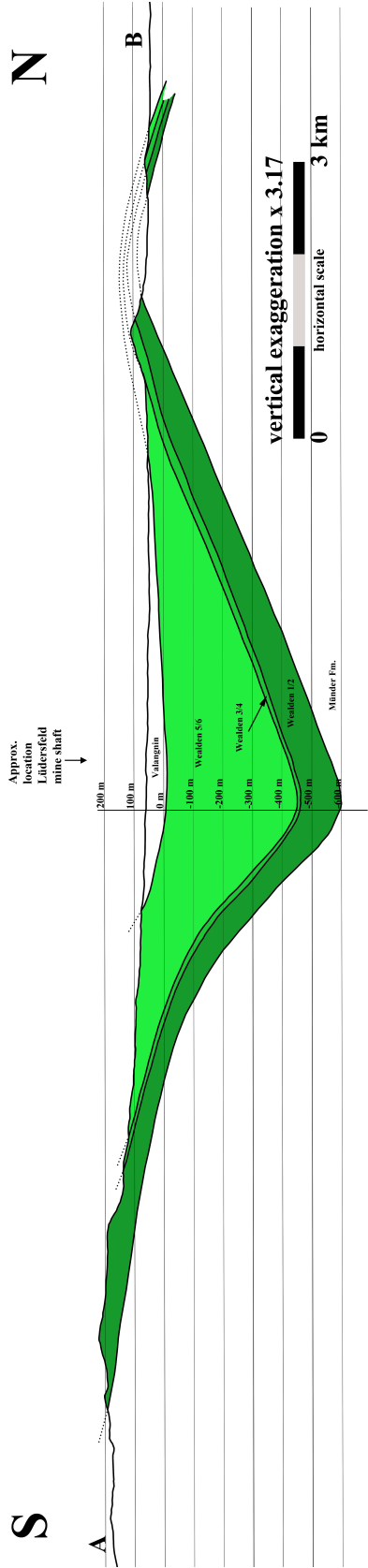
Figure 2.6: Cross-section of the Stadthagen syncline with the German Wealden geology in the subsurface between the Bückeberge Hills and the Rehburg anticline. The Lüdersfeld mine shaft profile (cf. Krassmann 2010) was used to correlate the surface observations in the central, deepest part of the syncline.

3 Sample Material

In August 2011, a number of 17 samples were collected from the area north, east and south of Stadthagen, Germany (c. 40 km W of Hanover). The map in Figure 2.5 shows the localities where a number of samples from the German Wealden were collected. Also, a sample from the stratigraphic younger Valanginian was obtained. Each sampled outcrop will be described on the following pages including a description of lithology, stratigraphy and state of the outcrops, if applicable. Exact localities (coordinates), stratigraphy and lithology of the samples are summarized in Table 3.1.

3.1 Sample Locations, Outcrops & Lithology

Suitable localities for recovering the samples from the stratigraphic units of interest were identified using the digital geological map of Lower Saxony (NIBIS®Kartenserver 2011). Information from the map and literature (e.g. Fig. 2.5; Krassmann 2010) concerning quarries, mud pits, mine shafts or river slopes were used. For example, river signatures with close contour lines that indicate steep morphology and potential outcrops (e.g. section of *samples 3 to 7*). The areas of interest were then inspected in the field and suitable outcrops were sampled. The outcrops comprised river slopes, newly dug trenches and abandoned quarries.

The different localities of the samples were chosen approximately in N-S direction in order to obtain a cross-section of the Stadthagen syncline that is indicated in Figures 2.5 and 2.6.

Nearly all of the described samples belong to the German Wealden (Lower Cretaceous), only *sample 17* belongs to the Valanginian (according to geological map in Fig. 2.5; cf. Table 3.1).

Table 3.1: The table displays from left to right the sample numbers, the internal lab numbers of BGR, a descriptive location name, X and Y coordinates according to Gauss Krüger system (prime meridian: 3. − 9°), the E and N UTM coordinates (zone 32U) calculated from the Gauss Krüger coordinates, the stratigraphy and the lithology. The stratigraphy is related to information from the geological map and also cross-referenced with the lithology to pinpoint Wealden units more precisely.

Sample Nr.	Sample Nr. (BGR)	Location	X coord.	Y coord.	UTM E	UTM N	Stratigraphy	Lithology
1	1103405	Eulenburg (rd trench)	3514580	5791390	514500	5789514	Wealden I	Shale
2	1103406	Eulenburg (rd trench)	3514320	5791508	514240	5789632	Wealden I	Shale
3	1103407	SE Obernwöhren	3517076	5795564	516995	5793686	Wealden III	Shale
4	1103408	SE Obernwöhren	3517234	5795431	517153	5793553	Wealden II	Sandstone
5	1103409	SE Obernwöhren	3517281	5795311	517200	5793434	Wealden I	Shale
6	1103410	SE Obernwöhren	3517281	5795311	517200	5793434	Wealden I	Carbonate
7	1103411	SE Obernwöhren	3516751	5795796	516670	5793918	upper Wealden	Sandstone
8	1103412	E Heuerßen	3519508	5799360	519426	5797481	upper Wealden	Shale
9	1103413	Mine shaft Lüdersfeld	3516098	5803345	516017	5801464	Wealden	Coal
10	1103414	Mine shaft Lüdersfeld	3516098	5803345	516017	5801464	Wealden	Bass
11	1103415	Mine shaft Lüdersfeld	3516098	5803345	516017	5801464	Wealden	Siltstone
12	1103416	Düdinghauser Mt.	3519829	5808684	519747	5806801	Wealden I/II	Shale
13	1103417	Düdinghauser Mt.	3520106	5808796	520023	5806913	Wealden III/IV	Shale-Sandstone
14	1103418	W Düdinghausen	3519944	5809124	519862	5807241	Wealden I/II	Shale
15	1103419	S Düdinghauser Mt.	3519724	5808159	519642	5806276	Wealden	Coal
16	1103420	Hagenburger Holz	3520214	5810026	520131	5808143	Wealden V/VI	Shale
17	1103421	Pollhagen	3513130	5806498	513050	5804616	Valanginian	Shale

Samples 1 & 2 are from a location c. 2.5 km NNW of the village of Rehren (Auetal). Here, a newly dug trench on the side of the forest road allowed retrieving fresh material.
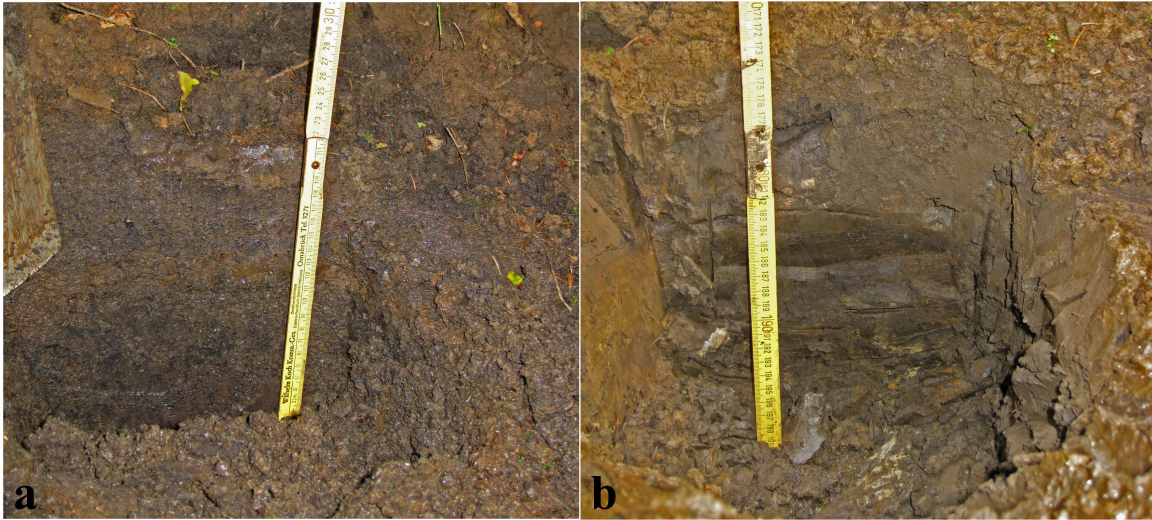
Figure 3.1: Photographs of the outcrops of sample 1 (a) and 2 (b). Please note that the yellow to light brown color on the margins of the photographs is due to correction of contrast and other values to make the scale better visible. The color of the horizon of interest, however, is not altered.

- **Sample 1** – According to the geological map, the Wealden sediments are overlain by Drenthe-stage (Saale-Glacial) sediments. The clayey material of the Wealden was recovered from a trench at the side of the road and comprises many up to 2 cm large dark brown to dark grey shale fragments. The matrix is fine-grained and of the same color as the fragments.

- **Sample 2** was recovered further uphill from where *sample 1* was taken. The geological map indicates Lower Wealden covered by quaternary sediments. On first sight, the outcrop appears fine-grained (muddy) and shows a dark brown color. When washed, the sample showed that many up to 2 cm large shale fragments were contained in the sample (similar to *sample 1*).

Samples 3 to 7 are from an area approx. 1 km SE Obernwöhren, just SE of Stadthagen. Good outcrops along a creek allowed us to recover five samples from the embankment (except for *sample 7*) ranging from Lower to Upper Wealden comprising carbonate, sandstone and shales.
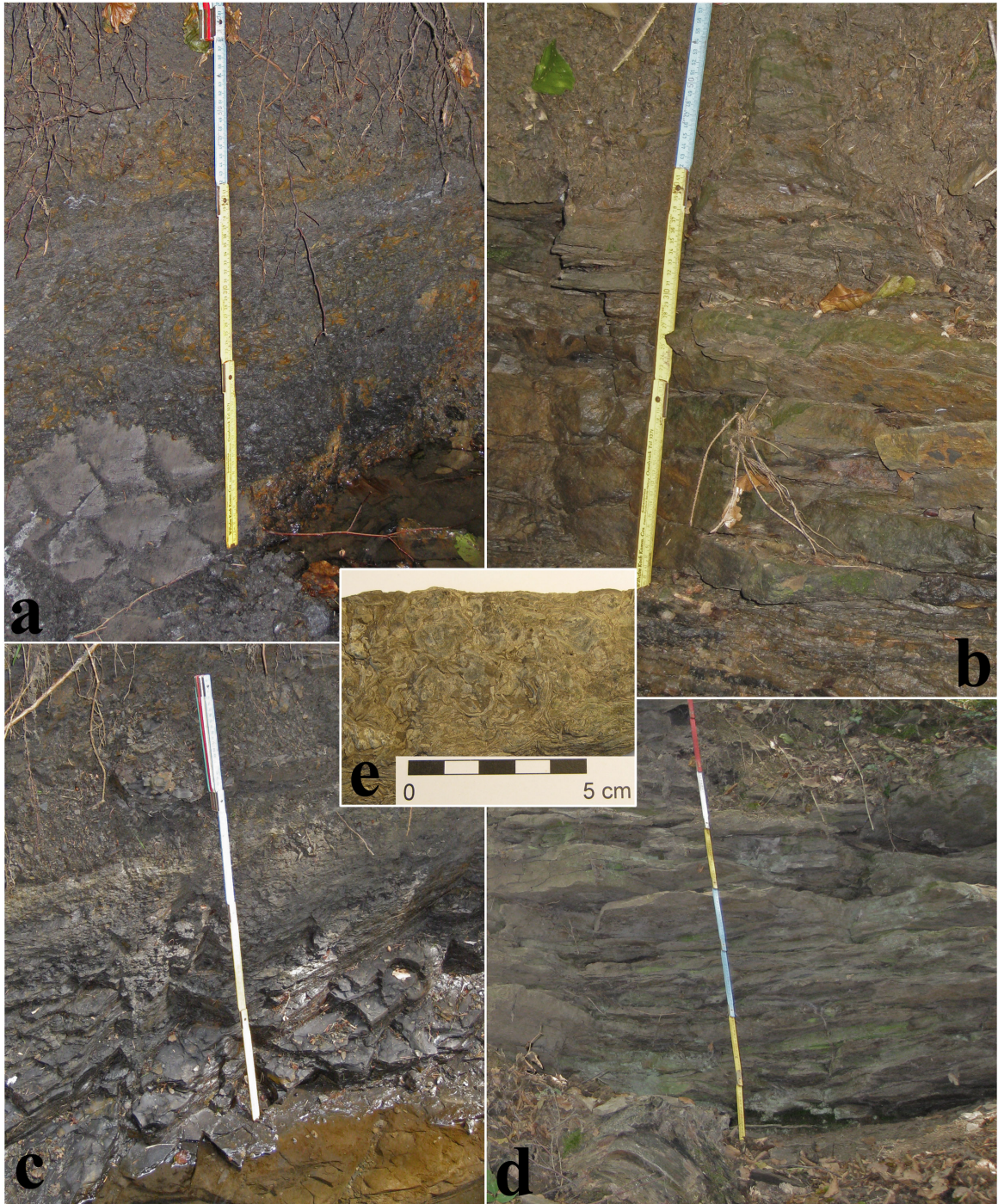
Figure 3.2: Photographs of the outcrops where samples 3 (a), 4 (b), 5 (c) and 7 (d) were taken. (e) is a fragment of sample 6 after washing.

- **Sample 3** – The picture in figure 3.2a shows the Wealden III sediment layers at the river bank. A fresher sample from a few centimeters inside the c. 2 m-high embankment was taken. Up to 2 cm large dark grey shale fragments were obtained.

- **Sample 4** – According to the geological map (Fig. 2.5), the stratigraphy changes from Wealden III to Wealden II. The sample recovered here is a light brown to yellowish ('rusty') sandstone. The outcrop consists of several 5 to 10 cm thick layers and is well maintained from weathering.

- **Sample 5** comprised dark shales. There are banks of several centimeters and finer, smaller scale layering of only a few millimeters. The outcrop and the shale appear to be a bit weathered; however, the material is very hard and resistant. In between the shale layers a carbonate bank was found (see *sample 6*).

- **Sample 6** was recovered from a carbonate layer in the hanging wall of the layer where *sample 5* was recovered. The rock contains many fossils (bivalves of up to 2 cm and gastropods of up to 1.5 cm) that will not be further characterized at this point. The photo of figure 3.2e shows the cleaned rock.

- **Sample 7** was recovered further downstream and not directly at the creek but upslope. Towards the village of Obernwöhren the valley of the creek becomes wider and deeper. At the NE slope of the valley a large outcrop of sandstone was discovered and a sample of the hard-wearing rock retained. The outcrop consisted of centimeter to decimeter thick beds of yellowish, fine-grained sandstones.

Sample 8 is from a small creek coming out of a forest just E of Heuerßen, a few kilometers E of Stadthagen. At this location the change from the Upper Wealden shale layer to the overlaying sandstone layer was obvious. Figure 3.3 shows the shale fragments of several centimeter that are incorporated in the muddy to silty and grey to purple matrix.

Samples 9, 10 & 11 The village of Lüdersfeld (c. 5 km NE of Stadthagen) is known for its coal mine that was finished building in 1952 up to a depth of over 500 m but whose operation stopped only 9 years later in 1961 due to economic reasons. *Samples 9, 10 & 11* were collected from
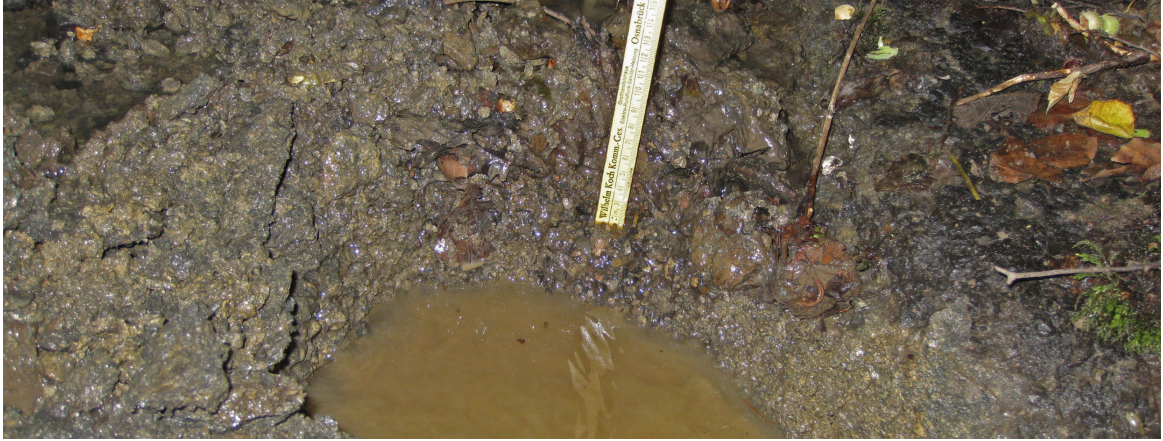
Figure 3.3: Sample 8

Figure 3.4: Samples (a) 9, (b) 10 & (c) 11 collected from the Lüdersfeld mine heap.

the Lüdersfeld mine heap that still exists today. Three samples of different appearances were recovered under the assumption that these were from different depths of the former mine shaft. *Samples 9, 10 and 11* consisted of a coal, a carbonaceous shale (bass; including a plant imprint) and a siltstone (with vein-like streaks), respectively (cf. Figure 3.4).

Samples 12 to 16   About 12 km NE of Stadthagen lies the village of Düdinghausen that is name-giving for the small Düdinghauser Hill – that is part of the hills of the Rehburger Anticline – where these samples were recovered. In this area the Wealden units reach the surface whilst creating an anticlinal structure. Some decades ago the outcropping coal seams that ran through these hilly areas were exploited. It was possible to obtain rock samples from the rims of abandoned pits where coal seams used to be mined. *Sample 15* is a coal from a mine heap near to the location of the other outcrops of this area.

- **Sample 12** was collected at the end of an elongated pit where there were slopes of shale. Apparently, the coal seam ended here or became too deep to mine so that the mining activity stopped and the pit was abandoned. The shale recovered here is dark grey to black and consists of mm-thick plates. The sediments of the outcrop are strongly weathered. However, digging into the walls allowed retrieval of fresher samples from the slope.

- **Sample 13** was taken from an outcrop that was a few hundred meters away from the outcrop of *sample 12*. It consists of silty sandstone and shows less vulnerability to weathering. The outcrop is made up of massive c. 5 cm thick beds of rock that show a light brown to yellowish color.

- **Sample 14** comes from an outcrop a few hundred meters further away from *sample 13* and was dug out of a creek bed. Many up to 5 cm large but only a few millimeters thick shale chips were retrieved. The shales were black, soft and could be easily broken. On the photo of Figure 3.5d it is seen how the water of the river filled the newly dug hole and, faintly, the harder material under a soft, muddy cover is visible.

- **Sample 15** was taken from a mine heap. The shiny black coal is well preserved and massive (see Figure 3.5c).

- **Sample 16** was collected from the outskirts of a flooded pit that according to the geological map is an 'island' of Wealden V/VI surrounded by a cover of quaternary sediment.
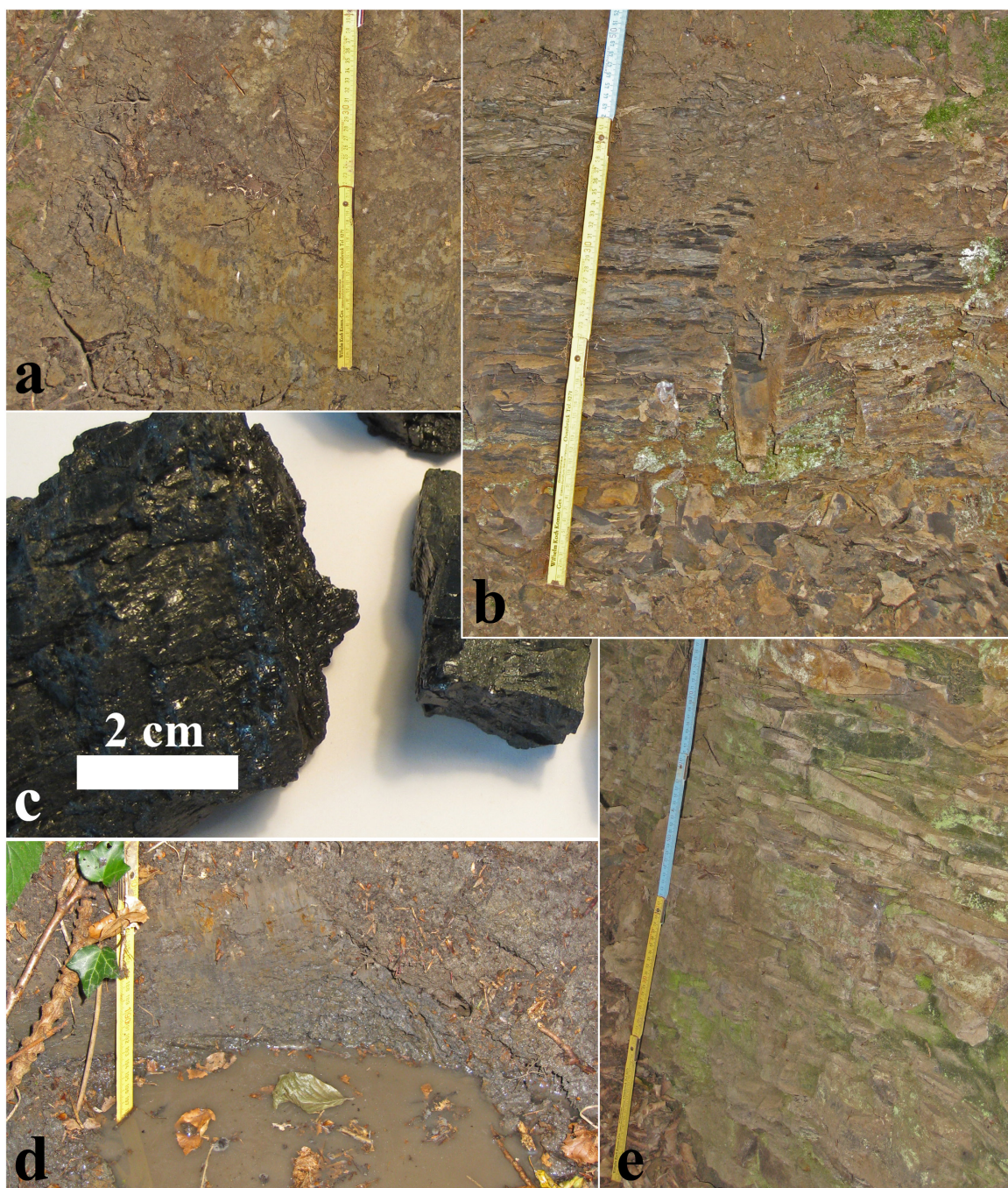
Figure 3.5: Outcrop photographs of samples (a) 16, (b) 12, (d) 14 and (e) 13. Photo (c) is the coal (*sample 15*) after washing.

Sample 17   was taken from a small dried out creek bed in a forest N of Pollhagen (c. 7 km N of Stadthagen). According to the geological map this area is characterized as Valanginian (Lower Cretaceous). The sediment recovered (see Figure 3.6a) had a very fine-grained clayey matrix and showed a light brown to light grey color. However, after washing the sample only crystals (probably calcite or gipsum) and a few rock fragments remained (cf. Fig. 3.6b).
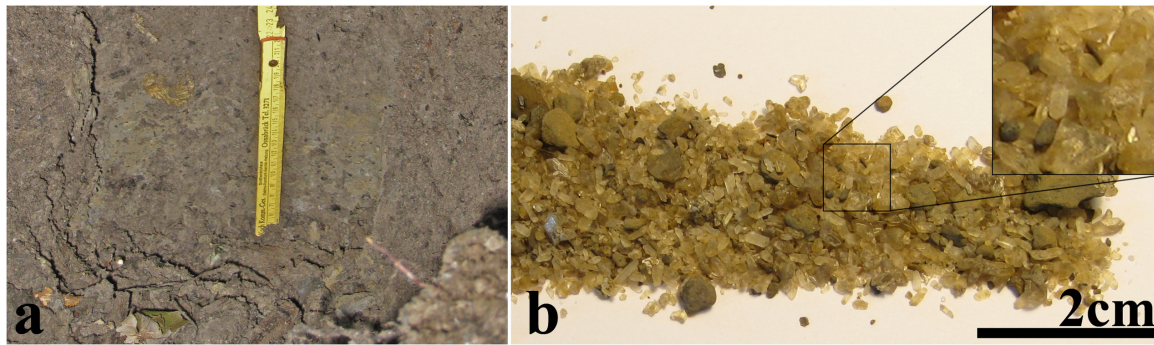
Figure 3.6: Photographs of outcrop & sample 17. (a) is the sample location and (b) is the sediment in the washed state

In summary, the samples comprised mainly shales (1, 2, 3, 5, 8, 12, 14, 16 and 17) but also sandstones (4, 7 and 13), a carbonate (6) and two carbon-rich coals, a siltstones and a bass (9, 15, 11 and 10, respectively) each of them characteristic for one of the six different Wealden units.

As seen on the geological map (Figure 2.5), the sample locations were positioned to approximate a N-S profile and to facilitate the construction of the cross-section of Figure 2.6.

4 Methods

The collected samples were prepared for analytical purposes in the labs of the BGR, Hanover. At first, the samples were washed thoroughly and portions were split for the different analytical methods. The marked samples were documented with photographs.

Besides geochemical analyses, basic physical properties have been determined. An aliquot of each sample was subjected to standard density and porosity measurements using Micrcometrics AccurPyc 1330 and GeoPyc 1360 pycnometers (cf. appendix, Table A.11).

The material used for geochemical analyses was broken up into grains of mere 1 mm in diameter with a jaw crusher before the grain sizes were further decreased to about 100 µm with a disc mill.

4.1 X-Ray Fluorescence

The x-ray fluorescence (XRF) analysis is assigned to the sub-department of *Inorganic Geochemistry* at the BGR. The analysis provides the major and minor elemental composition of given samples.

For this method 1 g of the sample material is annealed at 1030 °C in a muffle furnace for 10 minutes. The weight difference before and after the annealing stands for volatile and instable compounds such as water or carbonates that were liberated from the sample during heating. The samples with a weight difference smaller 25 % are supplied with 5 g of $LiBO_2$ and 25 g of $LiBr$; samples with losses greater 25 % are supplied with 2.5 g of $LiBO_2$, 2.415 of $Li_2B_4O_7$ and 25 g of $LiBr$. The mixtures are homogenized (i.e. melted in $PtAu$-crucibles at 1200 °C for 20 minutes) into pellets.

The XRF analysis is carried out by two wavelength dispersive x-ray spectrometers with an applied output power of 2.7 kW for the rhodium x-ray anode (type PANalytical AXIOS) and the chrome x-ray anode (type PW2400). Different reference materials and standards are used to ensure quality control. The results are evaluated and corrected using *SuperQ 4* software.

According to Rousseau (2006), the concentration of each analyte (element measured) can be expressed as a product of the calibration constant, the measured net intensity of the analyte and a factor that corrects for the effects of the matrix composition of the analyte, which can be calculated from

$$\|C_i = K_i I_i M_{is}\|$$

where C_i is the concentration of the analyte i, K_i the calibration constant of i, I_i the measured net intensity of i and M_{is} is the correction factor for matrix effects of specimen s on i. Matrix effects comprise mainly adsorption and enhancement.

4.2 Carbon and Sulfur Elemental Analysis

The carbon and sulfur elemental analyses are performed on a LECO CS-200 apparatus. Total carbon (TC) and total sulfur (TS) contents are measured separately from the total organic carbon (TOC; C_{org}) content in the samples. For every measuring campaign several carbon and sulfur standards are analyzed beforehand for purposes of calibration of both the software and apparatus. Every 12th measurement is reserved for a standardized sample in order to allow better reproducibility. Peters et al. (2005a) describe the LECO method and display information on source rock and organic matter quality (cf. Table 5.1).

From each ground sample material, c. 180 mg are weighed and filled into a crucible where it is covered by the melting agents (accelerants) tungsten and iron. The sample amount can go as low as 25 mg if the color is dark and a higher content of organic carbon assumed.

The sediments in the crucibles are burned in a high frequency induction furnace at 1800 °C under oxygen supply. Sulfur is oxidized to SO_2 and carbon is oxidized to CO and CO_2. Gases are flushed with oxygen as a carrier gas first through a water trap to remove water vapor and then through a SO_2-specific infrared cell where the total sulfur content of the sediment is measured by infrared absorption. In a catalysis furnace the gases are heated to 350 °C in order to further oxidize CO to CO_2 and SO_2 to SO_3. Latter compound will react with the cellulose filter in the

sulfur trap to form H_2SO_4 in order to be removed from the system before the total carbon in the system is measured in a CO_2-specific infrared cell.

Total organic carbon is measured in a similar way. However, inorganic carbon is first removed off line using 10 %-hydrochloric acid (HCl) in a decarbonatization step. The samples are then dried in a drying oven for several hours. The same filters described above are used with these analyses, however, only the carbon is measured. In order to remove leftover chlorides from the decarbonatization process the gases are flushed through a chloride trap removing all hydrogen chloride gas. The measured carbon concentration represents the total organic carbon expressed as weight percent (wt.-%).

The carbonate measurements are the result of the difference between the two carbon content measurements (C_{org} and TC).

4.3 Rock-Eval Pyrolysis

RockEval-pyrolysis is one of the most important tools in the oil and gas industry because it is a simple method that can be performed quickly on a rock sample to estimate the hydrocarbon potential. The Rock-Eval method quickly determines type of organic matter, thermal maturity and hydrocarbon potential of a given sample. Essentially, it is a simplified simulation of the thermal formation of natural hydrocarbons in a rock sample.

The analyses are performed on a Rock-Eval-6-Analyzer type Classic S3 produced by Vinci-Technologies. A short summary of the Rock-Eval method is also found in Killops & Killops (2005) whereas Behar et al. (2001) give extensive information on different Rock-Eval 6 versions as well as insights into additional measurements possible with these methods (e.g. oxidation process).

After obtaining the C_{org} results from the LECO analyses (see above), 20 to 200 mg of the powdered sample material – depending on C_{org} content – is weighed into small crucibles. The crucibles are placed on an auto sampler and subsequently analyzed by the machine. The Rock-Eval pyrolysis (see Figure 4.1 for a schematic overview of the method) is an automated analysis
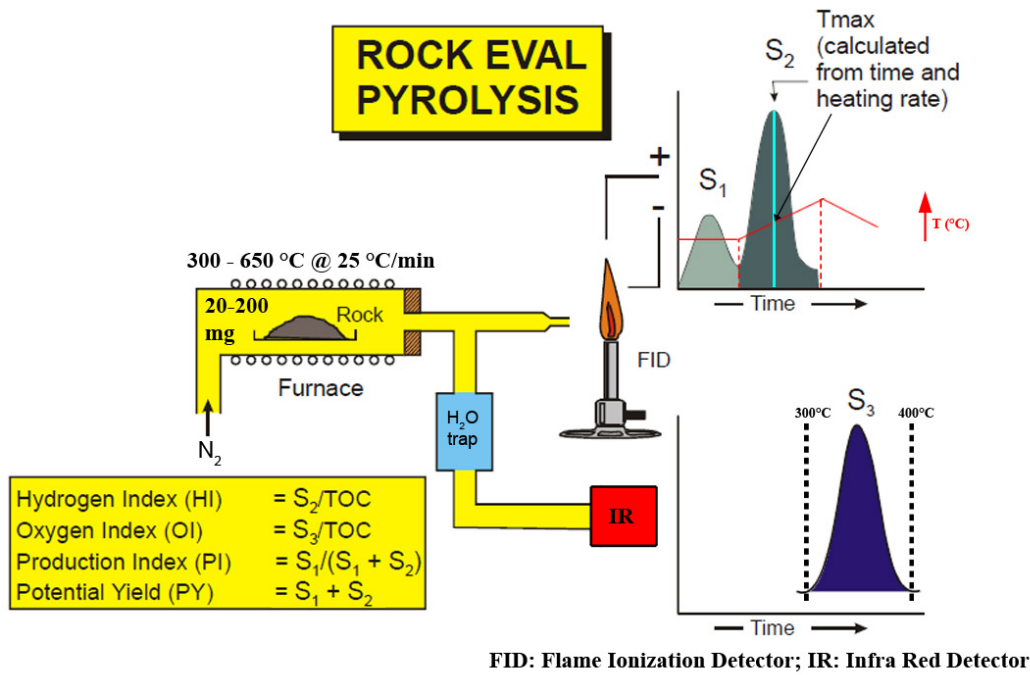
Figure 4.1: Figure shows the essential setup of the Rock-Eval method with its classical output diagrams. The figure was modified after IGI Ltd (2004) to fit the Rock-Eval 6 Classic Plus S3 apparatus that was used for the Rock-Eval pyrolysis in this thesis.

process where the sample is introduced into the pre-heated pyrolysis oven that has a temperature of 300 °C. Using nitrogen (N_2) as a carrier gas the volatile hydrocarbons are thermally desorbed for three minutes. At this temperature the kerogen is not affected whereas the so called free hydrocarbons that are liberated from the sediments are measured by a flame ionization detector (FID) and later referred to as S_1 peak (mg HC per gram of rock). During an experiment the temperature of the oven rises constantly at 25 °C/min up to 650 °C while the thermal decomposition of the kerogen takes place and releases newly generated hydrocarbons that are detected by the FID and referred to as S_2 peak (mg HC/g rock). An infrared (IR) cell measures the amount of CO_2 that is released from the kerogen during the heating phase of 300 to 400 °C. The recorded amount of CO_2 serves as a measure for the amount of oxygen in the kerogen and is referred to as S_3 peak (mg CO_2/g rock). The temperature at which a maximum of hydrocarbons are produced (T_{max}) can be a measure of the thermal maturity that a sample has experienced under natural conditions. This figure increases with increasing maturity of the sample and is therefore also referred to as a measure of thermal maturity. Figure 4.1 shows the

previously described curves as well as the T_{max}-temperature and how it is obtained.

Using the S_1, S_2, S_3 peaks and the C_{org} content it is possible to calculate fundamental parameters for the assessment of the hydrocarbon potential of rocks (productivity index PI, hydrogen index HI, oxygen index OI, compare Fig. 4.1).

4.4 Hydrocarbon Extraction and Fractionation

In a series of steps the hydrocarbons of the samples are extracted, fractionated and analyzed for the hydrocarbon they contain. Aliphatic, aromatic and hetero compounds (molecules containing N, S, & O) as well as asphaltenes are the fractions that are obtained. The methods are described in the following chapters.

4.4.1 Solvent Extraction

The so called accelerated solvent extraction (ASE) of hydrocarbons is carried out with the ASE 350 device of Dionex Corporation (cf. Richter et al. 1996). The cells that hold the sediment are made of stainless steel and have sizes of 11, 34 and 100 ml (which to use depends on the amount of C_{org} in the samples). Figure 4.2 shows the configuration of the components that comprise a cell of the type that is described below. The steel cylinders have steel caps on each side. The caps are protected from the contents of the cylinder by inserting cellulose filters at the contact of the sample material with the caps and by a layer of inert sea sand between the filter and the sample material itself. Depending on the C_{org} content of the sediments, 5 to 20 grams are weighed and mixed with sea

Figure 4.2: Configuration of the ASE cells used for the solvent extraction in this thesis.

sand to decrease clumping and increase permeability inside the steel cell. Before closing the cells, 25, 50 or 100 µl (more solvent if C_{org} is lower) of a standardized control solution (mixture of deuterized hydrocarbons: hexadecane-d34 (18,14 mg), icosane-d42 (13,40 mg), hexatriacontane-d74 (14,52 mg) and perylene-d12 (14,80 mg) in toluene) are added on the upper cellulose filter for controlling purposes. For each analytical sequence with the ASE 350 a cell with standardized material as well as a blank cell with sea sand is prepared and supplied with the right amount of control solution (i.e. 25 µl for the standardized material and 100 µl for the blank value). The ASE 350 analyzer uses dichloromethane (DCM, CH_2Cl_2) as a solvent that is vaporized after the extraction is completed. The vaporization is done with either a TurboVap®LV of Zymark or a TurboVap®II of Caliper Life Sciences for about 30 minutes until only an approx. 1 cm column of liquid remains in the glass.

4.4.2 De-sulfurization of Extracts

Elemental sulfur has to be removed to prevent analytical problems with the gas chromatography and mass spectrometric investigations. Therefore, granulated copper is activated in 10 % hydrochloric acid (HCl) at 60 °C for one hour. The copper is subsequently rinsed with distilled water and then cleaned with acetone and DCM. In the next step the copper is added to the extracts to react with the elemental sulfur (black oxide coating on the copper granular will form if S is present). If new copper grains do not coat with black oxide all free sulfur has been removed. The degree of oxidation is documented. The de-sulfurized solution is filtered into pre-weighed glasses, dried and weighed to determine the amount of extracts.

4.4.3 Clean-up of Extracts

The extracts obtained after the de-sulfurization were weighed and at this point the extraction/fractionation process separates into two branches. The samples that account for 15 mg of extract or more will be fractionated (see following chapters) and the samples with less than

15 mg undergo a so called clean-up. This procedure creates a cleansed aliphatic fraction removing other compounds like asphaltenes, NSO- and aromatic compounds. The separation is carried out on a column filled with silica. Iso-hexane is used as a solvent to remove aromatic and hetero-compounds. The eluate is collected in GC-vials and dried before being handed over to the GC analysis (Chapter 4.5).

4.4.4 De-asphalting of Extracts

The de-asphalting that the samples with extract amounts of more than 15 mg undergo prevent precipitation of the asphaltenes in the silica gel traps during subsequent liquid chromatography. The samples are dissolved in a mixture of 2 ml of DCM and 60 ml of petroleum benzene (mixture 1:30) and stored in the dark for 12 hours to prevent photo oxidization of the polar resins and to precipitate the asphaltenes. Afterwards, centrifugation for 15 minutes at 3000 rpm enforces settling of the asphaltenes at the bottom of the glass. The solution (mixture of aliphatic, aromatic and hetero-compounds) is separated from the precipitated asphaltenes and both fractions are each dried and weighed.

4.4.5 Liquid Chromatography

The liquid chromatography simply separates the residual solution into aliphatic, aromatic and hetero-compounds using the medium pressure liquid chromatography method (MPLC; cf. Radke et al. 1980).

MPLC uses different solvents to separate the aliphatic, aromatic and hetero-compounds. The stationary phase of the chromatographic process is a column of silica gel which is activated at 240 °C for 12 hours. At first, the mixture that is to be fractionated is dripped on the silica gel that is retained in a 3 ml glass cartridge, the pre-column, by a teflon frit on the bottom and top end. The pre-column is dried over night at 40 °C and the leftover DCM is removed with N_2 gas. The main column, a 17 ml glass cartridge, is also filled with silica gel retained by teflon frits.

The two columns are mounted in the apparatus.

The main column that is pre-rinsed with iso-hexane and the pre-column are both connected to the iso-hexane source. Iso-hexane is the first eluent and as a mobile phase it will adsorb the analyte (aliphatic fraction) and transport it into the sample glass. Due to covalent bonding forces the other fractions remain in the silica column until the mobile phase is changed. Subsequently, a solvent consisting of a mixture of DCM and iso-hexane (1:2) is used to elute the aromatic fraction and a solvent consisting of DCM and methanol (2:1) is used to elute the third fraction, the hetero-compounds. The speed at which the solvents flow through the system is 2.5 ml/min. Each analyte is rinsed with c. 30 ml of solvent filling a 30 ml glass for each fraction that will contain the solvent and corresponding eluent. At the end each eluate is vaporized and the remaining, dried fractions in the glasses are weighed and transferred into small vials for later GC analysis (see below).

4.5 Gas chromatography

The aliphatic fractions obtained from MPLC are analyzed with gas chromatography using an Agilent HP 6890 gas chromatographer (GC). The GC separates the analyte and provides retention times resulting in quantitative and qualitative values for the n-alkanes and the isoprenoids pristane and phytane in the samples.

The samples are placed on an auto sampler and after configuration of the software the GC operates fully automatically. In the GC the sample materials (i.e. aliphatic fractions) are separated into components by taking advantage of their chemical and physical properties. The sample material is vaporized and sent through a column of different stationary phases. After

Table 4.1: Temperature program of the Agilent HP 6890 GC

time (min)	heating rate ($°C$/min)	temperature ($°C$)
2.5	isotherm	70
4	20	150
42.5	4	320

vaporization the analyte is carried by Helium (mobile phase; flow of $29\ cm/s$) through a non-polar Agilent *HP Ultra 1* column of 50 m length, 0.2 mm inner diameter and 0.11 µm thick inner non-volatile liquid film (stationary phase). Latter film retains and releases the analyte into the mobile phase depending on the analyte's volatility and affinity for each phase across the column (Peters et al. 2005a). With increasing temperature the analytes move through the column at higher speeds. If the temperature program is the same for each run (see Table 4.1), it will take the same components always the same time to pass the column and reach the analyzer resulting in comparable chromatograms for each sample in terms of the component's position on the x-axis on the chromatograms. The gradually-heating temperature program (cf. Table 4.1) is chosen to allow the analytes eluting early in the analysis (lower retention) to separate correctly at lower temperatures while speeding up the analysis by allowing analytes with higher retention times to pass the column quicker by applying higher temperatures.

4.6 Carbon isotope analysis of organic matter and hydrocarbon fractions

Carbon isotopic analysis is performed on the samples to obtain carbon isotope ratios of bulk organic carbon and the fractions (aliphatics, aromatics and hetero-compounds).

The analysis is done with an isotope-ratio mass spectrometer Delta^{Plus}® of Finnigan MAT Corp. coupled to a Carlo Erba elemental analyzer NC 2500 and hence the name of the method, EA-IRMS (cf. Muccio & Jackson 2009 and see Fig. 4.3).

In dependence of the amount of organic carbon in the sediment samples up to 20 mg of each sample are placed in Ag-melting pots and decarbonatized using hydrochloric acid (HCl). After having dried over night at 70 °C the melting pots are placed on an auto sampler and subsequently introduced into an oxidizing furnace where the organic contents burn at 1020 °C to form CO_2, NO_x, SO_2 and H_2O. Helium as a carrier gas delivers the burned gases into the adjacent reducing furnace to convert NO_x to NO_2 and to remove excess oxygen. A magnesium perchlorate trap extracts water as well as HF- and HCl-compounds from the analyte mixture

(cf. Figure 4.3a). In the last step a chromatograph separates CO_2, NO_x and SO_2 from each other.

The CO_2 is analyzed in the mass spectrometer (Fig. 4.3b) in order to obtain the ratios between the molecular masses of 44 to 45 and 44 to 46 of the carbon dioxide. The molecular masses (amu=atomic mass units) come to be as follows: $44 = {}^{12}C^{16}O^{16}O$, $45 = {}^{13}C^{16}O^{16}O$, ${}^{12}C^{17}O^{16}O$ or ${}^{12}C^{16}O^{17}O$ and $46 = {}^{12}C^{17}O^{17}O$ (Werner & Brand 2001). The carbon isotope ratios are given as $\delta^{13}C$ values in per mill. The calculation is done using the following equation after Muccio & Jackson (2009)

$$\delta^{13}C = \left(\frac{\left(\frac{{}^{13}C}{{}^{12}C}\right)_{sample} - \left(\frac{{}^{13}C}{{}^{12}C}\right)_{standard}}{\left(\frac{{}^{13}C}{{}^{12}C}\right)_{standard}} \right) * 1000 \qquad [\permil]$$

The automated regulation and computation of the isotope ratios is done by the ISODAT software from Finnigan MAT Corp. The measurements are reported as carbon isotope ratios relative to the VPDB (Vienna Pee Dee Belemnite) standard (Ghosh & Brand 2003).

For ensuring the quality of the analyses, each sample is measured twice and the difference between both must not exceed ± 0.2 ‰. If the difference is in fact larger, the measurements are repeated. The reproducibility of the results is therefore ± 0.1 ‰ and a measuring accuracy of this instrument (± 0.01 ‰) is proven by the usage of calibrated internal standards.
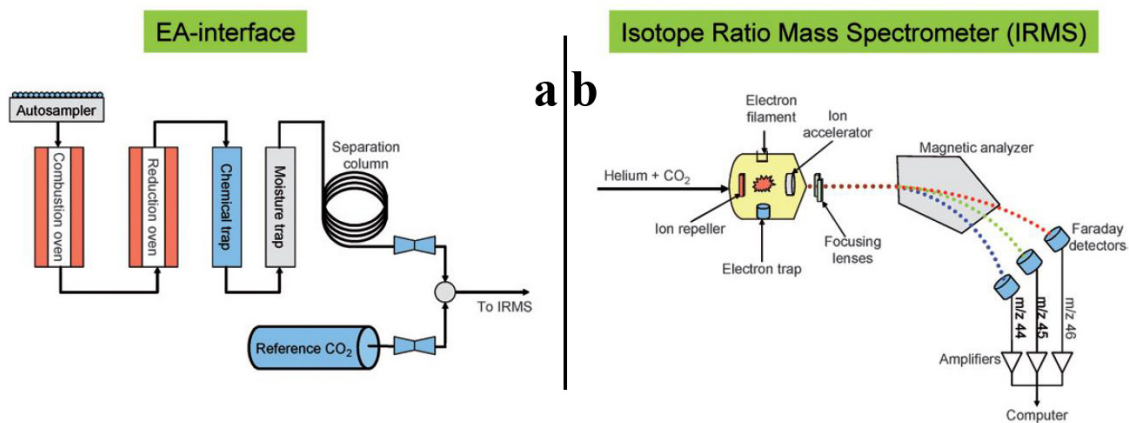
Figure 4.3: Schematics of the basic EA-IRMS method similar to the apparatus used in for the carbon isotope analysis in this thesis. (a) EA. (b) IRMS (from Muccio & Jackson 2009).

4.7 Gas Geochemistry

Gas geochemical methods of Faber & Stahl (1983) allow the desorption of hydrocarbon gases from sediments.

The desorption of gases is a complex process involving a vacuumed glass tube system (cf. Fig. 4.4), heated phosphoric acid (H_3PO_4) to separate the hydrocarbons from the sediment, concentrated caustic potash (KOH) to bind the carbon dioxide (CO_2) and a drying line to remove the vapor out of the gas mixture. Moreover, the apparatus is subdivided into three main parts as seen from Figure 4.4: the sediment flask (A), the caustic potash flask (B) and the section with the drying line (E) and sample vial (D).

At first, c. 100 g of sediment are weighed and placed in the sediment flask (A) of the apparatus and water is added before the system is evacuated to remove the extrinsic air. Next, 50 ml of concentrated (85%) ortho-phosphoric acid is dripped from a burette (C) slowly onto the sediment and the pressure, temperature and time are monitored and noted. Further monitoring takes place after half of the acid has entered the system and once all the phosphoric acid is filled into the sediment holder. The gas freed from the sediment passes through the caustic potash, which removes the carbon dioxide. The pressure is constantly monitored and should not exceed c. 1000 mbar (i.e. atmospheric pressure). Once the phosphoric acid has mixed with the sediment-water mixture and the reactions have ceased, the sediment flask containing the sediment, acid and water is carefully heated. After the boiling point is reached (approx. 60 to 70 $°C$ since the pressure in the system is typically low) the mixture is kept boiling for 10 minutes. The gas has now entirely escaped the sediment and water is carefully inserted into the sediment flask (A) for cooling reasons but also to push the gas that has accumulated in the tubing system of the apparatus towards the drying line (E) and into into the vial (D). Water is added until c. 1000 mbar of pressure in the system are reached.

The vial (D, 20 ml), the drying line (E) and the part of the tubing until the point where the water has been filled up to comprise a known volume because the water is only filled up
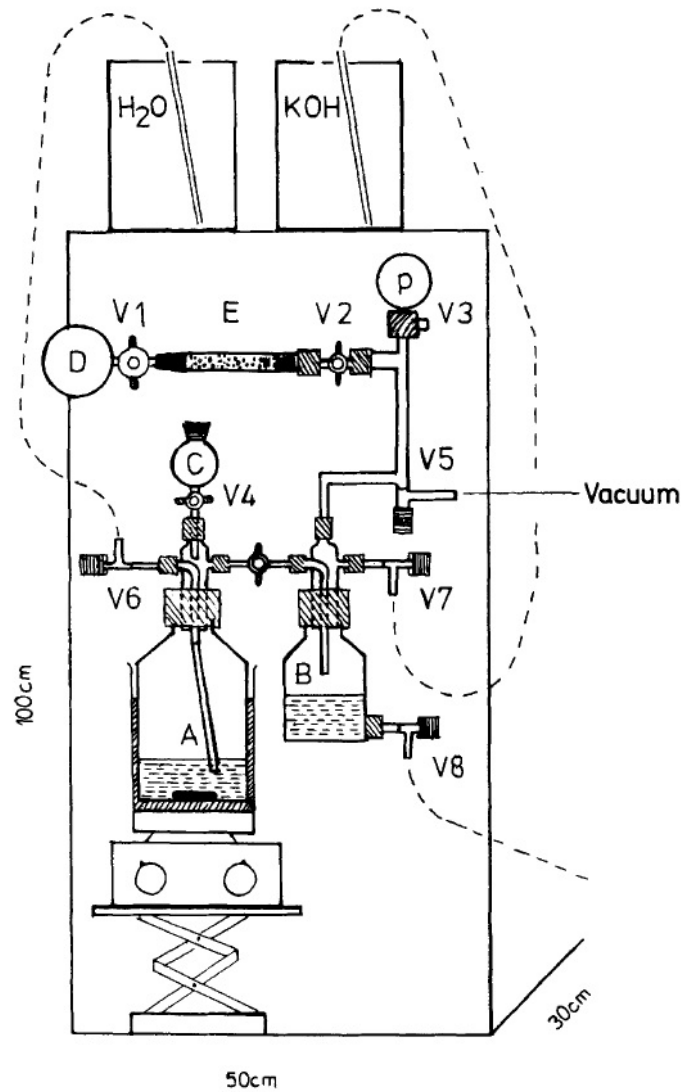
Figure 4.4: Sediment degassing apparatus. A is the sediment flask, B is the CO_2 extracter (caustic potash flask), C is the phosphoric acid (H_3PO_4), D is the vial to hold the gas for analysis, E is the drying line and V1 to V8 are different valves to control the gas, air and liquid flow (from Faber & Stahl 1983).

to predefined points between valves V5 and V3 of the apparatus (cf. Fig. 4.4). Which of the predefined points between V5 and V3 is reached with the water level depends on the amount of gas and hence the pressure in the system. Finally, the measured volume and pressure are used to calculate the amount of gas released from the sediment.

The recovered gas sample is analyzed in a GC (set-up is given in Faber & Stahl 1983) to obtain concentrations of the gases methane to pentane and isotopic analysis is performed on samples with sufficient gas concentrations using the method given in Faber & Stahl (1983).

5 Results & Discussion

Results obtained from analytical methods (see Chapter 4) are compiled and discussed in this chapter taking advantage of interpretative diagrams from the literature. Generally, the depositional environment may be evaluated through geochemical methods as shown in Chapter 5.1.

Also, the oil and gas potential as well as the maturity of the organic matter can be investigated through organic geochemistry. Organic matter is altered by a series of processes after deposition. Through a series of consecutive and random re-polymerization and polycondensation reactions during diagenesis, parts of the extant biomass in the sediments are converted into geopolymers which, together with selectively preserved biopolymers, undergo further chemical transformations into increasingly condensed and insoluble kerogens. At greater depths and higher temperatures catagenesis and subsequently metagenesis takes place converting kerogen into hydrocarbons that form oil and gas (Kahl 2010, Killops & Killops 2005, Tegelaar et al. 1989, Tissot & Welte 1984). Although geochemical parameters commonly measured in hydrocarbon research will undergo changes related to the above described alteration of the organic matter, it is still possible to use geochemical tools for a comprehensive hydrocarbon assessment. Chapters 5.1 to 5.3 will give examples on basic methodologies for the assessment of the depositional environment and hydrocarbon potential.

According to macroscopical field observations, the samples are derived from different sediment types and comprise shales, a carbonate, sandstones and coals. This classification will be kept consistently throughout the following chapters. All analytical data are documented in the Tables A.1 to A.11 of the appendix.

5.1 Environment

Elemental analyses provide data on the concentration of elements (major and minor elements and additionally carbon and sulfur) of the samples and help to classify and geochemically characterize sediments using published interpretative diagrams (Herron 1988, Brumsack 1989, Dean
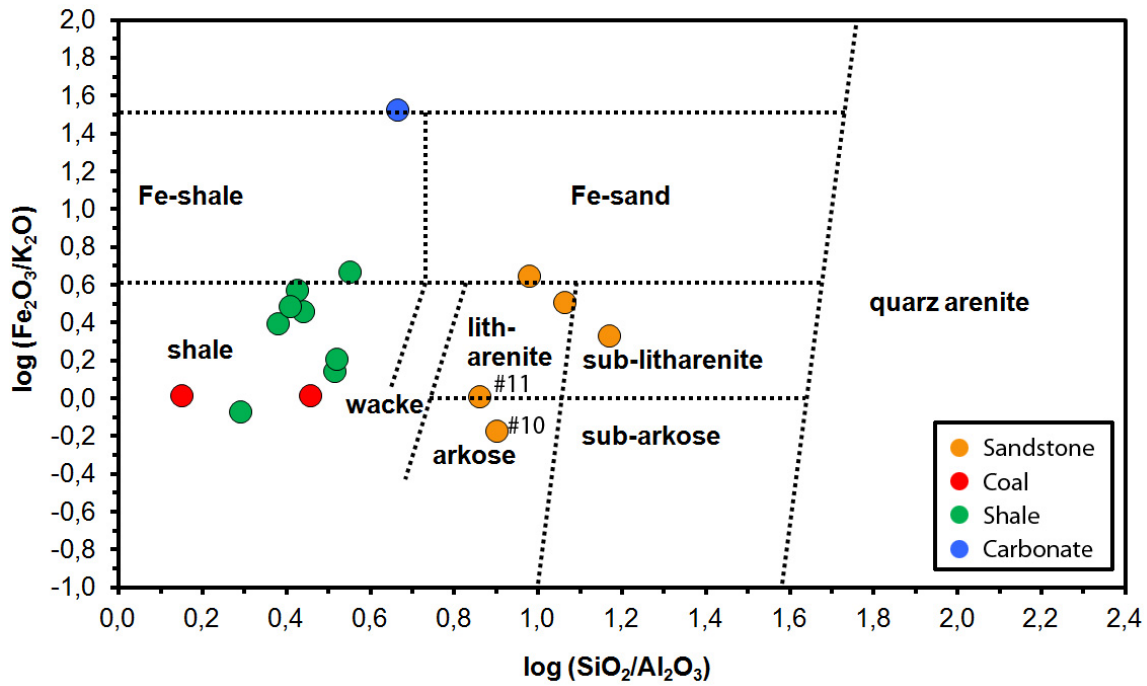
Figure 5.1: Common sandstone classification applicable for terrigenous sands and shales (modified after Herron 1988).
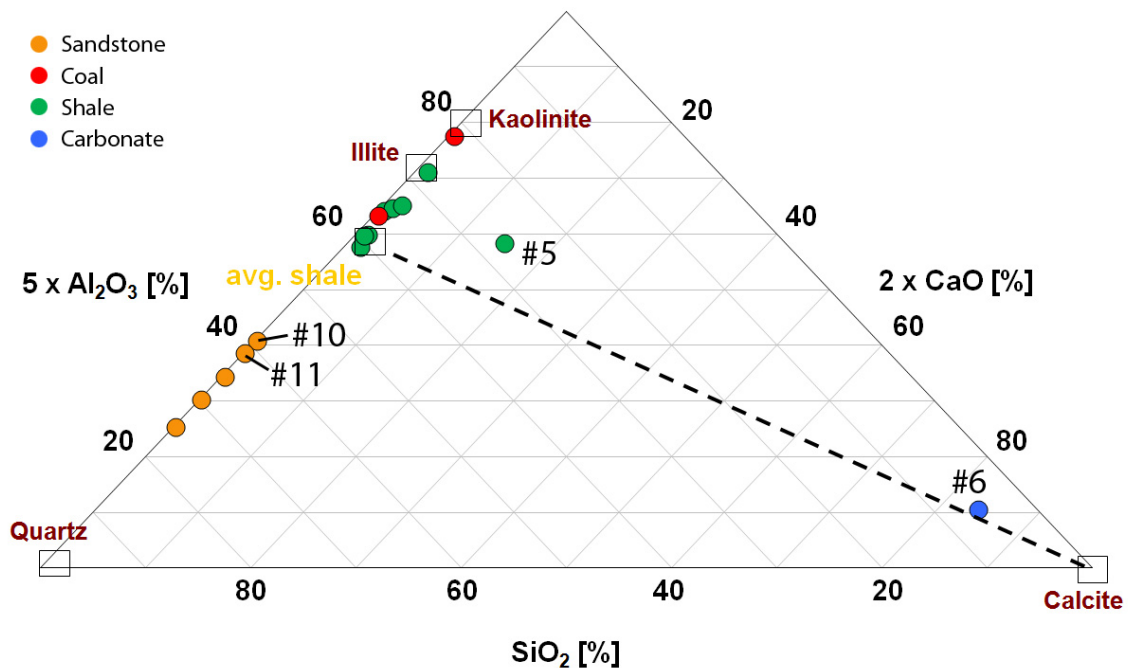
Figure 5.2: Major element components obtained from XRF analysis of the sediments (*Sample 1 to 16*) of the Stadthagen syncline. Classification diagram modified after Brumsack (1989).

& Arthur 1989, Hiete 2004).

X-ray fluorescence (cf. Chapter 4.1) provided data on major and minor elements in the samples. The analytical results are found in Tables A.1 and A.2 of the appendix. The following ranges of some key values were recorded: Fe_2O_3 varies from 0.6 to 10.6 wt.-% and K_2O from 0.1 to 3.4 wt.-% resulting in a $\log(Fe_2O_3/K_2O)$-ratio of -0.2 to 1.5. In the same way SiO_2 and Al_2O_3 vary from 6.6 to 87.9 wt.-% and 1.4 to 26.3 wt.-%, respectively, resulting in a $\log(SiO_2/Al_2O_3)$-ratio of 0.2 to 1.2. Furhter XRF data we use are the CaO (ranging from 0.0 to 47.2 wt.-%), the Na_2O (ranging from 0.0 to 0.5 wt.-%) and the Fe content (ranging from 0.2 to 3.7 wt.-%). The analytical results are compiled in several interpretative diagrams (cf. Figures 5.1, 5.2, 5.3, 5.4 and 5.5).

Herron (1988) suggested a classification for terrigenous sands and shales according to their geochemical $\log(Fe_2O_3/K_2O)$ and $\log(SiO_2/Al_2O_3)$-ratios. In general, the $\log(Fe_2O_3/K_2O)$-ratio is thought to be a measure for mineralogical stability. Samples comprising feldspars, mica and quartz contain low amounts of iron and high amounts of potassium, hence a low ratio. Higher ratios point to more unstable mineral assemblages and thus a proximal sediment source with more lithic fragments.

Figure 5.1 compiles the results of some XRF data (cf. appendix, Tables A.1 and A.2) indicating that the field observations (see Table 3.1) support the geochemical classification. The carbonate sample has a high $\log(Fe_2O_3/K_2O)$-ratio due to its lack in K-bearing rock-forming minerals such as mica or feldspar (mean wt.-% of K_2O in (a) the shales: 2.73 wt.-%; and (b) in the carbonate: 0.095 wt.-%). The Fe_2O_3 value, on the other hand, is comparable to that of the other shale samples.

When displayed in the ternary diagram of Figure 5.2 (major elements, Al_2O_3, SiO_2 and CaO) the shales plot on the aluminum-enriched side of the diagram whereas the sandstones plot nearer to the Si side of the diagram. The carbonate (*sample 6*) and the shale enriched in carbonate (*sample 5*) plot apart from the group of the other sediments and towards the Ca corner

of the diagram. The two coals seem to have similar mineralogy as most of the shales. Figure 5.2 further suggests that the shales likely comprise a mixture of common shale minerals (e.g. illite and kaolinite) as they plot near the 'average shale' composition. The five samples classified macroscopically as sandstones show a significantly higher proportion of SiO_2 than the shales.

In Figures 5.1 and 5.2 two sandstones (*samples 10 and 11*) stick out from the other sandstones. In the former figure the two samples plot in the arkose range of the diagram whereas on the latter figure they appear to be more enriched in aluminum compared to the rest of the sands. It could mean that *samples 10 and 11* contain feldspars since arkoses usually contain high amounts of feldspars and feldspars are also generally enriched in aluminum.

A more detailed mineralogical view of the samples is shown in Figure 5.3. The diagram plots some important aluminium phyllosilicates (e.g. mica or clay minerals) and tectosilicates (e.g. feldspars) in comparison to our samples. The figure helps to identify the general sediment composition. Our samples in Figure 5.3 differ from each other in the relative amount (the three oxides in the plot are normalized to 100 %) of K_2O that they contain. Except for *samples 4 and 7* the sediments lie on a mixing line between illite and muscovite on the K_2O-rich end and kaolinite, smectite, chlorite and anorthite on the K_2O-poor end. The samples may be composed of these minerals. It is further seen that each lithology group has a similar composition in terms of the relative amounts of Al_2O_3, Na_2O and K_2O. One exception is *sample 8* which plots on the K_2O-poor end of the mixing line together with the two coals (cf. Figure 5.3).

One further method for elemental analysis is the LECO method (cf. Chapter 4.2), that provided data on the amount of total carbon (TC), total organic carbon (TOC; C_{org}) and total sulfur (TS) in the samples. The data is compiled in Table A.3 of the appendix. With these values the amount of carbonate, organic matter and clastic sediment can be calculated as well.

$$Clastic = 100 - (\%\ Organic\ Matter + \%\ Carbonate + \%\ Sulfur) \qquad [\%]$$

with

$$Organic\ Matter = \frac{C_{org}}{0.85} \qquad [\%]$$
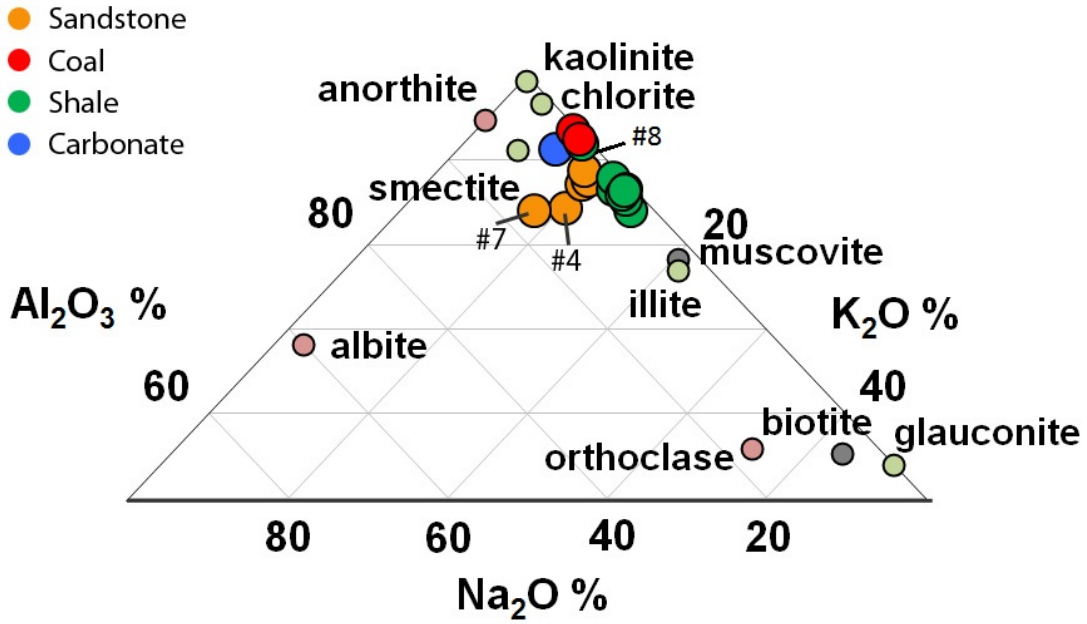
Figure 5.3: Samples of the Stadthagen syncline in comparison to aluminium phyllosilicate and tectosilicate minerals as they may be found in sediments. Only the upper, relevant half of the diagram is shown. Al_2O_3, SiO_2 and CaO are normalized to 100 %. Mineral data from Herron & Matteson (1993), cited after Hiete (2004).
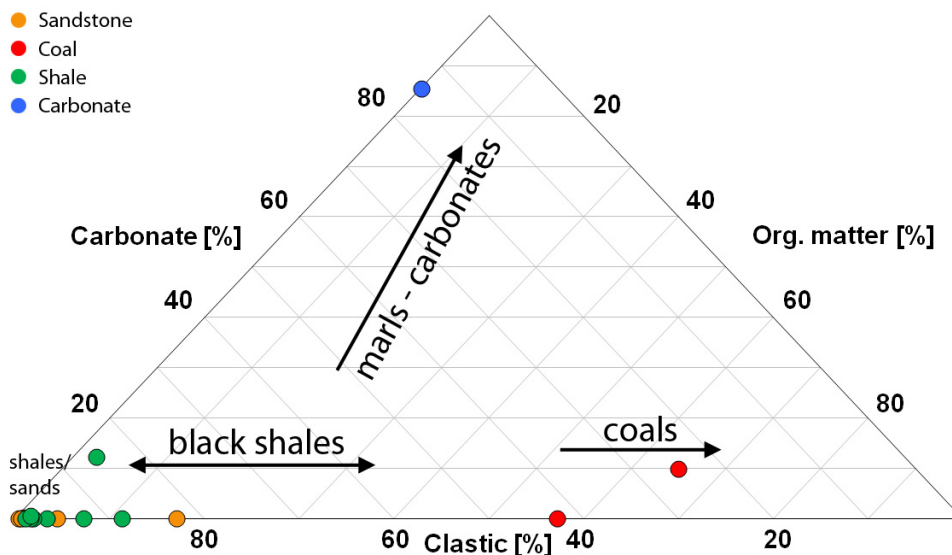
Figure 5.4: Simple discrimination between clastic, organic matter and carbonate relative portions in sediments according to data obtained from LECO analysis.
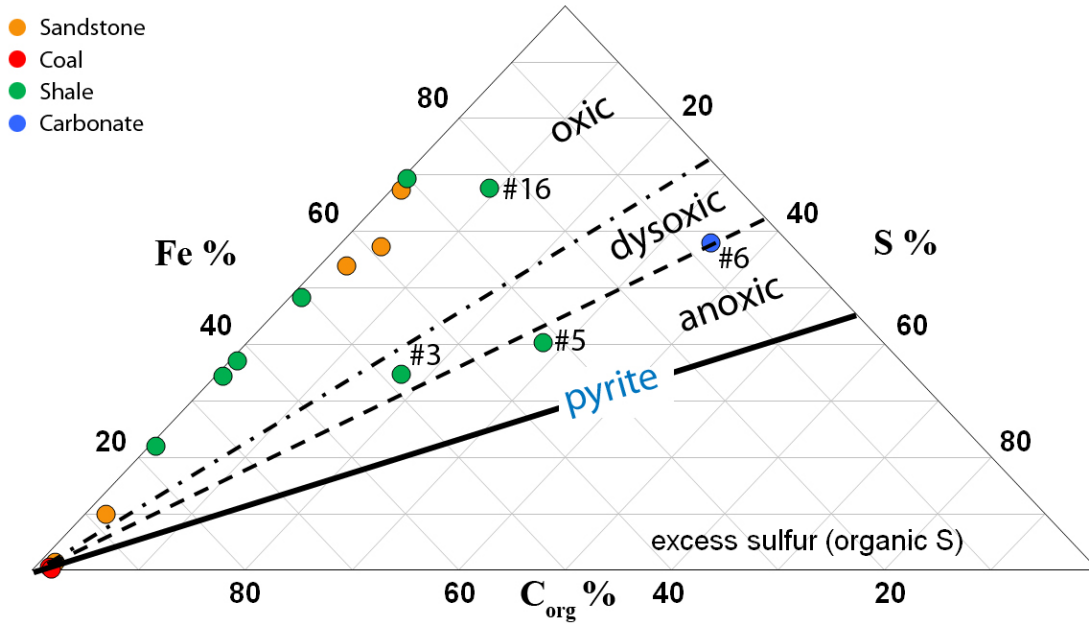
Figure 5.5: Classification of the depositional environment according to carbon, iron and sulfur relative contents (after Dean & Arthur 1989).

where the constant 0.85 denotes the conversion factor of C_{org} into organic matter since it is assumed that 85 % of organic matter is C_{org} (cf. Dahl et al. 2004 and Peters et al. 2005a).

The relative amount of carbonate is calculated with

$$Carbonate = C_{carb} * 8.33 \hspace{4cm} [\%]$$

where the factor 8.33 results from the conversion of C_{carb} to $CaCO_3$ (Correns 1949).

The data shows ranges for C_{org} of 0.15 to 55 wt.-% resulting in calculated amounts of organic matter (OM) of 0.17 to 65 wt.-%. The amount of total sulfur in the samples is low. Apart from *sample 5* (TS 1.77 wt.-%) the TS values range from 0.02 to 0.87 wt.-%. From the difference of TOC to TC the carbonate was calculated to ranges of 0 to 85.47 wt.-%. Relative amounts of clastics in the sediment is between 13.6 and 99.6 wt.-%.

The C_{org} values can be looked at with respect to the lithology. The C_{org} values in the shales range from 0.93 to 9.57 wt.-%. The two coals show values of 48.4 and 55 wt.-%. The data of the carbon and sulfur elemental analysis is displayed using interpretative diagrams in Figures 5.4, 5.5, 5.7, 5.10 and 5.13.

Figure 5.4 discriminates between the clastic fraction, the organic matter and carbonate in

the sediments, and indicates that the clastic fraction dominates the sediment samples.

One of the coals is shown to contain 10 % of carbonate. This, however, results from a statistical error in the carbonate calculation from LECO measurements (see Section 4.2) that is only possible due to the extremely high amount of organic carbon in a sample. In comparison, XRF data shows that the Ca, Mg and Fe content (main elements to form carbonates) is of similar magnitude in the coals as it is in the sandstones. The sandstones contain no significant amount of carbonate. The samples plot on the bottom axis that connects *organic matter %* and *clastic %* and are separated only by their content of organic matter (Fig. 5.4).

The geochemical investigations help to identify the depositional environment, as seen from sulfur and organic carbon contents. The depositional environment can be classified according to the availability of oxygen. Using the relative amounts of sulfur, iron and organic carbon the redox environment can be classified into oxic, dysoxic and anoxic environments. In Fig. 5.5 these areas are separated by lines of constant ratio between Fe and S. The solid line describes the S to Fe ratio of pyrite (pyrite: FeS, ratio of 1.15:1). Pyrite can form in oxygen-depleted environments as the result of reducing reactions of sulfur and iron (Dean & Arthur 1989, Killops & Killops 2005). The samples plot in the area of the diagram that indicates an oxic environment during deposition (except for *samples 3, 5 and 6* that plot in the field defined as dysoxic to anoxic). The lack of pyritization is caused by a lack of sulfur in the sediments because the content of iron outweighs the sulfur content by far (cf. app. Tables A.1 and A.2). The coals, however, have a larger S:Fe ratio than the rest of the samples (1.68 and 4.15 for *samples 9 and 15*, respectively) but due to the high amount of C_{org} they plot in the corner of C_{org}. The high pyrite ratio in the case of the coals is the result of an extremely low iron content rather than a high amount of sulfur in the sample. The lack of pyrite in the other samples may be caused by a lack in reactivity of the organic matter similar to the organic matter in the Albian sediments of Rachold & Brumsack (2001).

The overall depositional environment in the marginal eastern part of the Lower Saxony

Basin was oxic (see Fig. 5.5). An oxic environment is plausible because the samples come from near the shorelines of the lake at the time of deposition. Rivers and deltas transporting sediments into the area of deposition were probably able to rework the sediments during transport and prior to deposition.

5.2 Organic Facies

Sediment transport and deposition often coincides with the type of organic matter and organic facies. Geochemical data is therefore utilized to evaluate the organo-facies of the sediments which may also be described in terms of kerogen types. Kerogen is the sedimentary organic matter insoluble in organic solvent and is considered to be the most essential ingredient to hydrocarbon formation.

There are three different types of kerogen: types I, II and III. Although the borders are fluent, each type is characteristic in terms of origin. Type I kerogen comprises mainly lipid material (especially long-chain aliphatics) derived from alginites but also bacterial matter that is generally deposited in lacustrine environments. Type III kerogen is characterized by low H/C and high O/C ratios. It originates from higher land plants and is prone to generate gas at higher maturities. Type II kerogen may be a mixture between the other two types. However, Tissot & Welte (1984) state that Type II kerogen is usually related to autochtonous organic matter (mixture of phytoplankton, zooplankton and microorganisms) that deposits with marine sediments under reducing conditions. Type I and II kerogens are prone to produce oil (Tissot & Welte 1984 and Killops & Killops 2005).

The more specific methods applied to obtain the data used in the further assessment of the depositional environment comprise Rock-Eval pyrolysis, hydrocarbon extraction from sediments, fractionation of extracts and GC analysis of aliphatics as well as stable carbon isotope analysis of the sediments and extracts.

Rock-Eval pyrolysis (cf. Chapter 4.3) measured S_1, S_2 and S_3 values for each sample (see
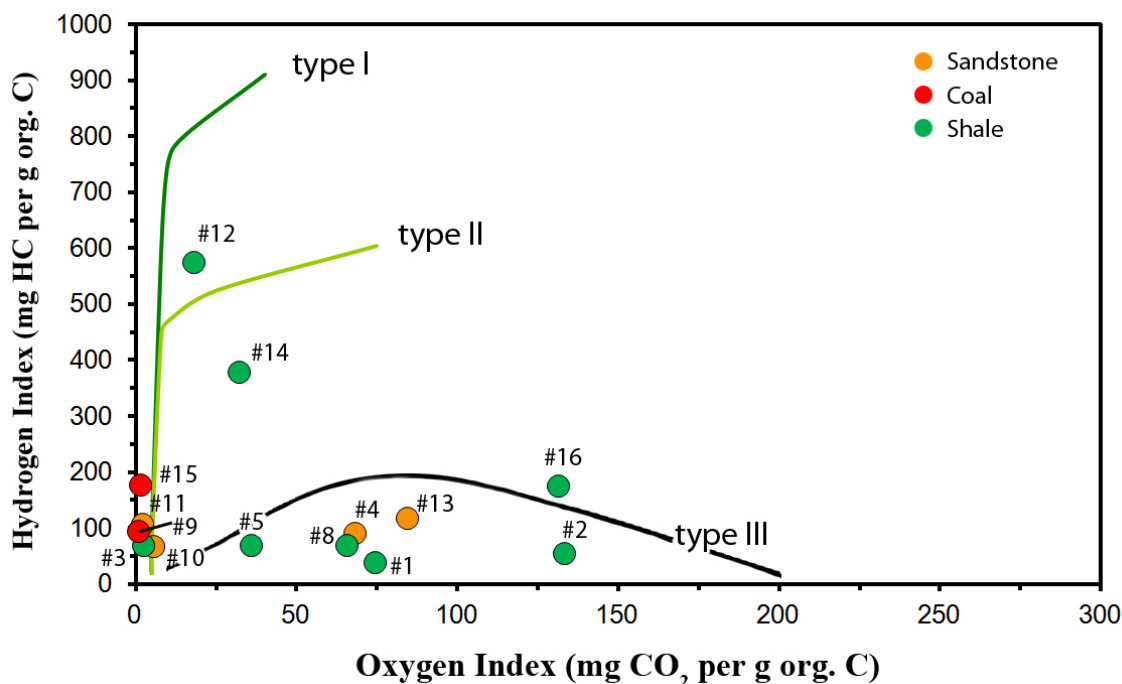
Figure 5.6: Modified van Krevelen diagram plotting the hydrogen index against the oxygen index obtained from Rock-Eval pyrolysis of whole rock samples (after Tissot & Welte 1984).

appendix Table A.4 for analytical results). S_1 values in the samples range from 0.01 to 2.76 mg HC/g $rock$, S_2 values from 0.65 to 98.04 mg HC/g $rock$ and S_3 values range from 0.2 to 2.14 mg CO_2/g $rock$.

Together with the C_{org} values (cf. app. Table A.3) the S_2 and S_3 values can be normalized according to the C_{org} content in the samples to obtain the hydrogen (HI) and oxygen (OI) indices, respectively. HI values range from 40 to 576 mg HC/g $Corg$ and indicate a wide variety of organic matter (type I to III) which is also shown by the large range of the OI values (1 to 133 mg CO_2/g $Corg$). The widespread ranges of the Rock-Eval pyrolysis values indicate different types of organic matter and the higher values show that some samples exhibit good source rock potential (cf. Table 5.1 and Peters et al. 2005a).

Rock-Eval data is compiled in several interpretative diagrams (see Figures 5.6, 5.10, 5.11, 5.12 and 5.13).

Analogously to a so called van Krevelen-diagram (Tissot & Welte 1984) the HI and OI values can be plotted against each other to discriminate and characterize types of organic matter (cf.
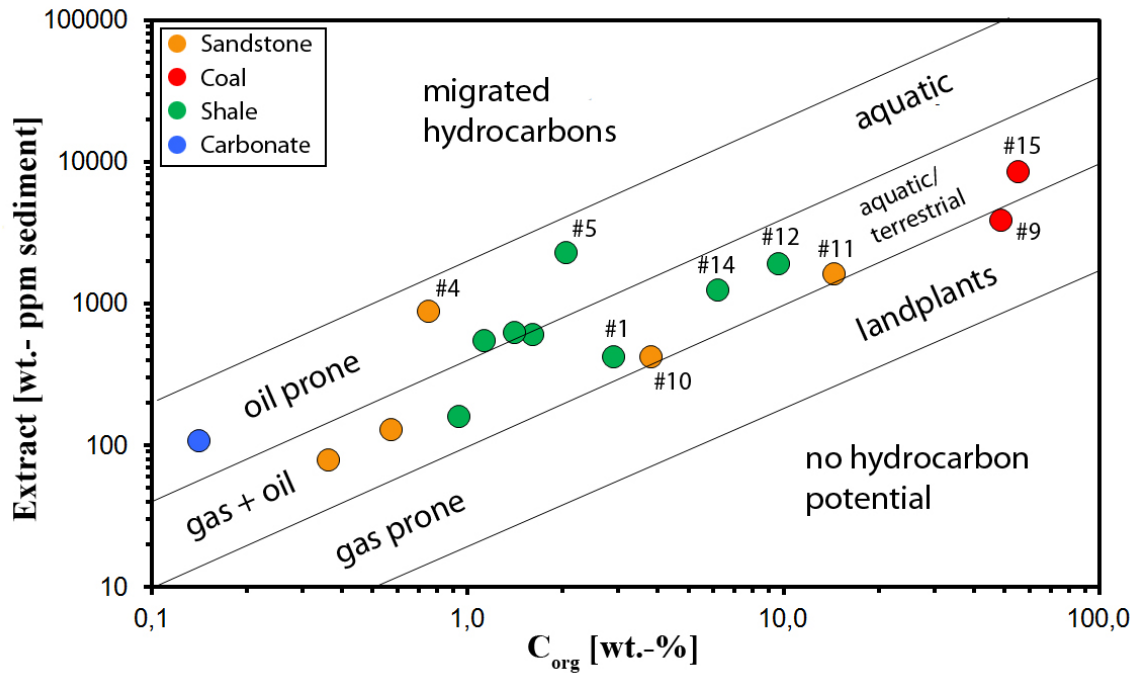
Figure 5.7: Amount of extractable hydrocarbons (ppm with respect to sediment weight) and amount of total organic carbon of the investigated sediments (after Akrout et al. 2011 and Peters et al. 2005a).

Fig. 5.6).

In Figure 5.6 we see that the samples mainly comprise type III organic matter (low HI and wider range of OI values). This indicates that the origin is most likely terrestrial (Tissot & Welte 1984). *Samples 12 and 14* (cf. Chapter 3) have a much higher HI value than the others and likely represent type I and II organic matter. Therefore, the samples likely contain aquatic organic matter. The solid lines in Fig. 5.6 represent the maturation paths of samples comprising different types of organic matter. The lines also indicate that the samples likely come from sediments of different maturities (cf. Chapter 5.3).

In further geochemical investigations the hydrocarbons of the sediments were extracted (cf. Chapter 4.4.1). The analytical results of the extraction and fractionation processes are found in the appendix (Tables A.5 and A.6). The extract yields range from 1.31 to 43.42 mg or 80 to 8654 ppm (per weight of sediment) with mean values of 11.1 mg and 1481 ppm, respectively. These values are used in the interpretative diagram of Figure 5.7 where the amounts of extracts are compared to the C_{org} content (e.g. Akrout et al. 2011, Peters et al. 2005a). Due to the variety of

organic matter most of the samples are both oil and gas prone. Algae-rich precursor material is likely more oil prone than land plant precursors.

In order to further characterize the extracted hydrocarbons, the aliphatic fractions have been analyzed by gas chromatography (cf. Chapter 4.5). GC traces of the n-alkanes are depicted in Figures A.1 to A.16 of the appendix. For more details with respect to the interpretations below and gas chromatogram analysis refer to Peters et al. (2005a) and Peters et al. (2005b).

Samples 1 and 2 that are of sediments of Wealden I show bi- and trimodal distributions of the n-alkanes, indicating mixtures of different organic precursor materials which likely consist of terrestrial and different phytoplankton sources (cf. Figs. A.1 and A.2).

Samples 5 and 6 were also obtained from Wealden I sediments, however, they differ significantly in their n-alkane distribution (cf. Figs. A.5 and A.6) compared to *samples 1 and 2*. The low concentration in the range of C_{24} to C_{40} and the strong predominance of the lighter homologues suggests that *samples 5 and 6* have experienced a higher thermal stress in comparison to *samples 1 and 2*. The same interpretation applies to *sample 3* that was obtained from Wealden III sediments.

Sample 4 was obtained from Wealden II sediments and shows a bimodal distribution of the n-alkanes (Fig. A.4), suggesting different aquatic organic precursors. The same is true for *sample 8* coming from the Upper Wealden. *Sample 7*, which also is from the Upper Wealden, likely experienced a strong thermal overprint similar to that observed for *sample 5 and 6* as indicated by the n-alkane distribution seen in Fig. A.7.

Samples 9, 10, 11 and 15 – which were all obtained from mine heaps related to the mining activity at Lüdersfeld – show characteristics of a stronger thermal overprint of the organic matter (cf. Figs. A.9, A.10, A.11 and A.15, respectively) similar to those discussed above (i.e. *samples 3, 4, 5, 6 and 8*).

Sample 12, obtained from Wealden I/II sediments at the Rehburg anticline, shows four modes in the n-alkane distribution (Fig. A.12) indicating different organic precursors. *Sample*
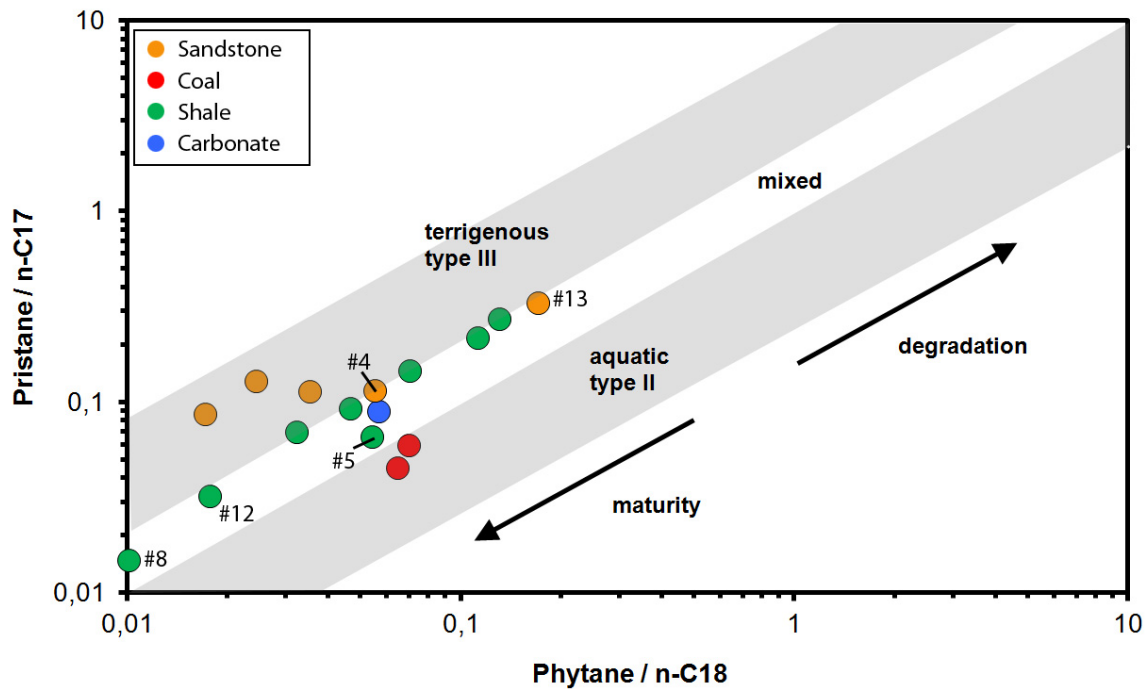
Figure 5.8: Plot of pristane/n-C17-ratio vs. phytane/n-C18-ratio from chromatograms obtained from the aliphatic fractions of the extracted hydrocarbons of the sediment samples. It can be used to infer oxygen availability within the depositional system and also the type of organic matter (modified after Peters et al. 1999).

14 is also derived from Wealden I/II sediments and likely contains at least two different aquatic organic precursors as indicated by the n-alkane spectrum of Figure A.14. A similar observation is made for *sample 13* that comes from Wealden III/IV sediments (cf. Fig A.13).

Finally, *sample 16* – which is obtained from Wealden V/VI sediments – seems to come from thermally more mature organic matter (Fig. A.16).

As thermal maturity has likely altered the n-alkane distribution in some samples, we investigate the typical isoprenoid/n-alkane ratios for their organo-facies signal below.

The pristane/n-C17 and phytane/n-C18 ratios (see appendix, Table A.7) that give significant insight into the organic facies, have values between 0.015 to 0.329 and 0.010 to 0.171, respectively. These values are compiled in Figure 5.8.

Pristane/n-C17 and phytane/n-C18 ratios are helpful to discriminate between terrigenous and aquatic organic matter, respectively (cf. Fig. 5.8). However, with increasing maturity of the rocks the ratios of pristane/n-C17 and phytane/n-C18 become smaller and on the opposite they

increase with the degree of biodegradation because aerobic bacteria attack the n-alkanes first (Peters et al. 1999).

The samples probably are of both terrigenous type III and aquatic type II organic matter with a dominance of the land plant precursors as suspected by Fig. 5.8. All the sandstones plot in or near the zone indicating type III organic matter. The isoprenoid to n-alkane ratio of the shales and of the carbonate indicates type III organic matter whereas the two coals seem to be of type II. This shows that the coals might contain algal organic matter.

Most of the samples plot at lower pristane/n-C17 and phytane/n-C18 ratios and indicate that the sediments are thermally mature. Due to the thermal overprint of the sediments an in depth study related to classical biomarkers (Peters et al. 2005a) was not possible and also concentrations of the relevant compounds (steranes and hopanes) were close to the detection level.

Besides basic molecular indicators, carbon isotopic analysis can be applied for gaining insight into the origin and type of organic matter. Peters et al. (2005a) state that when analyzing the C_{15+} stable carbon isotopic ratios of the respective aromatic and saturated fractions of an oil it is possible to distinguish between terrigenous and aquatic organic matter.

Stable carbon isotope ratios of the hydrocarbon fractions of the samples range from -29.1 to -24.4 ‰ and from -31.1 to -26.9 ‰ for the aromatic and aliphatic fractions, respectiveley (cf. Figure 5.9).

Sofer (1984) published an isotopic relationship for terrestrial and aquatic organic matter. The canonical (CV) variable is a statistical parameter, which is computed according to the equation:

$$CV = -2.53\,\delta^{13}C_{sat} + 2.22\,\delta^{13}C_{aro} - 11.65$$

where $\delta^{13}C_{sat}$ and $\delta^{13}C_{aro}$ are the isotopic ratios of the aliphatic and aromatic fractions, respectively.
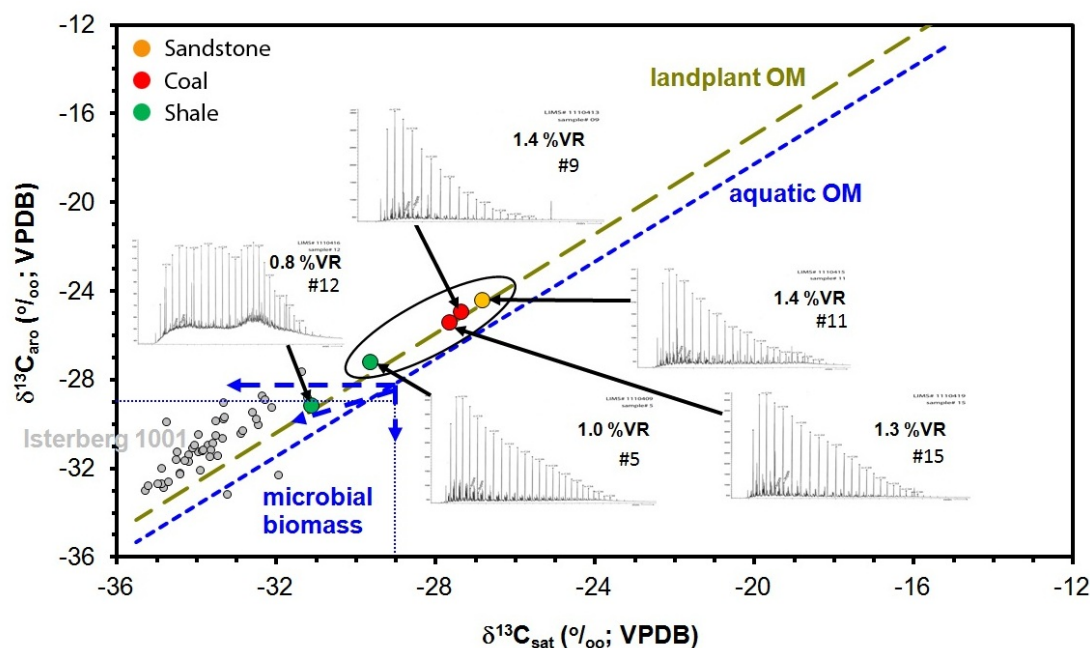
Figure 5.9: Stable carbon isotopic data of the aromatic and saturated fraction of five selected samples are separated into terrestrial and aquatic organic matter. Other German Wealden data is shown in gray for comparison (Kahl 2010). Samples plotting in the blue rectangle are most likely influenced by microbial biomass (modified after Sofer 1984).

The stable carbon isotope analysis was performed on the saturated and aromatic fractions of the extracted hydrocarbons (cf. Chapter 4.6). The complex fractionation was performed only on samples that yielded 15 mg of extract or more. Therefore, isotopic data is only available for five different fractionated samples (cf. appendix Tables A.5 and A.6 for the results on extracts and Table A.8 for results on carbon isotopes).

In Figure 5.9 the five analyzed samples are plotted with respect to the statistical analysis of Sofer (1984). The thermal maturities, sample numbers, sample types (colors) and respective chromatograms of the n-alkanes ($C_{15} - C_{40}$) are included on the diagram. Samples comprising light isotopes (isotopic ratios lower than -29 ‰ $\delta^{13}C$) plot in the area 'microbial biomass'. Microbial biomass influences the aromatic and saturated fraction differently (personal comm. U. Berner and BGR database; cf. also Peters et al. 2005a). Therefore, a shift from aquatic to terrigenous organic matter may be observed due to the higher abundance of ^{12}C-rich molecules in the aliphatic fraction (e.g. *sample 12*, see blue vectors in Fig. 5.9). The Wealden samples from the

Isterberg 1001 core that have a dominant microbial biomass influence are shown on the diagram for comparison (Kahl 2010, Berner et al. 2010). Of the five fractionated samples only *sample 12* seems to have microbial influence because it plots in the region of the Isterberg 1001 samples.

Although the molecular composition of the selected samples (Fig. 5.9) does not allow to genetically characterize the extracts, the carbon isotopic composition of the aliphatic and aromatic fractions clearly point to terrestrial organic precursors in the coals (*samples 9 and 15*) and the carbon rich siltstone (*sample 11*).

5.3 Hydrocarbon Potential & Thermal Maturity

Rock-Eval pyrolysis and hydrocarbon extraction methods allow to characterize the hydrocarbon potential of organic-rich sediments. Peters et al. (2005a) summarized parameters that describe hydrocarbon source rocks and their potential to generate hydrocarbon (cf. Table 5.1).

Values of S_2 and the C_{org} are depicted in Figure 5.10. With respect to the classification suggested in Table 5.1 the C_{org} values in the samples range from fair to excellent (most of the shales plot in the fields good to very good). Five samples have excellent C_{org} values. However, the low values of S_2 results in a poor generative potential for most of the samples. Five samples (same five that have the high C_{org}) have very good to excellent generative potential due to much higher S_2 values.

A similar picture arises from the concentration of bitumen extracts shown in Figure 5.7 (Chapter 5.1). Generally, the source rock potential in Figure 5.7 increases from the lower left to the upper right of the diagram (Akrout et al. 2011). The extract amounts in Fig. 5.7 approximate the hydrocarbons already generated whereas the S_2-values in Fig. 5.10 describe the remaining hydrocarbon potential.

Thermal maturity has a significant imprint on the remaining hydrocarbon potential. With increasing maturity the remaining hydrocarbon potential decreases. Rock-Eval analysis data (cf. app. Table A.4) indicate thermal maturities (T_{max}) of the samples between 434 and 476 °C.
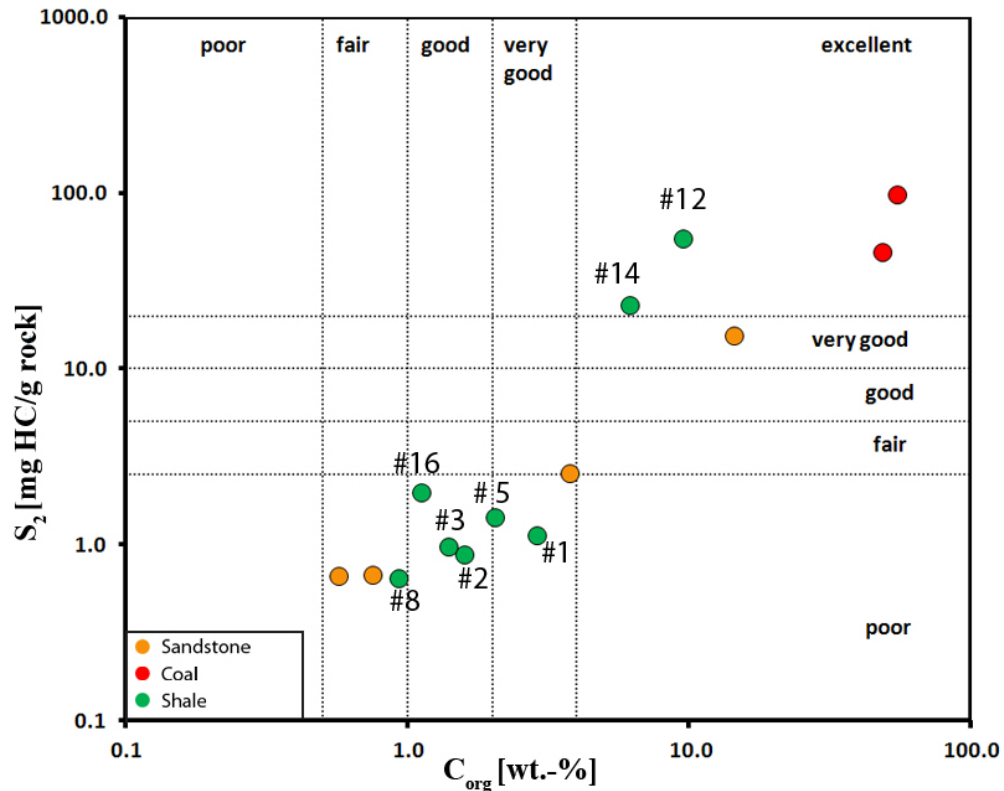
Figure 5.10: Generative potential of the sediments obtained from Rock-Eval S_2 data and C_{org} values. The ranges for the classifications of poor, fair, good, very good and excellent are taken from Peters et al. (2005a).
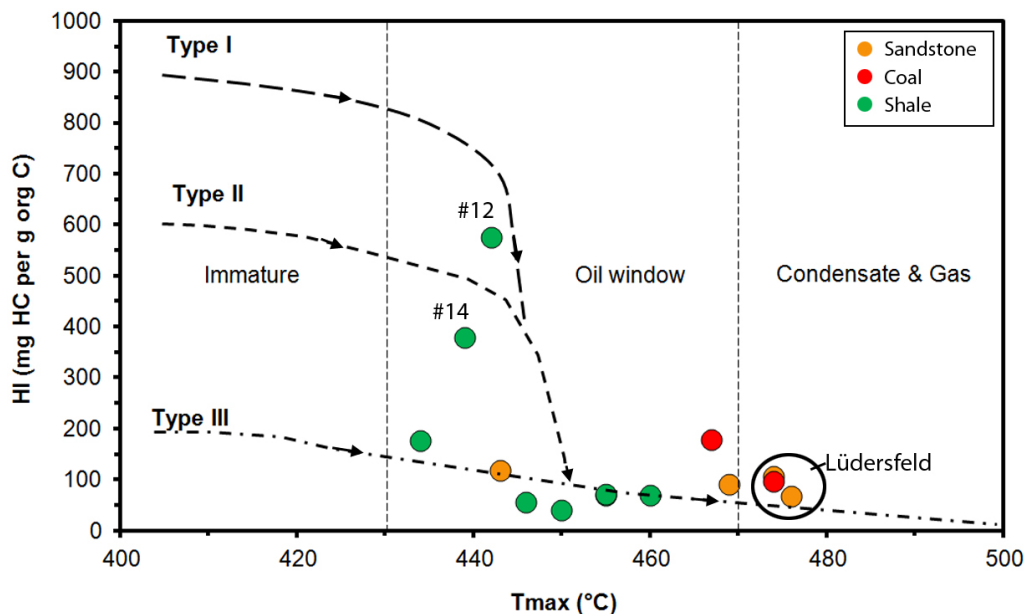
Figure 5.11: Typical Rock-Eval pyrolysis plot displaying type of organic matter (deduced from hydrogen index) and thermal maturity. Oil and gas window are plotted according to values from Peters et al. (2005a).

Table 5.1: (a) Generative potential (quantity) of immature source rock, (b) kerogen type and quality of expelled products, and (c) Thermal maturity. TAI: thermal alteration index, PI: production index (Peters et al. 2005a, modified after Peters & Cassa 1994).

Potential (quantity)	C_{org} (wt.-%)	Rock–Eval S_1	(mg/g rock) S_2	Bitumen (ppm)	Hydrocarbons (ppm)
Poor	<0.5	<0.5	<2.5	<500	<300
Fair	0.5−1	0.5−1	2.5−5	500−1000	300−600
Good	1−2	1−2	5−10	1000−2000	600−1200
Very Good	1−2	1−2	10−20	2000−4000	1200−2400
Excellent	>4	>4	>20	>4000	>2400
(a)					

Kerogen (quality)	Hydrogen Index (mg hydrocarbon/g TOC)	S_2/S_3	Atomic H/C	Main product at peak maturity
I	>600	>15	>1.5	Oil
II	300−600	10−15	1.2−1.5	Oil
II/III	200−300	5−10	1.0−1.2	Oil/Gas
III	50−200	1−5	0.7−1.0	Gas
IV	<50	<1	<0.7	None
(b)				

Maturity	Maturation R_o (%)	T_{max} (°C)	TAI	Generation Bitumen/C_{org}	Bitumen (mg/g rock)	PI ($S_1/(S_1+S_2)$)
Immature	0.2−0.6	<435	1.5−2.6	<0.05	<50	<0.10
Mature						
Early	0.60-0.65	435-445	2.6-2.7	0.05-0.10	50-100	0.10-0.15
Peak	0.65-0.90	445-450	2.6-2.7	0.15-0.25	150-250	0.25-0.40
Late	0.90-1.35	450-470	2.9-3.3	-	-	>0.40
Postmature	>1.35	>470	>3.3	-	-	-
(c)						

T_{max} is the temperature at which a peak production of hydrocarbons from kerogen is reached during pyrolysis. With increasing maturity of the sediments the thermal energy needed to break the kerogen bonds in order to produce hydrocarbons increases as well. Therefore, the higher the maturity the higher the T_{max}. However, T_{max} is also dependent upon the type of organic matter since different macerals are more easily broken apart than others (Killops & Killops 2005). Investigations of Kahl (2010) show that type I kerogens need higher Rock-Eval temperatures to transform into hydrocarbons and thus Rock-Eval pyrolysis may indicate much higher thermal maturities than actually experienced in the subsurface (see also Banerjee et al. (1998) and literature cited therein).

The higher the maturity of a sample, the higher the amount of hydrocarbon that has already

Table 5.2: Back-calculation of S$_2$* using HI values observed in Fig. 5.12 of the shales of this thesis.

sample #	C_{org} wt.-%	HI* mgHC/g orgC	S$_2$* mg/g
1	2,88	200	5,76
2	1,6	200	3,20
3	1,4	700	9,80
5	2,04	700	14,28
8	0,93	1100	10,23
12	9,57	1100	105,27
14	6,14	600	36,84
16	1,12	200	2,24

been generated from the organic matter (Peters et al. 2005a). Rock-Eval pyrolysis measures the remaining generative potential of the samples. The true initial generative potential is related to immature samples. However, information on the initial hydrocarbon potential is needed when it comes to the evaluation of the oil and gas generation within shales (Jarvie et al. 2007).

In order to restore the initial hydrocarbon potential of the mature sediments a simple method may be used which deviates slightly from the more sophisticated approaches given in Dahl et al. (2004), Peters et al. (2005a) and Berner (submitted).

The Rock-Eval pyrolysis data HI and T_{max} can be used to create a plot (Fig. 5.11) where the curves of the three types of organic matter follow a path from high HI to lower HI values when the thermal maturity increases. Fig. 5.11 shows that most samples have reached the stage of the oil window. The three samples collected from the Lüdersfeld mine heap are at the beginning of the condensate and wet gas window.

Figure 5.12 shows the development of general HI values with respect to thermal maturity given as vitrinite reflectance equivalent (Dahl et al. 2004 and Banerjee et al. 1998).

The equivalents of vitrinite reflectance (VReq. in %) which is commonly used in petroleum exploration have been calculated (cf. Peters et al. 2005a) using the measured T_{max} values of the samples.

$$VR_{eq} = 0.018\,T_{max} - 7.16$$

Ranges of VReq. vary between 0.65 and 1.41 % for the sample set.
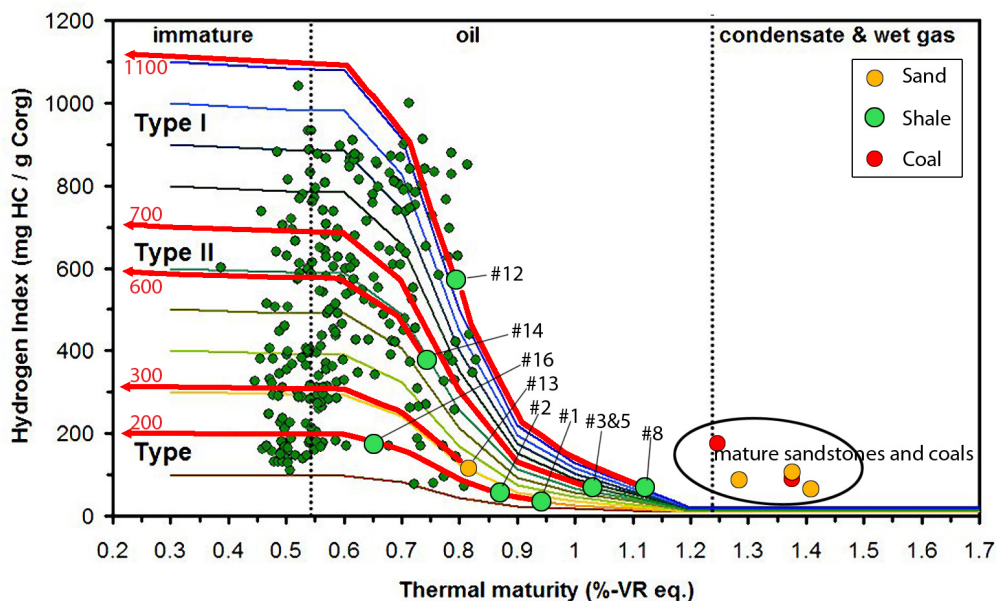
Figure 5.12: Back-calculation of *HI* with decreasing maturity. Whilst immature (i.e. %-VR eq. lower than c. 0.55), *HI* is constant but decreases rapidly when entering the oil window. Green dots are data points from samples of the BGR database. The red arrows back-trace the maturity path of each sample. The approximate original *HI** values are indicated by red numbers.
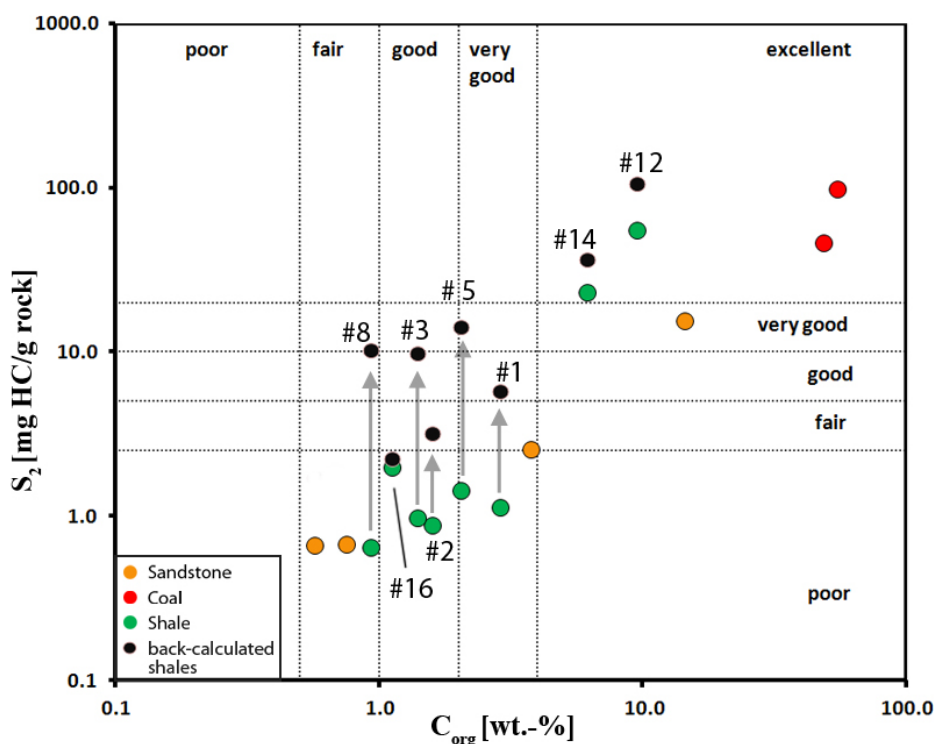
Figure 5.13: Generative potential of the sediments obtained from Rock-Eval S_2 data and C_{org} values. The ranges for the classifications of poor, fair, good, very good and excellent are taken from Peters et al. (2005a). Additionally a *HI** (and hence S_2*) reconstruction is given for each of the shales by the black dots above from where the according shales plot (see text for more detail).

The shales of this research were plotted on the diagram of Figure 5.11 and followed back to immaturity in order to get an approximate value of the original HI. The observed $HI*$ values (Fig. 5.12) are then calculated into S_2*. $HI*$ is converted into S_2* by calculating:

$$S* = (C_{org} * HI*)/100.$$

The theoretical S_2* values for immature equivalents of the samples (cf. Tab. 5.2) are integrated in Figure 5.13 (black dots; strong increases in S_2 are indicated by black arrows). Although C_{org} values decrease significantly with increasing maturity they were not back-evaluated because it would exceed the scope of this thesis.

From Table 5.2 it is obvious that sediments of *samples 3, 5, 8, 12 and 14* contain organic matter which shows excellent hydrocarbon generation potential, suggesting that the eastern Wealden basin (eastern Lower Saxony Basin) could be a good target for shale oil and gas exploration.

5.4 Gas Geochemistry

The gas geochemical analyses are performed on the gases obtained from the de-gassing method (cf. Chapter 4.7). If enough gas was available the stable carbon isotopic ratio of the gases were measured as well. Isotopic $\delta^{13}C_{CH_4}$ (methane) and $\delta^{13}C_{C_2H_6}$ (ethane) composition is available for *samples 5, 7, 14 and 16*. The isotopic $\delta^{13}C_{C_3H_8}$ (propane) composition is available for *samples 5, 7 and 16*. The amounts in the other samples were too low to provide reliable measurements.

Appendix Tables A.9 and A.10 display the results of the gas geochemical analysis. The $C_1/(C_2 + C_3)$-ratio of these samples are between 4.11 and 6.72. The $\delta^{13}C_{CH_4}$ (methane) isotope ratios in the samples ranged from -47.15 to -38.02 ‰ whereas the isotope ratios of $\delta^{13}C_{C_2H_6}$ (ethane) and $\delta^{13}C_{C_3H_8}$ (propane) ranged from -32.69 to -26.82 ‰ and -31.49 to -24.37 ‰, respectively.

Natural gases can be formed by thermogenic or microbial processes (Schoell 1988). Molecular as well as the isotopic compositions help to distinguish between different genetic processes.
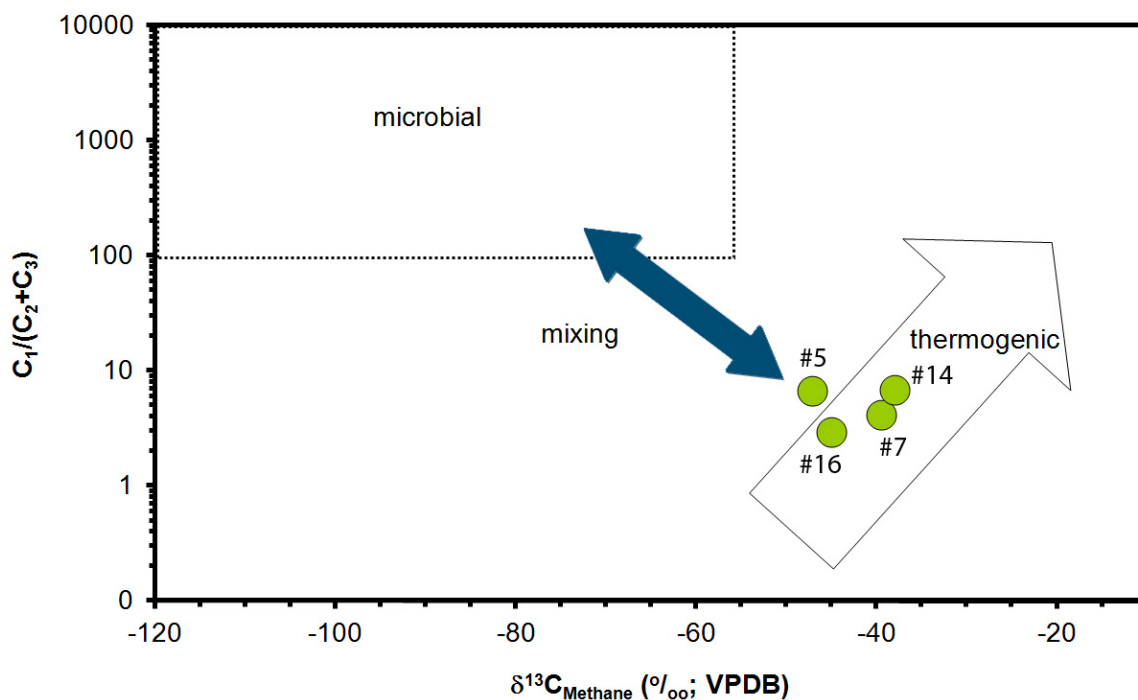
Figure 5.14: Interpretative 'Bernard' diagram comparing molecular $C_1/(C_2+C_3)$ and isotopic $\delta^{13}C_{CH_4}$ compositions of the natural gases extracted from the sediments. Only four samples yielded enough gas for methane isotopic analysis (after Whiticar 1990).

Microbial processes form mainly methane, whereas thermogenic processes also form significant amounts of higher homologues (e.g. ethane and propane, cf. Schoell 1988). Microbial methane usually contains higher amounts of light isotopes (^{12}C) whereas thermogenic methane is enriched in the heavier ^{13}C isotopes with typical values more positive than $-55\,‰$. When thermal maturity rises, the amount of methane increases due to the cracking of higher homologues and hence the $C_1/(C_2 + C_3)$-ratio increases. With increasing maturity the gases become enriched in ^{13}C due to kinetic isotope fractionation processes (Berner et al. 1995).

Molecular ratios ($C_1/(C_2 + C_3)$) and methane isotope ratios (Fig. 5.14) suggest, according to Bernard (1978), that the hydrocarbon gases of the Wealden sediments are predominantly of thermogenic origin. However, a slight contribution of microbial methane seems to be likely for *sample 5* (Fig. 5.14). Carbon isotope ratios of methane, ethane and propane indicate again the predominance of thermogenic hydrocarbons (see Figs. 5.15a and 5.15b, cf. Berner et al. 1995 and Berner & Faber 1996). Maturity trends in Fig. 5.15 have been calculated according to Berner & Faber (1996) using an approximated isotope ratio for an averaged sappropelic Wealden kerogen
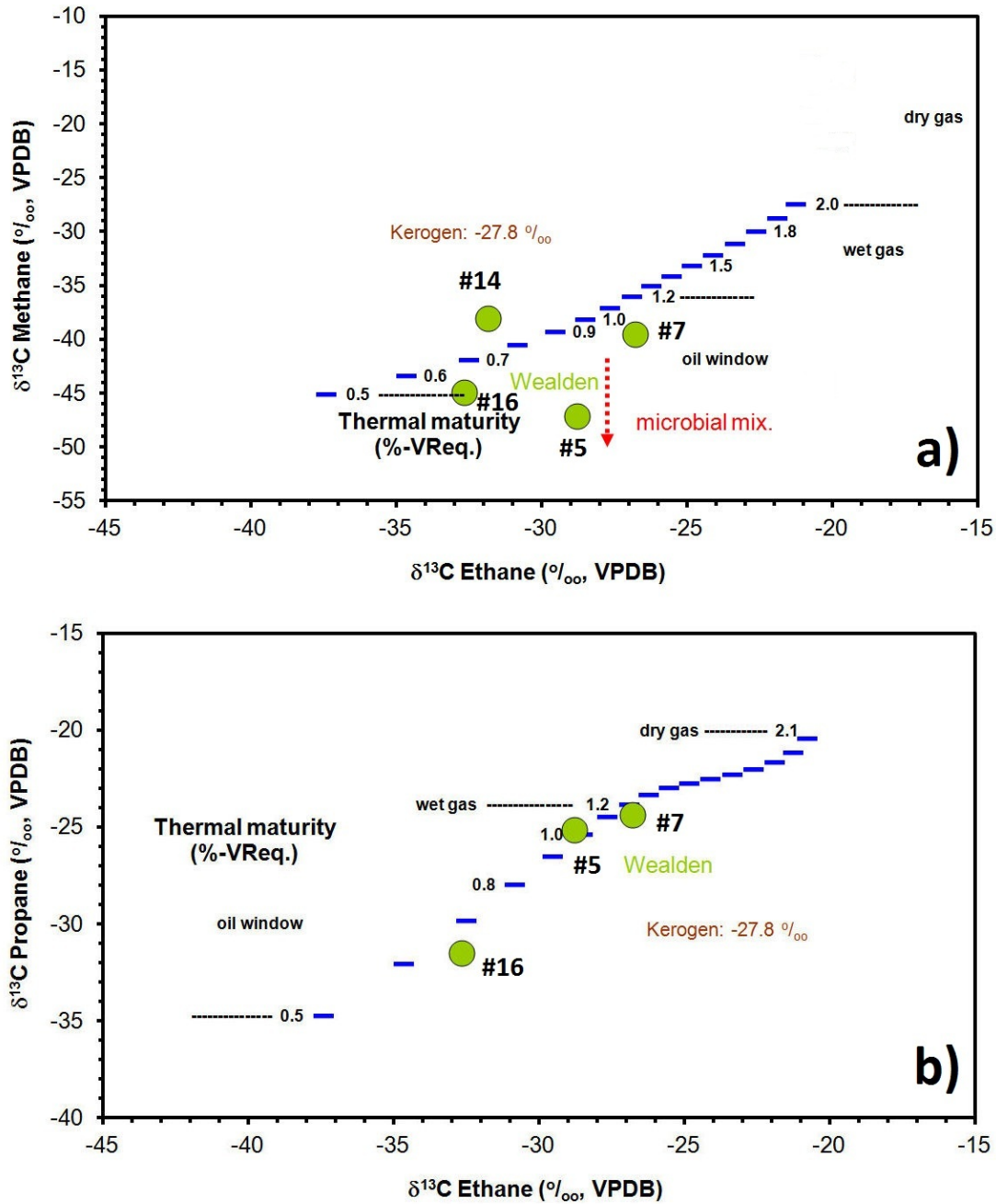
Figure 5.15: Maturity trends using isotopes ratios of methane, ethane and propane. Calculations according to Berner & Faber (1996).

using basic isotopic mass balance consideration (Berner & Faber 1988), which uses the isotopic composition of the hydrocarbon fractions given in Table A.10 of the appendix. Generally, carbon isotope ratios of methane, ethane and propane suggest that the gases were generated within the oil window (Tissot & Welte 1984) at maturities equivalent to 0.6 to 1.2 %-VR. The maturity values derived from the carbon isotope method are strongly supported by the T_{max} values derived

from Rock-Eval pyrolysis (Tab. A.4 in the appendix).

5.5 Restored Tectonic Movements (Subsidence & Uplift)

Thermal maturity of the organic matter in sediments can provide information about subsidence and tectonics. Rock-Eval pyrolysis provides T_{max} values that can be converted into equivalents of vitrinite reflectance (see Chapter 5.3).

The cross-section of the Stadthagen syncline is depicted in Figure 5.16 including the thermal maturities of the samples at their projected locations. A projection had to be applied since the sample sites were not exactly on the cross-section. However, the distance between the cross-section and the sample localities was small enough to allow this projection.

Fig 5.16 shows how the thermal maturity increases towards the basin center even though the age of the sediment decreases in the same direction. This must mean that the anticlines of the shoulders have formed after the basin had been buried to its maximum depth. The observed maturities suggest that the sediments were thermally overprinted during burial and retained the thermal signature after being up-lifted.
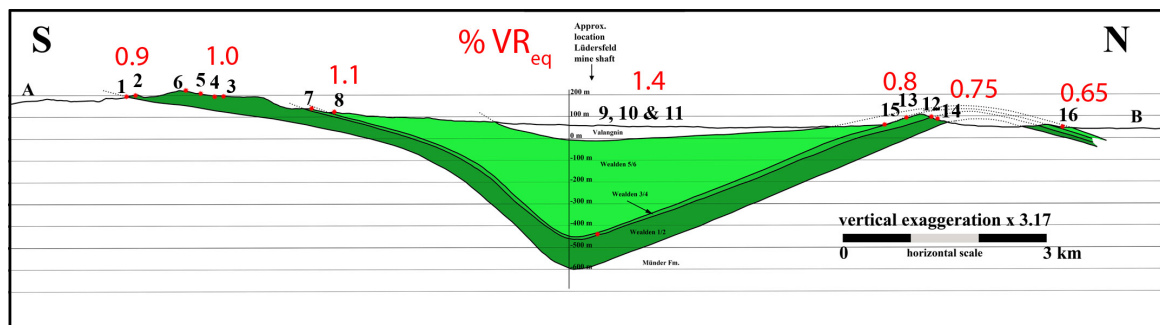
Figure 5.16: Cross-section from Figure 2.6 including projected sample locations and maturities.

In an attempt to restore the original burial, porosity measurements and an empirical shale compaction curve may help to obtain theoretical values of the maximum burial depths of the sediments.

Table A.11 of the appendix comprises the density and porosity measurements of the Wealden sediments. The porosity in the shales ranges from 7.4 to 28.8 %.
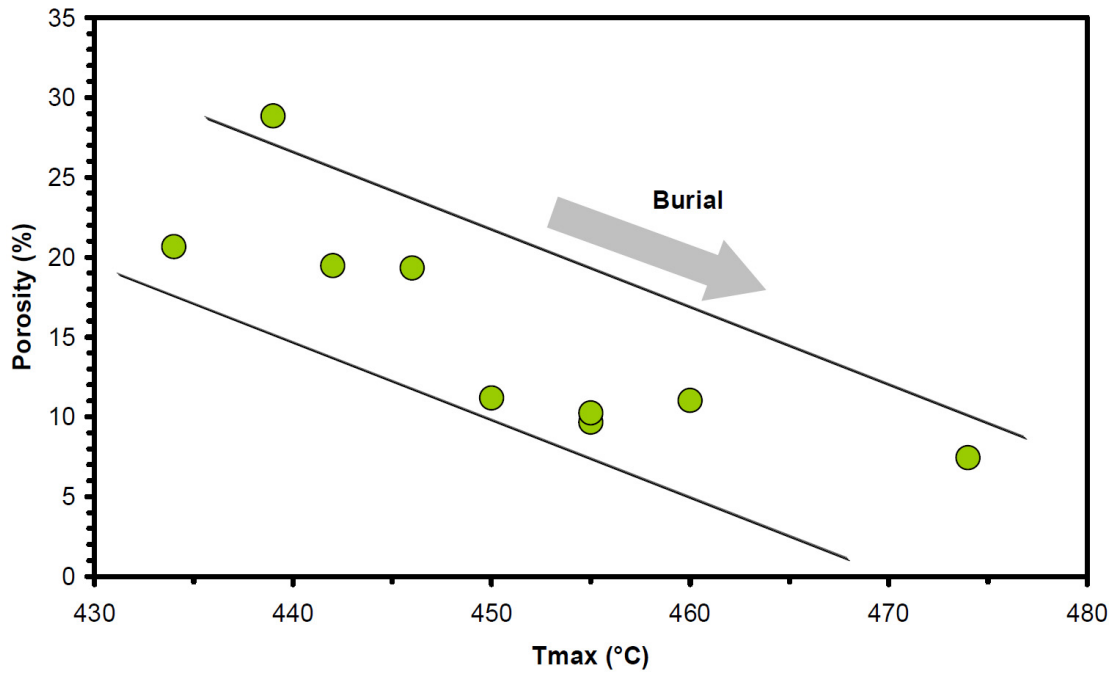
Figure 5.17: Increasing burial of Wealden sediments leads to increasing thermal maturity and decreasing porosity of shales.

The observed decrease of porosities with increasing thermal maturity in shales (Fig. 5.17) indicates that the sediments experienced significant burial in the past. Porosity and maturity data will be used to estimate the magnitude of burial the Wealden sediments have experienced in the Stadthagen syncline.

From standard assumptions on shale compaction (normal shale compaction after Baldwin & Butler (1985) is used as an example) burial depths may be estimated (Fig. 5.18a). The maximum burial is estimated from porosity to be in the order of 3600 m at Lüdersfeld. We compare the estimated burial with our calculated vitrinite reflectance data (cf. Peters et al. 2005a). The burial estimates derived from porosities that have likely been the deepest seem to fit a depth-maturity line (Fig. 5.18b), which also would reach 0.3 %-VR at the surface (immaturity criterion), suggesting that the upper most burial estimates from porosities might be too low.

Fig. 5.19 shows a depth-scenario in which the regression of Fig. 5.18b was used to estimate maximum burial in the region. Obviously the basin center sediments at Lüdersfeld experienced the deepest burial of about 3600 m (Wealden III/IV) and the values of the Rehburg anticline
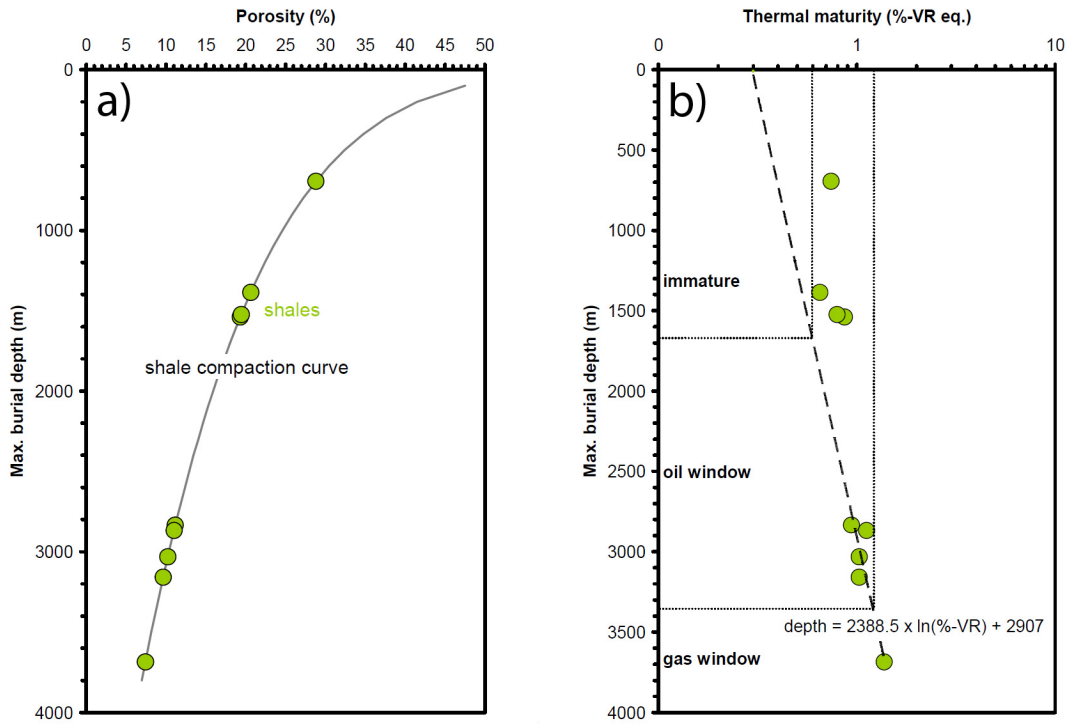
Figure 5.18: a) Increasing burial of sediments leads to decreasing porosity of shales with the example curve according to (Baldwin & Butler 1985) – b) estimated maximum burial and observed thermal maturities.
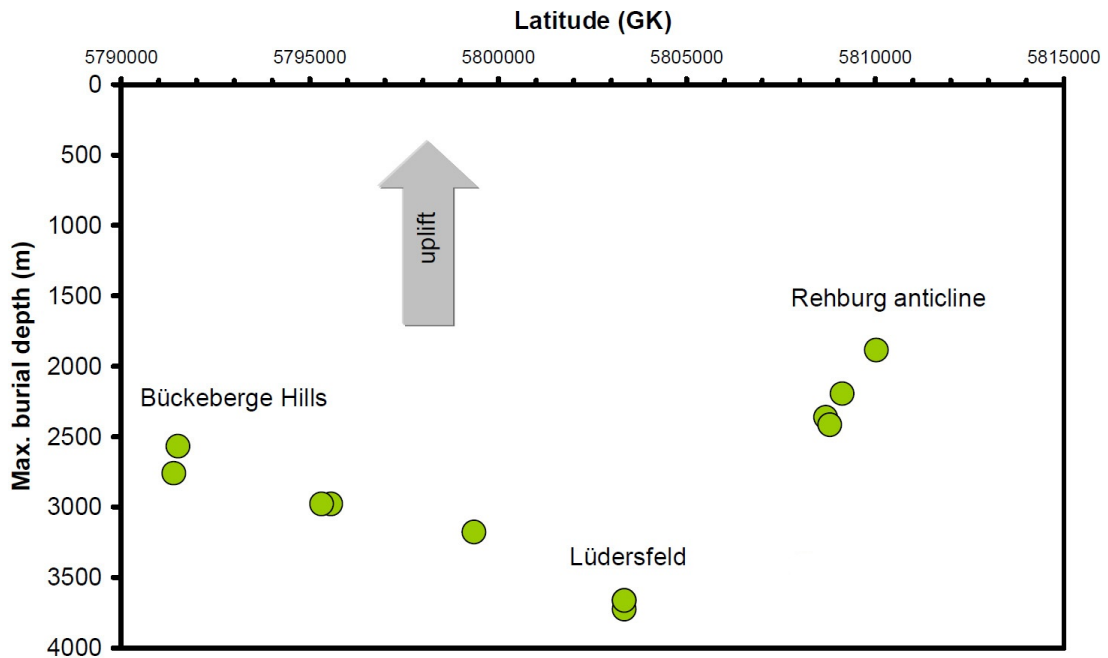
Figure 5.19: Paleoburial reconstruction using vitrinite reflectance and porosity data. After maximum burial the sediments were uplifted differentially. The southern part was uplifted stronger than the northern part.

suggest the lowest burial (about 1800 m; Wealden V/VI) in the region. The estimated maximum burial of the southern-most samples from the Bückeberge Hills may have reached a depth of about 2600 m (Wealden I/II).

The estimated burial depths of the samples seen in Figure 5.19 show that the sediments from the Bückeberge Hills are significantly deeper than the northern Rehburg anticline sediments. The large difference between the burial depth of the northern and southern shoulders suggests a differential uplift in which the southern part of the basin experienced a stronger uplift than the northern part.

Petmecky et al. (1999) point out that a northward tilt of the Lower Saxony basin happened in Oligocene and Miocene times. The fact that at present day topography the southern sediments are located at even higher elevations than the northern sediments supports the northward tilt hypothesis of Petmecky et al. (1999).

The vitrinite reflectance equivalents (Fig. 5.16) show a northward decrease away from the basin center. However, the cross-section of Figure 5.16 shows a significant folding of the northern basin shoulder which is not observed in the reconstruction of Figure 5.19. We therefore conclude that the folding of the Rehburg anticline happened after the period of maximum burial.

6 Conclusions

The samples obtained in the field come from different lithologies. Partly organic rich, lacustrine shales as well as coals and shore line or fluvial sandstones were collected which indicates significant variability in the Wealden depositional environment. The applied analytical methods (elemental analysis, Rock-Eval pyrolysis, hydrocarbon extraction and fractionation, GC and biomarker analysis, porosity measurements, gas geochemistry and stable carbon isotope analysis) revealed the following:

1. The sediments contained terrestrial (e.g. land plant) and partly aquatic (e.g. algae, bacteria) organic matter that deposited in mostly oxic environments. Three samples as well as the two coals appear to have deposited under dysoxic to anoxic conditions.

2. Hydrocarbon extracts indicate that the kerogen in the samples is generally oil and gas prone. This is also supported by n-alkane and isoprenoid data obtained from gas chromatography.

3. A simplified method for a reconstruction of the remaining hydrocarbon generative potential (Rock-Eval S_2 parameter reconstruction) showed that the samples of the Stadthagen syncline have significant hydrocarbon potential.

4. Thermal maturities (vitrinite reflectance equivalents) showed that the Bückeberge Hills and Rehburg anticline sediments of the Stadthagen syncline shoulders reached the oil window stage, whereas the sediments in the basin center sediments at Lüdersfeld have already attained wet gas window maturities. The thermal maturities are supported by carbon isotope ratios in methane, ethane and propane gases extracted from selected samples. Isotope analysis and gas geochemistry also show that *sample 5* from the Bückeberge Hills shows a microbial methane influence.

5. Paleodepth reconstruction of the samples showed that the Bückeberge Hill samples (esti-

mated burial of 2600 m, Wealden I/II) were buried deeper than the northern counterpart, the Rehburg anticline sediments (est. burial of 1800 m, Wealden V/VI). The burial of the Wealden III/IV coals of the Lüdersfeld mine shaft is estimated to be at c. 3600 m. Asymmetric burial and differential uplift is likely to have taken place in the Stadthagen syncline.

6. Although the study suggests excellent hydrocarbon potential for a number of the German Wealden shales of the Stadthagen syncline the vertical and horizontal variability in lithologies within the Wealden strata also suggests significant variability of the organic matter.

We demonstrate with our study that surface exploration helps significantly to evaluate the hydrocarbon system of gas shale plays.

7 References

Akrout, D., Affouri, H., Ahmadi, R., Mercier, E., Montacer, M. (2011): Source Rock Characterization and Petroleum Systems in North Ghadames Basin, Southern Tunisia. Resource Geology 61(3), 270–280.

Baldwin, B., Butler, C. O. (1985): Compaction Curves. AAPG Bulletin 69(4), 622–626.

Banerjee, A., Sinha, A., Jain, A., Thomas, N., Misra, K., Chandra, K. (1998): A mathematical representation of Rock-Eval hydrogen index vs T_{max} profiles. Organic Geochemistry 28(1-2), 43–55.

Behar, F., Beaumont, V., De B. Penteado, H. L. (2001): Rock-Eval 6 Technology: Performances and Developments. Oil & Gas Science and Technology - Rev. IFP 56(2), 111–134.

Bernard, B. (1978): Light hydrocarbons in marine sediments. Ph.D. thesis, Texas A and M University, Texas, USA.

Berner, U. (2011): The German Wealden, an unconventional hydrocarbon play? Erdöl Erdgas Kohle 127(7/8), 1–7.

Berner, U. (submitted): Assessing unconventional prospects – How important is migration? AAPG Bulletin .

Berner, U., Faber, E. (1988): Maturity related mixing model for methane, ethane and propane, based on carbon isotopes. Organic Geochemistry 13(1-3), 67–72.

Berner, U., Faber, E. (1996): Empirical carbon isotope/maturity relationships for gases from algal kerogens and terrigenous organic matter, based on dry, open-system pyrolysis. Organic Geochemistry 24(10-11), 947–955.

Berner, U., Faber, E., Scheeder, G., Panten, D. (1995): Primary cracking of algal and landplant kerogens: kinetic models of isotope variations in methane, ethane and propane. Chemical Geology 126, 233–245.

Berner, U., Kahl, T., Scheeder, G. (2010): Hydrocarbon Potential of Sediments of the German Wealden Basin. Erdöl Erdgas Kohle / OIL GAS European Magazine 126(6), 80–84.

Betz, D., Führer, F., Greiner, G., Plein, E. (1987): Evolution of the Lower Saxony Basin. Tectonophysics 137, 127–170.

Brumsack, H.-J. (1989): Geochemistry of recent TOC-rich sediments from the Gulf of California and the Black Sea. Geologische Rundschau 78(3), 851–882.

Correns, C. (1949): Einführung in die Mineralogie. Springer Verlag, Berlin, 414pp.

Dahl, B., Bojesen-Koefoed, J., Holm, A., Justwan, H., Rasmussen, E., Thomsen, E. (2004): A new approach to interpreting Rock-Eval S_2 and TOC data for kerogen quality assessment. Organic Geochemistry 35(11-12), 1461–1477.

Dean, E. W., Arthur, M. A. (1989): Iron-sulphur-carbon relationships in organic-carbon-rich sequences I: Cretaceous Western Interior Seaway. American Journal of Science 289, 708–743.

Doornenbal, J. C., Stevenson, A. G. (2010): Petroleum Geological Atlas of the Southern Permian Basin Area. EAGE Publications B.V. (Houten), 510pp.

Elstner, F., Mutterlose, J. (1996): The Lower Cretaceous (Berriasian and Valanginian) in NW Germany. Cretaceous Research 17, 119–133.

Faber, E., Stahl, W. (1983): Analytic procedure and results of an isotope geochemical surface survey in an area of the British North Sea. Geological Society, London, Special Publications 12(1), 51–63.

Ghosh, P., Brand, W. A. (2003): Stable isotope ratio mass spectrometry in global climate change research. International Journal of Mass Spectrometry 228, 1–33.

Herron, M., Matteson, A. (1993): Elemental composition and nuclear parameters of some common sedimentary minerals. Nuclear Geophysics 7(3), 383–406.

Herron, M. M. (1988): Geochemical classification of terrigenous sands and shales from core or log data. Journal of Sedimentary Petrology 58(5), 820–829.

Hiete, M. (2004): Umweltveränderungen in der Permo-Trias – geochemische Charakterisierung, Zeitreihenanalyse, Modellierung. Papierflieger, Clausthal-Zellerfeld, 1st edn., 330pp.

IGI Ltd (2004): The Program for Integrated Geochemical Interpretation, p:IGI – The p:IGI Geochemical Manual. Integrated Geochemical Interpretation Ltd., Bideford, UK.

Jarvie, D. M., Hill, R. J., Ruble, T. E., Pollastro, R. M. (2007): Unconventional shale-gas systems: The Mississippian Barnett Shale of north-central Texas as one model for thermogenic shale-gas assessment. AAPG Bulletin 91(4), 475–499.

Kahl, T. (2010): Ablagerungsraum und Kohlenwasserstoff-Potential von Sedimenten aus dem Deutschen Wealden 3 und 4 (Bohrung Isterberg 1001, westliches Niedersächsisches Becken. unpubl. diploma thesis, University of Cologne, Cologne.

Killops, S., Killops, V. (2005): An introduction to organic geochemistry. Blackwell Publishing, Oxford, UK, 2nd edn., 404pp.

Krassmann, T. (2010): Geologie und Bergbau des Schaumburger Landes und seiner Randgebiete – Teil 1 & 2. online publication at: www.mineral-exploration.de.

Littke, R., Scheck-Wenderoth, M., Brix, M., Nelskamp, S. (2008): Subsidence, inversion and evolution of the thermal field. *In:* Littke, R., Bayer, U., Gajewski, D., Nelskamp, S. (Eds.): Dynamics of Complex Intracontinental Basins – The Central European Basin System. Springer, Berlin, 125–153.

Muccio, Z., Jackson, G. P. (2009): Isotope ratio mass spectronomy. Analyst 134(2), 213–222.

Mutterlose, J., Bornemann, A. (2000): Distribution and facies patterns of Lower Cretaceous sediments in northern Germany: a review. Cretaceous Research 21, 733–759.

NIBIS®Kartenserver (2011): Geology. Landesamt für Bergbau, Energie und Geologie (LBEG) .

Peters, K., Fraser, T., Amris, W., Rustanto, B., Hermanto, E. (1999): Geochemistry of crude oils from eastern Indonesia. AAPG Bulletin 83, 1927–1942.

Peters, K. E., Cassa, M. R. (1994): Applied Source Rock Geochemistry. *In:* Magoon, L. B., Dow, W. G. (Eds.): The petroleum system – from source to trap. AAPG Memoir 60, Tulsa, Oklahoma, U.S.A., 93–120.

Peters, K. E., Walters, C. C., Moldowan, J. M. (2005a): The biomarker guide: I, Biomarkers and Isotopes in the Environment and Human History, vol. 1. Cambridge University Press, Cambridge, United Kingdom, 2nd edn., 490pp.

Peters, K. E., Walters, C. C., Moldowan, J. M. (2005b): The biomarker guide: II, Biomarkers and Isotopes in Petroleum Exploration and Earth History, vol. 2. Cambridge University Press, Cambridge, United Kingdom, 2nd edn., 704pp.

Petmecky, S., Meier, L., Reiser, H., Littke, R. (1999): High thermal maturity in the Lower Saxony Basin: intrusion or deep burial? Tectonophysics 304, 317–344.

Rachold, V., Brumsack, H.-J. (2001): Inorganic geochemistry of Albian sediments from the Lower Saxony Basin NW Germany: palaeoenvironmental constraints and orbital cycles. Palaeogeography, Palaeoclimatology, Palaeoecology 174, 121–143.

Radke, M., Willsch, H., Welte, D. H. (1980): Preparative hydrocarbon group type determination by automated medium pressure liquid chromatography. Analytical Chemistry 52(3), 406–411.

Richter, B. E., Jones, B. A., Ezzell, J. L., Porter, N. L., Avdalovic, N., Pohl, C. (1996): Accelerated Solvent Extraction: A Technique for Sample Preparation. Analytical Chemistry 68(6), 1033–1039.

Rousseau, R. M. (2006): Corrections for matrix effects in X-ray fluorescence analysis – A tutorial. Spectrochimica Acta Part B: Atomic Spectroscopy 61(7), 759–777.

Schoell, M. (1988): Multiple origins of methane in the Earth. Chemical Geology 71(1-3), 1–10.

Sofer, Z. (1984): Stable Carbon Isotope Compositions of Crude Oils: Application to Source Depositional Environments and Petroleum Alteration. AAPG Bulletin 68(1), 31–49.

Strauss, C., Elstner, F., Du Chene, R. J., Mutterlose, J., Reiser, H., Brandt, K.-H. (1993): New micropaleontological and palynological evidence on the stratigraphic position of the 'German Wealden' in NW-Germany. Zitteliana , 389–401.

Tegelaar, E. W., de Leeuw, J. W., Derenne, S., Largeau, C. (1989): A reappraisal of kerogen formation. Geochimica et Cosmochimica Acta 53, 3103–3106.

Tissot, B. P., Welte, D. H. (1984): Petroleum formation and occurence. Springer-Verlag, Heidelberg, Germany, 2nd edn., 699pp.

Vejbæk, O. V., Andersen, C., Dusar, M., Herngreen, G. F. W., Krabbe, H., Leszczyński, K., Lott, G. K., Mutterlose, J., van der Molen, A. S. (2010): Cretaceous. *In:* Doornenbal, J. C., Stevenson, A. G. (Eds.): Petroleum Geological Atlas of the Southern Permian Basin Area. EAGE Publications B.V. (Houten), 195–209.

Werner, R. A., Brand, W. A. (2001): Referencing strategies and techniques in stable isotope ratio analysis. Rapid Commun. in Mass Spectrom. 15, 501–519.

Whiticar, M. J. (1990): A geochemial perspective of natural gas and atmospheric methane. Organic Geochemistry 16(1-3), 531–547.

A Appendix – Analytical Results

Table A.1: X-ray fluorescence data of major elements (sample # cf. Table 3.1).

Sample #	SiO_2 wt.-%	Al_2O_3 wt.-%	TiO_2 wt.-%	Fe_2O_3 wt.-%	Fe wt.-%	K_2O wt.-%
1	59.21	18.16	0.97	4.36	1.52	3.12
2	57.30	16.12	0.89	10.56	3.69	2.26
3	51.15	26.27	1.11	2.90	1.01	3.41
4	79.29	8.36	1.25	4.55	1.59	1.02
5	44.78	18.76	0.79	7.39	2.58	2.97
6	6.56	1.42	0.07	3.18	1.11	0.10
7	87.91	5.97	0.68	1.28	0.45	0.60
8	63.76	19.34	1.35	2.54	0.89	1.57
9	20.74	14.72	0.47	1.00	0.35	0.97
10	76.90	10.61	1.48	1.23	0.43	1.20
11	68.97	8.66	0.90	0.67	0.23	0.99
12	49.83	18.09	0.94	7.77	2.72	2.69
13	84.18	7.31	0.67	2.42	0.85	0.75
14	49.41	18.57	0.86	10.52	3.68	2.80
15	21.55	7.52	0.42	0.60	0.21	0.58
16	51.94	20.34	1.01	9.34	3.27	3.04

Sample #	CaO wt.-%	MgO wt.-%	MnO wt.-%	Na_2O wt.-%	P_2O_5 wt.-%
1	0.47	0.98	0.03	0.32	0.11
2	0.61	0.95	0.23	0.24	0.19
3	0.48	1.29	0.01	0.19	0.07
4	0.15	0.66	0.04	0.54	0.12
5	6.31	2.16	0.24	0.25	0.31
6	47.24	1.02	0.23	0.04	0.06
7	0.07	0.28	0.02	0.54	0.08
8	0.38	0.61	0.17	0.14	0.06
9	0.10	0.40	0.00	0.06	0.13
10	0.09	0.38	0.01	0.37	0.08
11	0.05	0.26	0.00	0.24	0.03
12	0.19	0.80	0.05	0.11	0.11
13	0.05	0.21	0.10	0.17	0.14
14	0.39	0.99	0.05	0.24	0.18
15	0.08	0.22	0.00	0.04	0.14
16	0.67	1.68	0.19	0.17	0.27

Table A.2: X-ray fluorescence data of minor elements (sample # cf. Table 3.1).

Sample #	Ba mg/kg	Ce mg/kg	Co mg/kg	Cr mg/kg	Cu mg/kg	Ga mg/kg	La mg/kg	Nb mg/kg	Nd mg/kg	Ni mg/kg
1	274	90	5	120	38	25	53	20	26	31
2	308	102	26	105	34	21	55	24	33	112
3	354	119	12	166	31	34	51	25	39	58
4	185	83	31	85	14	10	48	29	22	56
5	334	78	24	111	40	24	36	19	17	99
6	74	87	6	6	14	2	17	6		9
7	81	59	10	51	9	6	38	17		9
8	203	81	48	117	10	25	39	31	21	42
9	154	70		107	26	21	44	14	14	16
10	136	72	16	116	26	13	36	32	13	23
11	150	53	9	83	12	10	33	20		14
12	274	103	20	111	26	23	55	22	37	67
13	84	85	14	67	12	8	35	17	32	20
14	236	88	37	110	57	24	38	20	17	113
15	138	151		60	15	10	62	11	53	15
16	319	99	25	126	28	27	43	23	28	68

Sample #	Pb mg/kg	Rb mg/kg	Sc mg/kg	Sr mg/kg	Th mg/kg	V mg/kg	Y mg/kg	Zn mg/kg	Zr mg/kg
1	27	150	27	205	17	143	38	89	190
2	39	116	10	134	18	137	48	162	225
3	25	202	21	186	25	246	31	72	164
4	10	48		119	16	61	62	163	481
5	182	151	19	176	18	152	34	40	126
6	6	14		2363	10	11	21	7	12
7	9	33		58	12	35	36	39	411
8	20	79	23	114	13	137	30	42	302
9	15	51	21	296	17	205	20	31	81
10	16	58	12	104	19	68	55	54	777
11	23	51	14	68	13	62	27	23	383
12	51	139	13	123	19	150	31	39	170
13	6	37	12	62	17	34	50	245	587
14	84	137	15	131	13	151	28	66	175
15	19	31	21	376	5	118	19	31	91
16	20	155	20	118	20	169	39	150	174

Table A.3: Carbon and sulfur elemental analysis. Carbonate is calculated by multiplying C_{carb} by 8.33 (see Chapter 4.2). The clastic proportion in the samples and the organic matter are calculated (cf. Chapter 5.1) using the C_{org} and S_{tot} values (for sample # cf. Table 3.1).

Sample #	C_{tot} wt.-%	C_{org} wt.-%	C_{carb} wt.-%	Carbonate wt.-%	S_{tot} wt.-%	Organic Matter wt.-%	Amount Clastic %
1	2.88	2.88	0.00	0	0.03	3.4	96.6
2	1.60	1.60	0.00	0	0.02	1.9	98.1
3	1.40	1.40	0.00	0	0.50	1.7	97.8
4	0.77	0.75	0.02	0.17	0.02	0.9	98.9
5	3.52	2.04	1.48	12.33	1.77	2.4	83.2
6	10.40	0.14	10.26	85.47	0.66	0.2	13.6
7	0.36	0.36	0.00	0	0.02	0.4	99.6
8	0.93	0.93	0.00	0	0.02	1.1	98.9
9	48.40	48.40	0.00	0	0.59	57.2	42.1
10	3.79	3.79	0.00	0	0.08	4.5	95.4
11	14.40	14.40	0.00	0	0.20	17.0	82.8
12	9.57	9.57	0.00	0	0.07	11.3	88.6
13	0.57	0.57	0.00	0	0.06	0.7	99.3
14	6.14	6.14	0.00	0	0.06	7.3	92.7
15	56.20	55.00	1.20	10.00	0.87	65.0	24.0
16	1.19	1.12	0.07	0.58	0.43	1.3	97.6

Table A.4: Rock-Eval pyrolysis data. PI: production index ($S_1/(S_1 + S_2)$), HI: hydrogen index in $mg\ HC/g\ orgC$, OI: oxygen index in $mg\ CO_2/mg\ orgC$ (sample # cf. Table 3.1).

Sample #	S_1 mg/g	S_2 mg/g	S_3 mg/g	T_{max} °C	C_{org} wt. − %	HI	OI	PI
1	0.07	1.14	2.14	450	2.9	40	74.3	0.06
2	0.07	0.88	2.13	446	1.6	55	133.1	0.07
3	0.16	0.98	0.03	455	1.4	70	2.1	0.14
4	0.02	0.68	0.51	469	0.8	91	68.0	0.03
5	0.68	1.44	0.73	455	2.0	71	35.8	0.32
6	n.a.	n.a.	n.a.	n.a.	0.1			
7	n.a.	n.a.	n.a.	n.a.	0.4			
8	0.01	0.65	0.61	460	0.9	70	65.6	0.02
9	1.43	46.38	0.35	474	48.4	96	0.7	0.03
10	0.16	2.55	0.20	476	3.8	67	5.3	0.06
11	0.79	15.42	0.27	474	14.4	107	1.9	0.05
12	0.17	55.13	1.73	442	9.6	576	18.1	0.00
13	0.01	0.67	0.48	443	0.6	118	84.2	0.01
14	0.10	23.27	1.96	439	6.1	379	31.9	0.00
15	2.76	98.04	0.68	467	55.0	178	1.2	0.03
16	0.06	1.98	1.47	434	1.1	177	131.3	0.03

Table A.5: Hydrocarbon extraction from sediments. After de-sulfurization: ADS; (sample # cf. Table 3.1).

Sample #	C_{org} %	Free sulfur [e.g. -, +]	Extract ADS [mg/g rock]	Extract ADS [ppm]
1	2.9		0.427	427
2	1.6		0.607	607
3	1.4		0.631	631
4	0.8		0.887	887
5	2.0		2.315	2315
6	0.1		0.109	109
7	0.4		0.080	80
8	0.9	++	0.162	162
9	48.4		3.890	3890
10	3.8	+	0.422	422
11	14.4	++	1.637	1637
12	9.6		1.930	1930
13	0.6		0.131	131
14	6.1		1.266	1266
15	55.0	+++	8.654	8654
16	1.1		0.548	548

Table A.6: Hydrocarbon fractions in sediments. Samples with more than 15 mg of extract are fully fractionated, whereas the rest are only separated into aliphatics and combined fraction of aromatics and NSO-compounds. Values refer to sediment amount: $mg/g_{sediment}$ (sample # cf. Table 3.1).

| Sample #	Extract [mg/g rock]	Aliphatics [mg/g rock]	Aromatics [mg/g rock]	NSO-compounds [mg/g rock]	Aromatics & NSO-compounds [mg/g rock]
1	0.427	0.180			0.072
2	0.607	0.235			0.124
3	0.631	0.434			0.118
4	0.887	0.274			0.077
5	2.016	1.668	0.150	0.219	
6	0.109	0.074			0.017
7	0.080	0.050			0.020
8	0.162	0.081			0.036
9	2.453	0.357	1.120	1.008	
10	0.422	0.043			0.292
11	1.257	0.393	0.461	0.419	
12	1.821	0.297	0.252	1.296	
13	0.131	0.033			0.039
14	1.266	0.496			0.514
15	5.076	1.078	2.316	1.664	
16	0.548	0.258			0.195
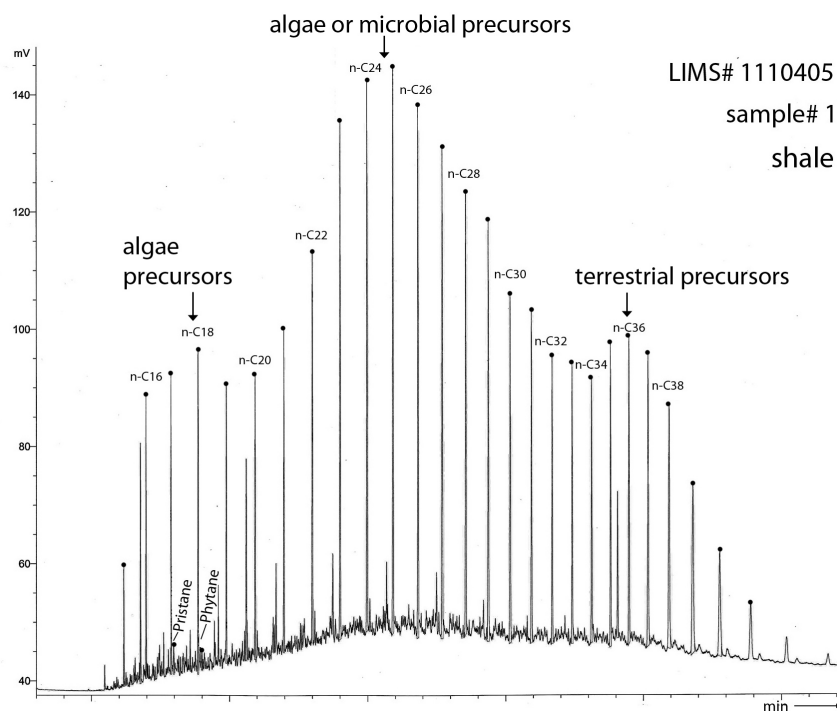
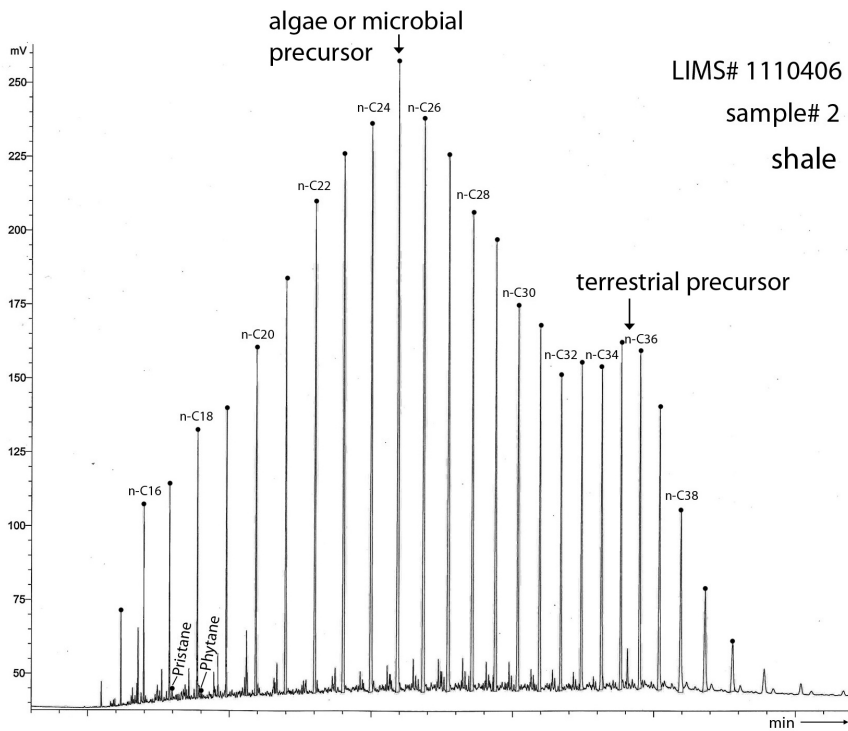Figure A.1: Gas Chromatogram Sample 1

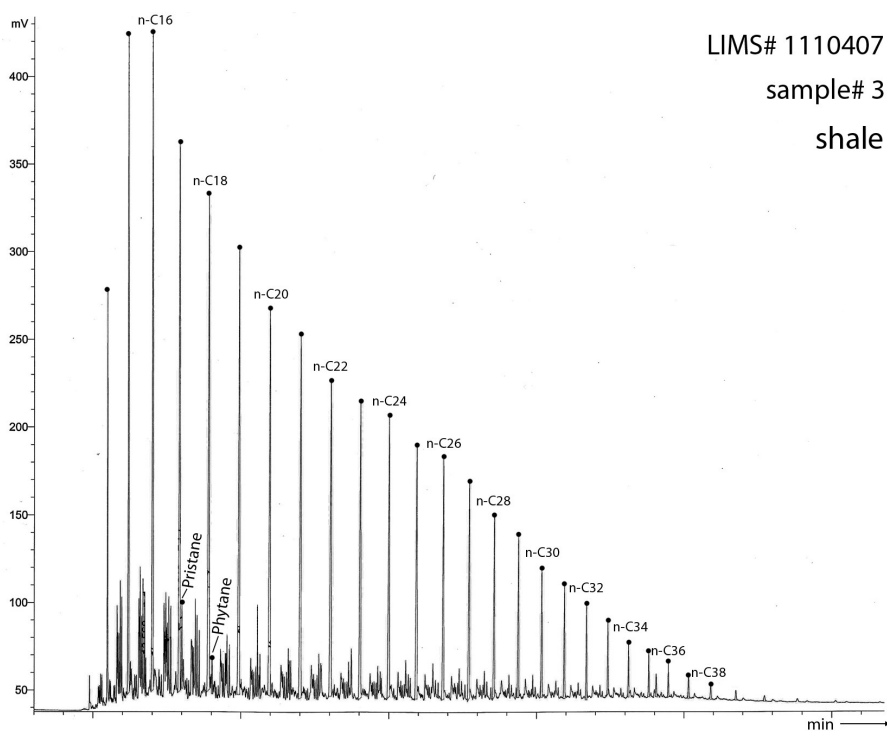Figure A.2: Gas Chromatogram Sample 2

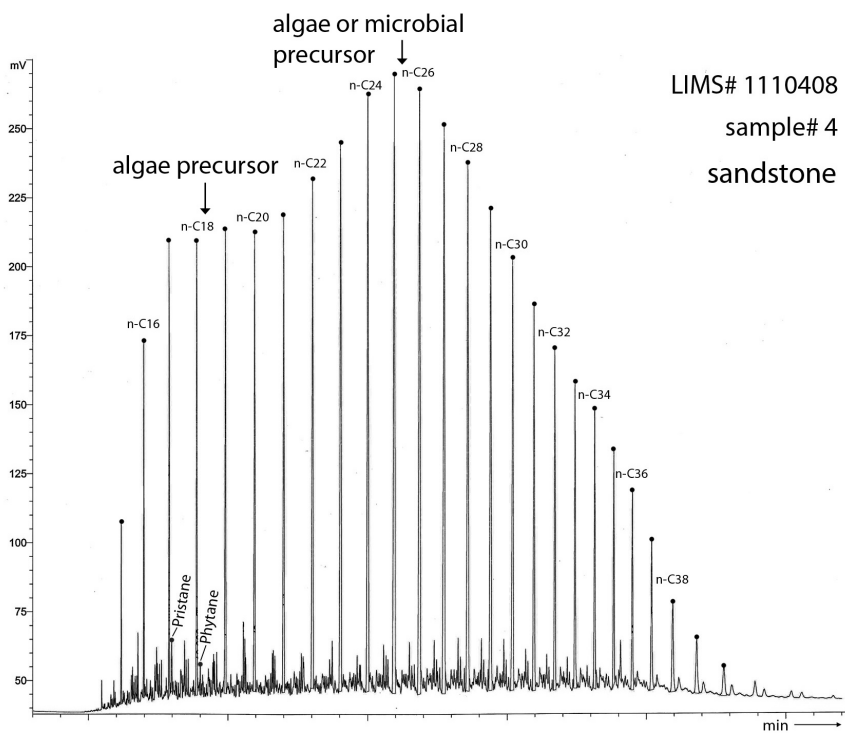Figure A.3: Gas Chromatogram Sample 3
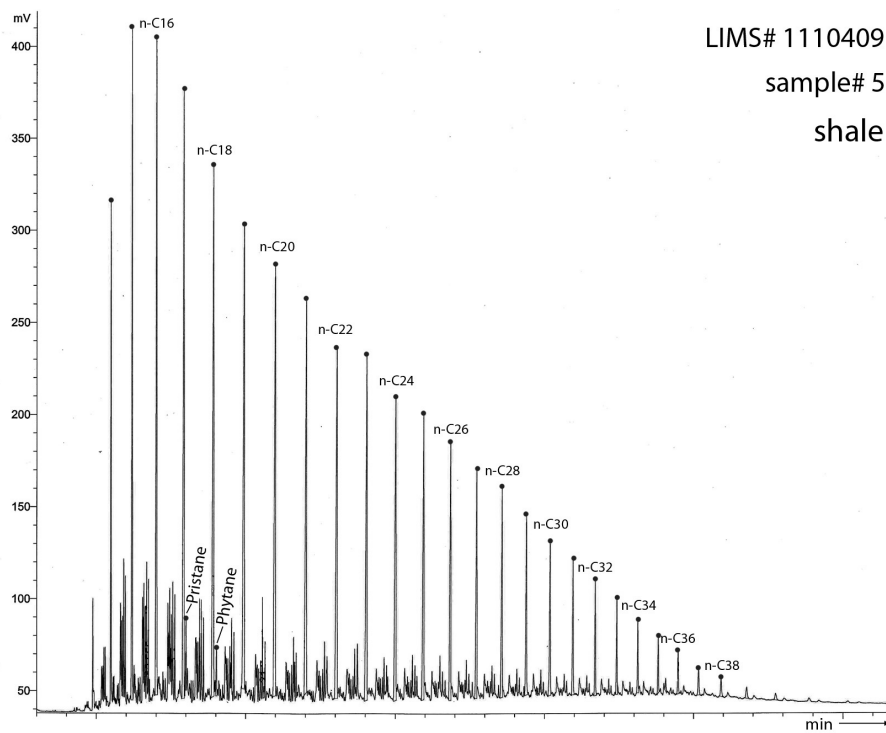

Figure A.4: Gas Chromatogram Sample 4

Figure A.5: Gas Chromatogram Sample 5

Figure A.6: Gas Chromatogram Sample 6

Figure A.7: Gas Chromatogram Sample 7

Figure A.8: Gas Chromatogram Sample 8

Figure A.9: Gas Chromatogram Sample 9

Figure A.10: Gas Chromatogram Sample 10

Figure A.11: Gas Chromatogram Sample 11

Figure A.12: Gas Chromatogram Sample 12
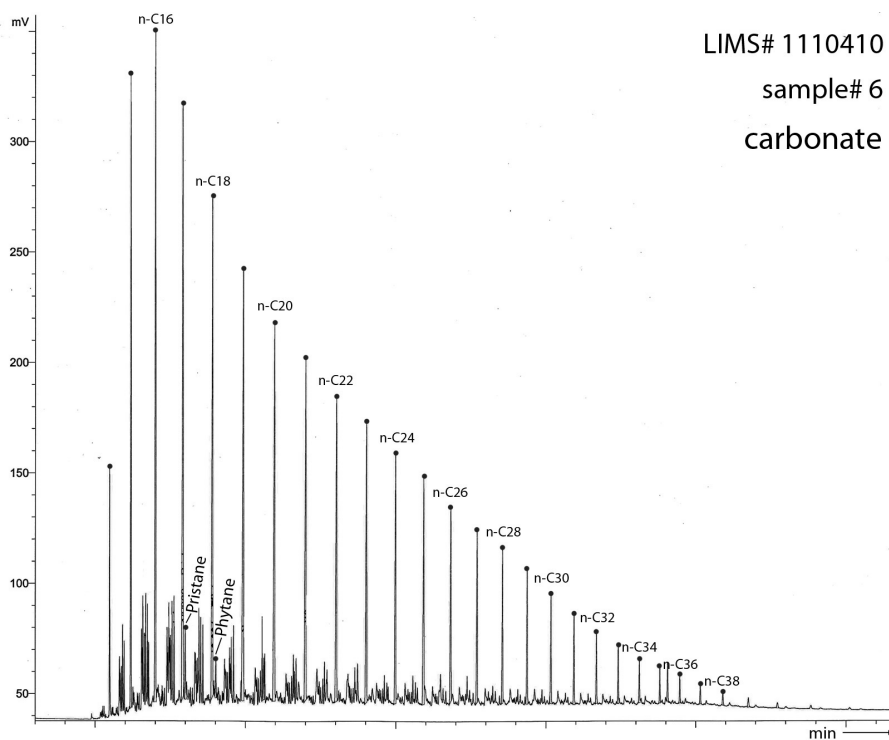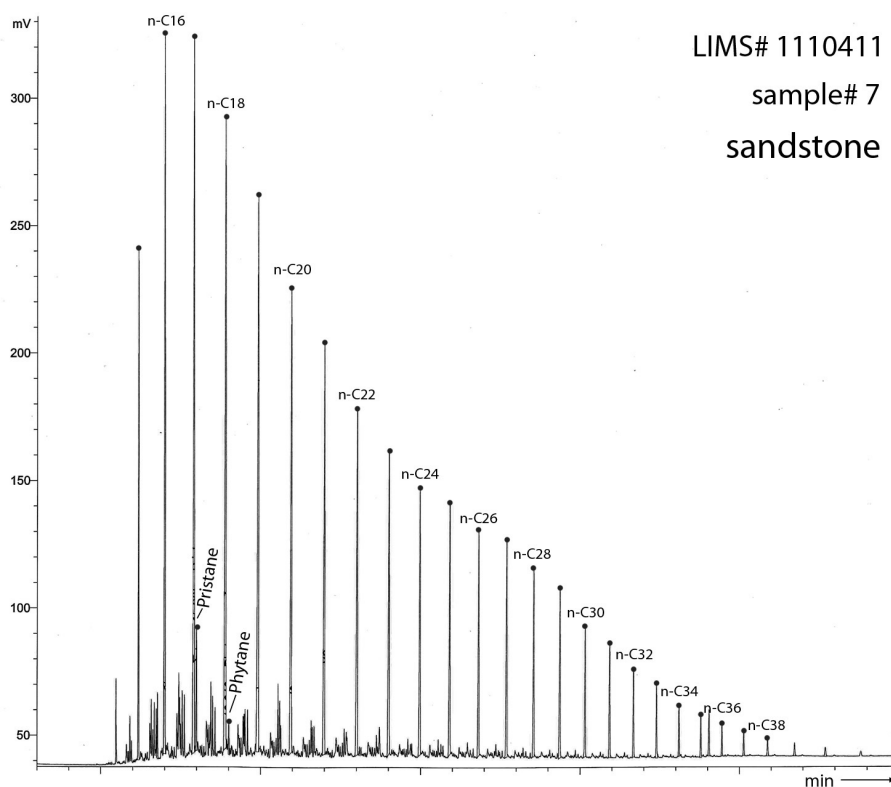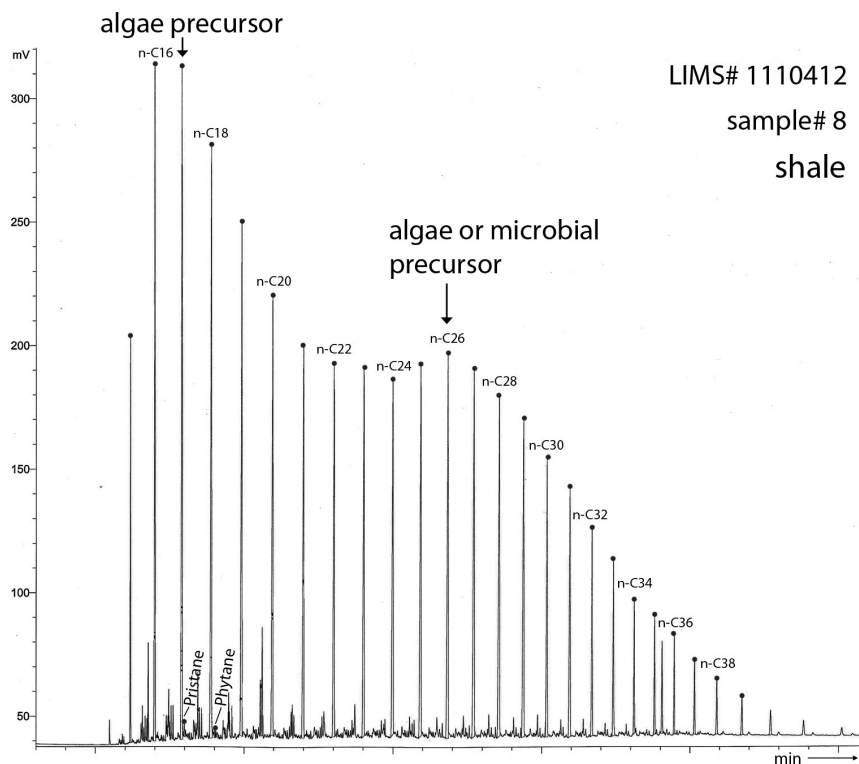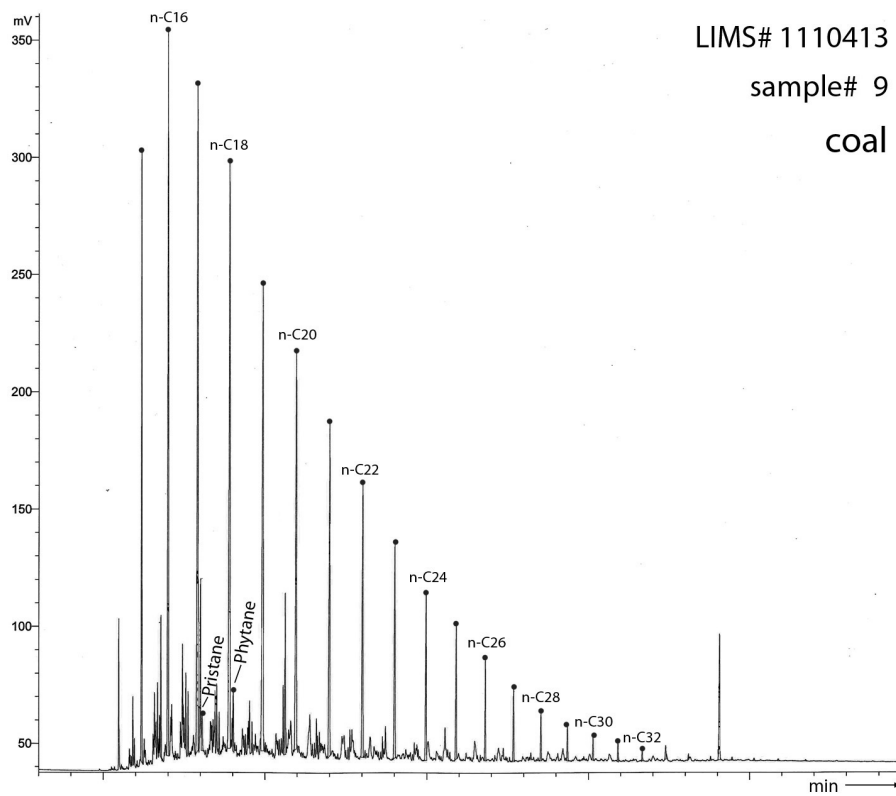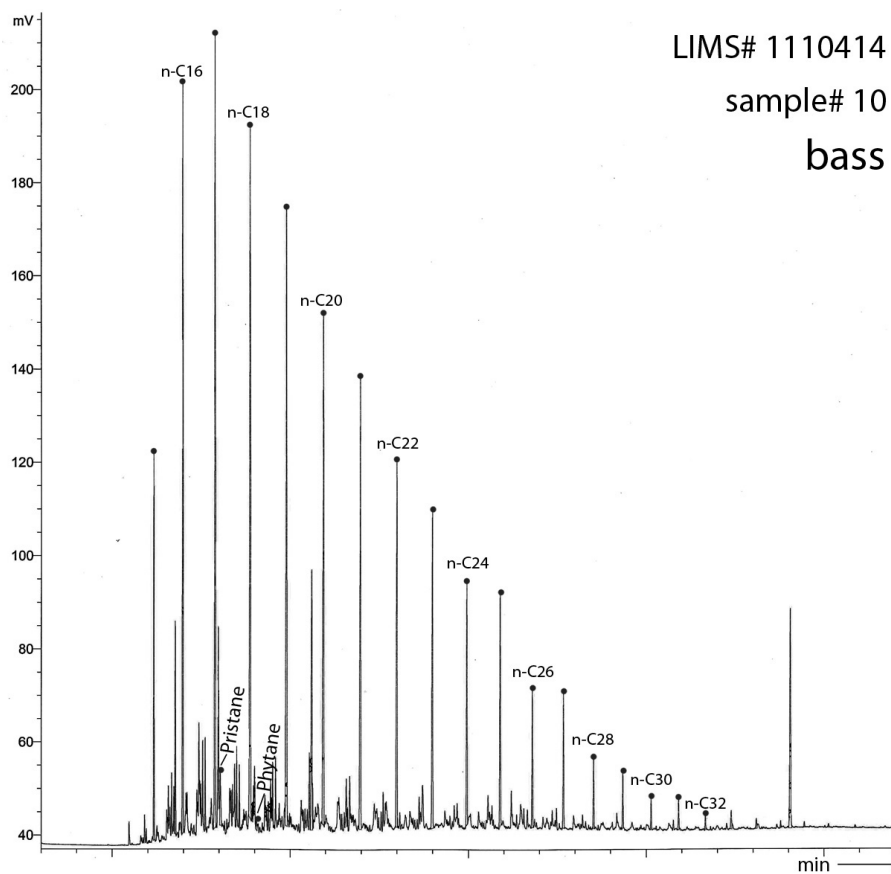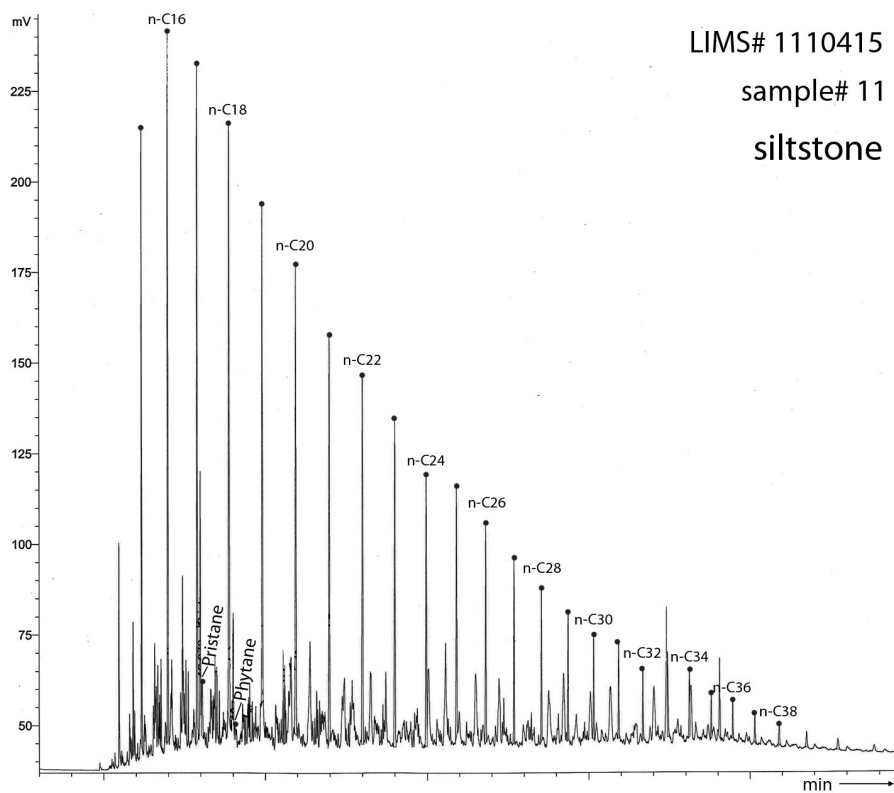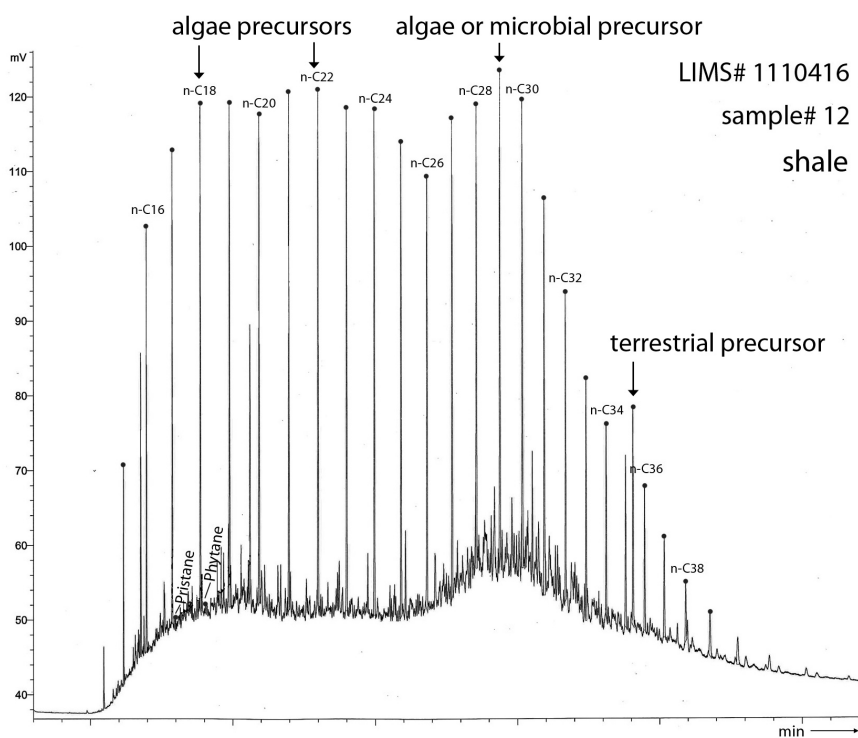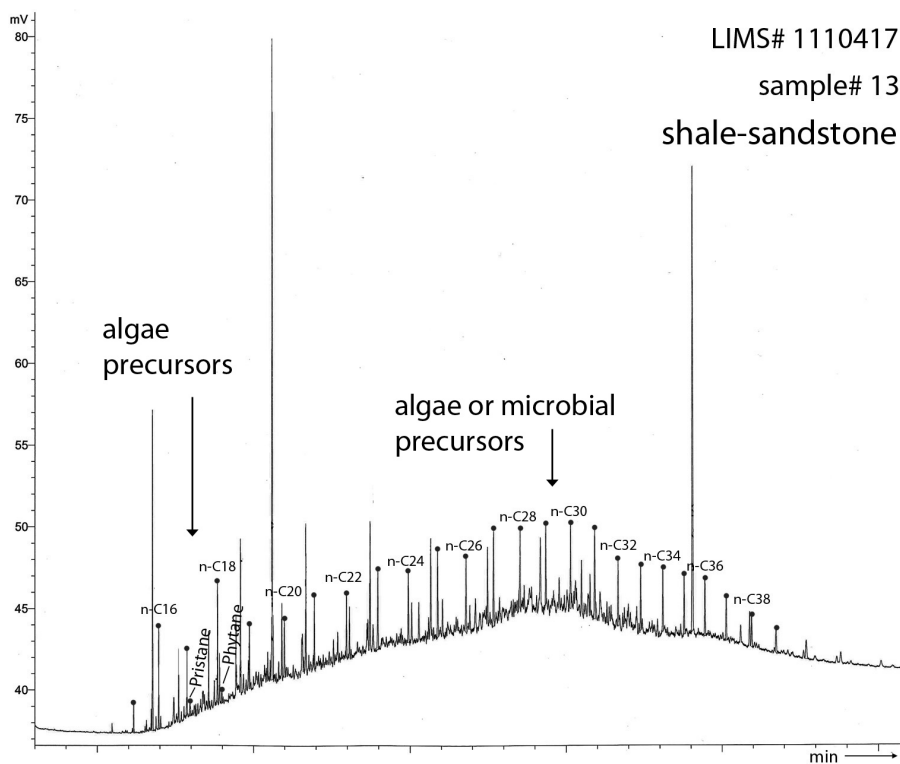
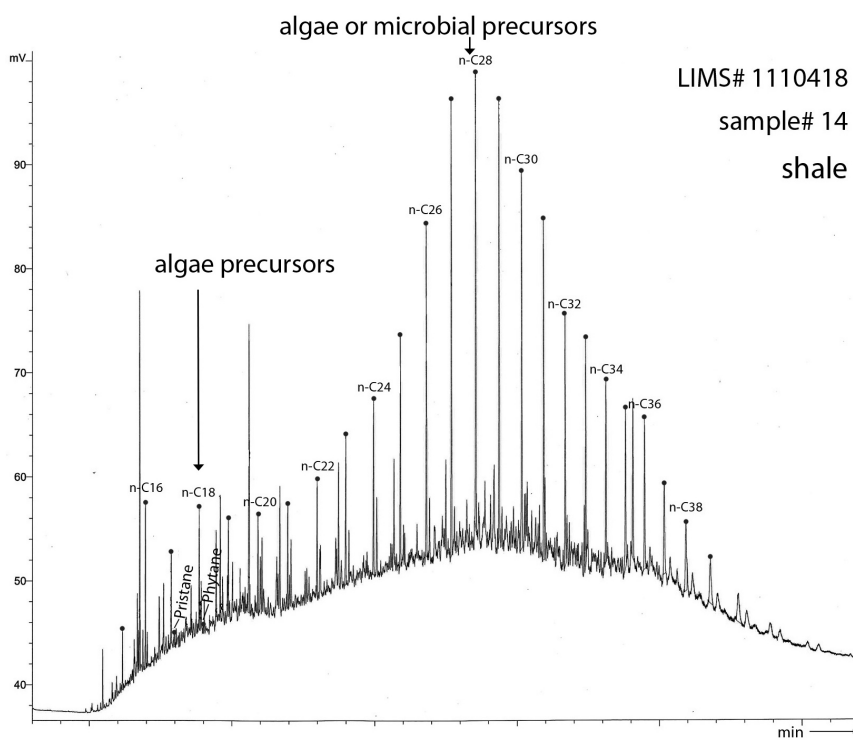Figure A.13: Gas Chromatogram Sample 13
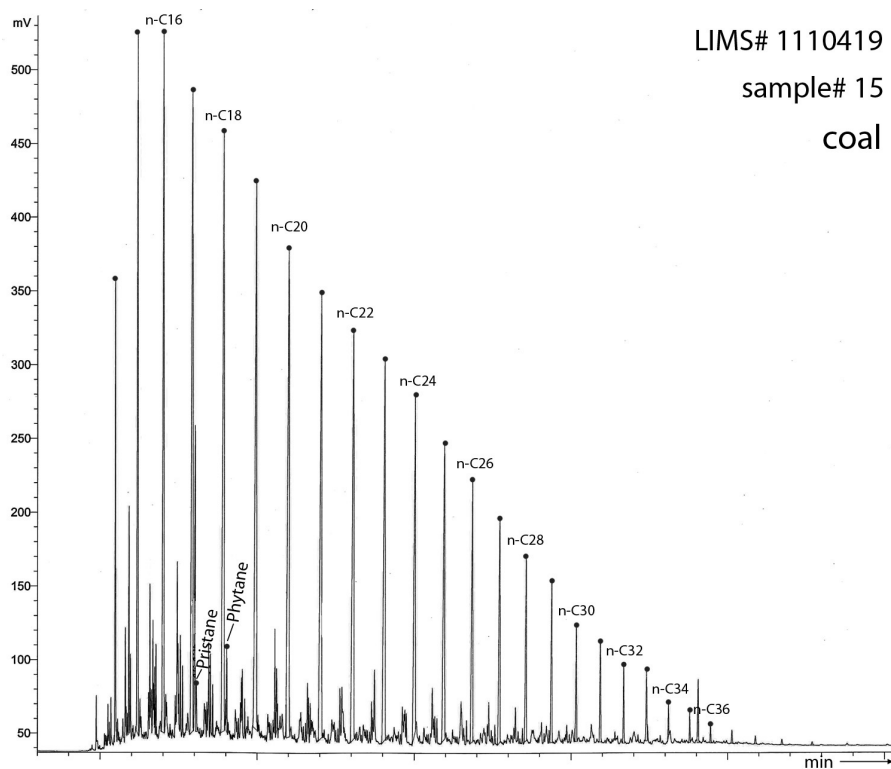

Figure A.14: Gas Chromatogram Sample 14
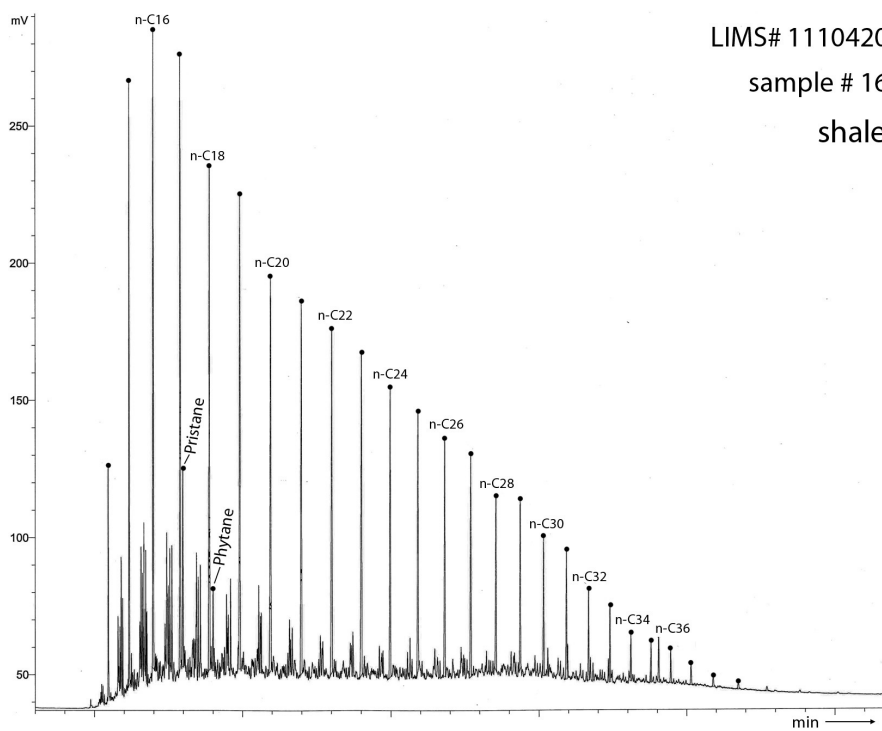
Figure A.15: Gas Chromatogram Sample 15

Figure A.16: Gas Chromatogram Sample 16

Table A.7: Gas chromatography analysis data of C15 to C40 in percentages of the sum of C15 to C40 (sample # cf. Table 3.1).

Sample #	C15	C16	C17	pri	C18	phy	C19	C20	C21	C22
1	0.69	1.65	2.12	0.31	2.49	0.18	2.26	2.38	2.91	4.15
2	0.36	0.84	1.09	0.08	1.51	0.05	1.90	2.68	3.72	4.91
3	7.59	9.29	9.41	0.87	8.79	0.41	8.21	7.38	6.84	6.05
4	0.65	1.55	2.55	0.29	3.15	0.17	3.57	3.75	4.24	4.94
5	6.95	8.37	9.00	0.59	8.72	0.47	8.01	7.47	6.71	6.25
6	7.48	10.31	10.58	0.95	9.59	0.55	8.84	7.70	6.74	5.89
7	4.44	9.23	11.54	1.32	11.01	0.39	9.84	8.23	6.93	5.77
8	2.45	6.52	8.09	0.12	7.78	0.08	6.79	5.72	5.18	4.85
9	8.00	13.44	14.68	0.88	14.06	0.99	11.63	8.96	7.17	5.46
10	4.01	10.44	13.39	1.16	13.13	0.23	11.68	9.72	8.24	6.48
11	6.31	9.19	10.32	1.34	10.22	0.25	8.00	7.92	7.01	6.27
12	1.43	3.05	3.85	0.12	4.60	0.08	5.02	4.95	5.47	5.63
13										
14	0.68	2.06	1.23	0.27	1.68	0.19	1.52	1.47	1.61	1.87
15	6.42	8.63	9.64	0.44	9.88	0.64	9.47	8.79	8.07	7.32
16	6.27	8.38	9.63	2.64	8.34	1.09	7.90	7.05	6.68	5.97

Sample #	C23	C24	C25	C26	C27	C28	C29	C30	C31	C32
1	5.72	6.33	6.87	6.58	6.05	5.02	4.63	4.03	3.54	3.09
2	6.58	7.58	8.24	7.60	7.04	5.85	5.22	4.39	3.81	3.31
3	5.61	4.93	4.51	3.95	3.45	2.73	2.33	1.75	1.57	1.18
4	6.19	7.06	7.92	7.89	7.61	6.64	5.80	4.89	4.07	3.29
5	5.76	5.11	4.57	3.94	3.41	2.87	2.47	2.09	1.73	1.38
6	5.29	4.50	4.04	3.31	2.84	2.28	2.03	1.59	1.36	0.99
7	4.89	4.09	3.66	3.23	3.05	2.52	2.32	1.75	1.47	1.02
8	4.87	4.88	5.34	5.47	5.57	4.97	4.59	3.64	3.20	2.31
9	4.11	3.06	2.26	1.52	1.10	0.74	0.52	0.34	0.32	0.18
10	5.59	3.93	3.89	2.21	2.04	1.01	0.80	0.48	0.48	0.26
11	5.65	4.74	3.99	3.28	2.65	2.10	1.72	1.47	1.26	1.00
12	5.89	5.72	5.58	5.27	5.46	5.34	5.78	5.46	5.10	3.34
13										
14	2.60	3.02	4.08	5.99	9.03	8.74	8.44	7.91	6.50	5.10
15	6.47	5.30	4.65	3.52	2.85	2.02	1.62	1.14	0.97	0.64
16	5.73	4.94	4.51	3.79	3.58	2.60	2.44	1.87	1.89	1.20

Table A.7 continuation

Sample #	C33	C34	C35	C36	C37	C38	C39	C40
1	2.94	2.91	3.36	3.80	4.39	4.49	4.15	2.93
2	3.32	3.44	3.77	3.75	3.41	2.74	1.82	1.01
3	0.83	0.60	0.50	0.40	0.31	0.24	0.16	0.11
4	2.84	2.35	2.07	1.92	1.65	1.33	0.96	0.64
5	1.07	0.78	0.65	0.53	0.43	0.31	0.23	0.15
6	0.79	0.58	0.48	0.39	0.31	0.24	0.20	0.13
7	0.88	0.56	0.52	0.37	0.31	0.26	0.21	0.18
8	1.95	1.30	1.14	0.91	0.77	0.63	0.51	0.37
9	0.25	0.09	0.07	0.06	0.04	0.04	0.04	0.00
10	0.35	0.18	0.09	0.09	0.06	0.06	0.00	0.00
11	1.48	1.12	0.65	0.52	0.49	0.42	0.34	0.29
12	2.74	2.08	2.11	1.81	1.49	0.97	0.96	0.69
13								
14	4.10	3.51	4.06	3.80	3.00	3.05	2.44	2.07
15	0.65	0.23	0.23	0.14	0.12	0.08	0.05	0.04
16	1.01	0.62	0.57	0.47	0.35	0.23	0.16	0.11

Table A.8: Stable carbon isotope analysis on hydrocarbon fractions. Results refer to VPDB (sample # cf. Table 3.1).

Sample #	Aliphatics ‰-$\delta^{13}C$	Aromatics ‰-$\delta^{13}C$
5	-29.67	-27.17
9	-27.39	-24.91
11	-26.86	-24.39
12	-31.13	-29.15
15	-27.68	-25.38

Table A.9: Geochemical analysis of sediment gases. Concentration in extracted gas: %-values normalized to the $\sum C_1 - C_3$. Concentration in dry sediment: ppb concentrations normalized to dry sediment weight (sample # cf. Table 3.1).

| Sample # | normalized to the $\sum C_1 - C_3$ | | | concentration normalized to dry sediment weight | | | C1/(C2+C3) |
	Methane %	Ethane %	Propane %	Methane ppb	Ethane ppb	Propane ppb	
1	81.7%	11.0%	7.3%	9.3	2.2	2.3	4.46
2							
3	93.8%	6.2%	0.0%	6.1	0.7	0	15.18
4	94.3%	5.7%	0.0%	11.7	1.2	0	16.57
5	87.0%	10.5%	2.5%	7911.8	1676.3	622.7	6.68
6							
7	80.4%	14.5%	5.1%	17.0	5.3	3.0	4.11
8	92.2%	7.8%	0.0%	3.8	0.6	0	11.87
9	27.5%	1.4%	71.1%	4.5	0.4	32.2	0.38
10	96.8%	3.2%	0.0%	9.6	0.6	0	30.37
11	91.1%	8.9%	0.0%	6.9	1.2	0	10.27
12	100.0%	0.0%	0.0%	2.6	0	0	
13	82.1%	11.3%	6.6%	5.0	1.2	1.1	4.59
14	87.1%	10.0%	2.9%	17.4	3.5	1.6	6.72
15	78.9%	12.1%	9.0%	4.6	1.2	1.4	3.74
16	74.5%	19.1%	6.4%	108.1	48.4	25.5	2.93

Table A.10: Stable carbon isotope analysis of selected sediment gases (sample # cf. Table 3.1). Analysis refers to VPDB.

Sample #	Methane ‰-$\delta^{13}C_{[CH_4]}$	Ethane ‰-$\delta^{13}C_{[C_2H_6]}$	Propane ‰-$\delta^{13}C_{[C_3H_8]}$
5	-47.15	-28.79	-25.12
7	-39.50	-26.82	-24.37
14	-38.02	-31.87	
16	-44.94	-32.69	-31.49

Table A.11: Data of density and porosity measurements (sample # cf. Table 3.1).

Sample #	True density g/cm^3	Bulk density g/cm^3	Shale Porosity %	Sand/Coal Porosity %
1	2.4322	2.1598	11.19	
2	2.629	2.1206	19.33	
3	2.5439	2.2979	9.66	
4	2.6957	2.2807		15.39
5	2.6531	2.3813	10.24	
6				
7				
8	2.5796	2.2951	11.02	
9	1.6727	1.5794		5.57
10	2.565	2.2825		11.01
11	2.3152	2.1428	7.44	
12	2.3054	1.8567	19.46	
13				
14	2.3864	1.6982	28.83	
15	1.9708	1.8056		8.38
16	2.6216	2.08	20.65	